BNL-1328

Subject Category: PHYSICS

UNITED STATES ATOMIC ENERGY COMMISSION

LEAKAGE OF GAMMA RADIATION THROUGH SPHERICAL AND CYLINDRICAL VOIDS

By
William W. Pratt
Herbert J. Kouts

August 25, 1952

Brookhaven National Laboratory
Upton, New York

Technical Information Service, Oak Ridge, Tennessee

DISCLAIMER NOTICE

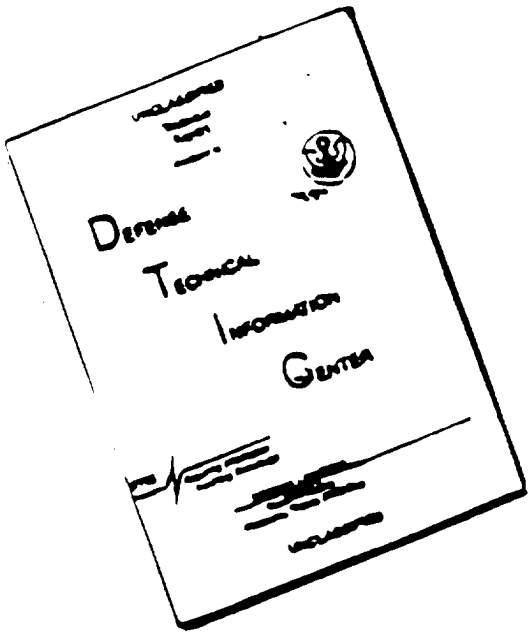

THIS DOCUMENT IS BEST QUALITY AVAILABLE. THE COPY FURNISHED TO DTIC CONTAINED A SIGNIFICANT NUMBER OF PAGES WHICH DO NOT REPRODUCE LEGIBLY.

Date Declassified: November 30, 1955.

Printed in USA, Price 45 cents. Available from the Office of Technical Services, Department of Commerce, Washington 25, D. C.

BNL-1328

LEAKAGE OF GAMMA RADIATION THROUGH SPHERICAL AND CYLINDRICAL VOIDS

By

William W. Pratt
Herbert J. Kouts

August 25, 1952

Work performed under Contract No. AT(30-2)-Gen-16.

Reactor Department
BROOKHAVEN NATIONAL LABORATORY
Associated Universities, Inc.
Upton, New York

LEAKAGE OF GAMMA RADIATION THROUGH SPHERICAL AND CYLINDRICAL VOIDS *

* The work reported here represents a continuation of the work described in BNL-158. The present report is intended for most purposes to supersede BNL-158, and a summary of the results presented in BNL-158 is included in the present report.

I. EXPERIMENTAL ARRANGEMENT

The measurements reported here were made in the BNL water tank shielding facility, which has been described in detail in BNL-139 (T-26). Measurements were made with: (a) a brass-walled GM counter, one inch in diameter by four inches in length, shielded on all sides by two and one-half inches of lead; and, (b) a graphite-walled ion chamber, one inch in diameter by four inches in length. The GM counter has the advantage of high sensitivity permitting measurements of high precision for the determination of the detailed shape of flux patterns. It has the disadvantage of an energy response which is enhanced in the high energy region of the spectrum, due to the heavy lead shield which is used to reduce the flux to a measurable value. The ion chamber has an approximately tissue-equivalent response to gamma ray flux but has too low a sensitivity to permit measurements with small voids.

The experimental arrangement is indicated in Figure 1, which shows the GM counter in position to measure the leakage through a spherical void. The tank is filled with water to a depth of 143.25 inches. An outlet is provided at the top of the tank, so that the water level remains constant when a void is placed in the tank. The counter or ion chamber is mounted with its axis of symmetry vertical and with a clearance

of one inch between the bottom of the detector and the water surface. Flux measurements are then made at various points in the horizontal plane.

A natural uranium source plate, 39-5/8" x 39-5/8" x 5/8", is mounted below the tank to provide a fission source of gamma rays and neutrons. The top surface of the source plate is shielded with boral from thermal neutrons scattered from the water tank. A plate of bismuth, 3-5/8" thick, is mounted below the source plate to suppress gamma ray leakage from the pile reflector. Even with the bismuth shield in place, the fraction of the gamma ray flux at the surface of the water tank which is attributed to the source plate is only about five per cent of the total flux. Thus, the gamma ray measurements are primarily characteristic of the pile gamma rays and those produced by neutron capture in the material surrounding the water tank facility.

II. MEASUREMENTS

A. Notation

The following notation is used in this report.

x = north-south coordinate of the detector axis, south is positive, north is negative.

y = west-east coordinate of the detector axis, east is positive, west is negative.

The center of the tank is taken as $x = y = 0$.

z = thickness of water between the detector center and the bottom of the tank.

$\bar{x}$, $\bar{y}$ = x and y coordinates of the center of the void.

$r = ((x - \bar{x})^2 + (y - \bar{y})^2)^{\frac{1}{2}}$, and is the radial distance of the axis of the detector from the center of the void.

D = diameter of a spherical or cylindrical void*.

H = distance of the top surface of a spherical void below the water surface.

L = length of a cylindrical void*.

N = detector response with a void present, expressed in counts per minute for the GM counter and in Roentgens per hour for the ion chamber.

No = detector response with no void present.

P = pile power in megawatts.

$I = \int_{\sigma}^{\infty} 2\pi r\,(N/No-1)dr$, the excess leakage integral which is a measure of the total radiation emerging from a shield due to the presence of a void.

W = width at half maximum of the curve (N/No-1) as a function of r.

* These are nominal dimensions only. The actual dimensions and wall thicknesses of the aluminum shells encasing the voids are given in Table 11.

B. Flux Pattern with No Void

Measurements were first made with no void in the water tank. The results are plotted in Figures 2 and 3. The emerging flux is seen to have a maximum value near the center of the tank. In the case of the ion chamber measurements (Figure 2), the flux pattern curves are fairly symmetrical about the center of the tank. In the case of the GM counter measurements (Figure 3), the flux pattern curves exhibit a maximum slightly to the south and to the east of the center of the tank. The shifting of the maximum to the south is attributed to the presence of the reactor cooling gap which is south of the water tank. The shifting of the maximum to the east may be the result of a thermal column on the west side of the water tank.

The fact that the displacement of the maximum in the flux pattern is observed with the shielded GM counter and not with the ion chamber is believed to be a consequence of the different energy response of the two detectors. The GM counter, enclosed in a two and one-half inch lead shield, is responsive only to the more penetrating components of the radiation emerging from the tank. Thus, the flux measured by this counter consists mainly of the primary radiation which originates at the bottom of the tank and emerges from the surface of the water with little or no scattering. The flux pattern measured by this counter is thus strongly dependent upon the flux pattern at the bottom of the tank. The ion chamber, on the other hand, responds to low energy secondary radiation with fair efficiency. The flux pattern measured by this detector is thus strongly influenced by scattering in the water, and only the more pronounced features (i.e., dropping off of flux near the tank wall) of the primary flux pattern are observed with this detector. Thus, the variation of flux with horizontal distance is much less in the ion chamber measurements than in the GM counter measurements, and the shifting of the maximum is not observed at all.

C. Flux Pattern with Voids

Measurements were made with spherical voids having diameters of four, six, eight, twelve, and eighteen inches; and with cylindrical voids having diameters of two, four, six, eight, twelve, and eighteen inches. The spheres were placed in the center of the tank, and flux patterns were measured as a function of the depth of the sphere below the water surface. The cylinders were placed in the center of the tank with the axis of symmetry vertical, and the top surface of the cylinder

barely submerged below the water surface. Flux patterns were measured as a function of cylinder length.

The pile power was monitored periodically by positioning the detector in a standard position and checking the detector response. During the course of the experiments, a BF_3 counter monitor with continuous recording was installed in a corner of the tank to correct for short time variations in pile power. The detector readings were corrected for resolving time (in the case of the GM counter), background, and pile power level.

The data are presented as the ratio of detector response N, with the void present, to the detector response No, with no void present. This may be expected, to a first approximation, to correct for the variation with position of the flux pattern with no void present.

In some cases, particularly in cases where the void was some distance below the water surface, the void was not positioned exactly in the center of the tank. This resulted in a shift in the peak of the flux pattern obtained; and the amount of miscentering could be determined and corrected for by observing the amount of this shift. Since the flux reaching the detector decreases as the height of the detector above the water surface is increased, it is necessary to correct the observed data for the decrease in observed flux due to the height of the detector above the water surface. This correction was obtained for $N/No(r = 0)$ as a function of D, H, and L by measuring No and N as a function of height of detector above the water surface for a variety of voids. In this way, a correction factor, F, is obtained which must be multiplied by the observed

$N/N_o(r = 0)$ to give the value corresponding to a detector at the surface of the water. This correction factor is given in Table 1. It is assumed that no correction is necessary in the case of the excess leakage integral, I, since the reduction in height of the flux pattern should be accompanied by a corresponding increase in width.

D. Results

The results of the sphere and cylinder measurements are presented in Tables 2 to 7 and in Figures 4 to 29. The GM counter sphere measurements have been reported previously in BNL-158, and individual flux pattern curves are not included in the present report.

Summaries of the sphere measurements are presented in Tables 2, 3, and 6 and in Figures 26 and 28. There is seen to be good agreement between the ion chamber and GM counter measurements in all cases where the precision is sufficient to afford an accurate comparison. These measurements are also in agreement with a semiempirical theory described in a separate report*. An interesting feature of the excess leakage integral curves (Figure 28) is the approximate independence of this integral on the depth of the sphere below the water surface.

Summaries of the cylinder measurements are presented in Tables 4, 5, and 7 and in Figures 27 and 29. There is a definite discrepancy between the ion chamber and GM counter results in the peak value of N/N_o, although the excess leakage integral curves show fair agreement. The discrepancies are believed to be attributable to the difference in energy response of the two detectors, and are discussed in a later section.

* Herbert J. Kouts, BNL Log No. C-6459 (in press)

III. SUPPLEMENTARY EXPERIMENTS

A. Effect of Detector Size

Since the dimensions of the lead shield surrounding the GM counter are not small compared to the void diameters, an experiment was carried out to determine the effect of the size of the shield on the width of the flux pattern curve. A shield was constructed which was open at the bottom, so that the end of the counter was unshielded. The sides and top of the counter were shielded by two and one-half inches of lead. A one inch diameter counter thus shielded should be equivalent to a one inch diameter disc-shaped counter. Flux pattern curves were obtained for a four inch diameter sphere with a counter shielded in this way and with a counter shielded in the manner described previously. No difference was observed in the half-width of the excess leakage curve ((N/No - 1) vs r); although the peak value of N/No was somewhat increased in the case of the partially shielded counter, because of the collimating effect of the open-ended shield. It is concluded from this that the effective diameter of the fully shielded GM counter is no greater than one inch, and the effect of counter size on the observed flux patterns should be small. The ion chamber was mounted, like the GM counter, with its axis vertical and thus presented a minimum area to the radiation from the tank.

B. Collimating Effect of the GM Counter Shield

Since the lead shield around the GM counter was cylindrical in shape with a flat bottom, as indicated in Figure 1, the counter may be expected to be more sensitive to radiation from directly below the counter than to radiation which comes obliquely from off the counter axis.

This is because the oblique radiation will have to penetrate somewhat more lead than the axial radiation. To test the influence of this effect, the lower end of the shield was rounded so as to present approximately the same amount of lead to radiation from all directions. Several of the flux pattern curves were repeated with the rounded shield. Although both N and No were increased, no significantly different values of N/No were observed with the new shield. It is concluded from this that the radiation to which the shielded GM counter responds is mainly the penetrating primary radiation which emerges in a nearly vertical direction from the tank.

C. Water Attenuation Curves

Attenuation curves in the water tank with no voids present were obtained with both the shielded GM counter and the ion chamber. In making the GM counter measurements, the water was drained from the tank in four inch steps and the counter was lowered so as to remain always one inch above the water surface. When the counting rate became too high for reliable counting, the pile power was decreased; and the decrease in source strength was determined by measuring the counting rate before and after the change in pile power. Background corrections were made by observing the decay rate and variation with water level of the counting rate with the pile shut down. Measurements with the ion chamber were made with the water tank full and at full pile power, the ion chamber being submerged at various depths in the water. Below a water depth of seventy-six inches, the ion chamber was replaced by a less sensitive chamber of essentially the same dimensions. The resulting attenuation curves are presented in Tables 8 and 9 and in Figure 30. These curves

are not corrected for the finite size of the source. The observed attenuation length in the water tank between fifty-five and one hundred forty-three inches of water is 31.6 cm as measured by the ion chamber and 36 cm as measured by the shielded GM counter. This appears to support the conclusion of the previous section that the shielded GM counter responds preferentially to the more penetrating components of the radiation.

D. Flux Pattern Throughout the Water Tank

Ion chamber measurements were made of the gamma ray flux throughout the water tank with no voids present. These measurements are presented in Figures 31 to 46. It is seen from these curves that the flux near the tank bottom is greater on the south side than on the north side and greater on the west side than on the east side. This is to be expected since the water tank is located north and east of the center of the pile. The greater variation in the north-south direction than in the east-west direction is to be attributed to the cooling gap which runs east and west through the center of the pile, and gives rise to a large amount of neutron streaming along the face of the pile reflector. Measurements at successively higher levels in the tank show less and less of this assymmetry; and after a level of about sixty inches is reached, the flux pattern curves are fairly symmetrical. The curves at all levels show a pronounced drop in the flux near the walls of the tank.

E. Angular Distribution Measurement

An attempt was made to measure the angular distribution of the gamma radiation emerging from the water tank with no voids present. A four inch by four inch by twenty-four inch lead collimator with a one inch diameter hole through the long axis was mounted above the water tank and aimed at the water surface in the center of the tank. A GM counter was mounted in the end of the collimator as shown in Figure 47. The angle between the collimator axis and the vertical axis of the tank was varied in the east-west plane, and at each angle the counting rate was observed. A background correction was obtained at each angle by filling the collimator with a lead plug. The counting rate, with background subtracted, was taken as a measure of the radiation reaching the counter through the hole in the collimator. In order to simulate the difference between the ion chamber and the shielded GM counter, the measurements were repeated with a two and one-half inch lead shield fixed inside the collimator directly in front of the counter. The results are presented in Table 10 and in Figures 48 and 49.

A collimation measurement of this type is subject to the criticism that there may be scattering of radiation by the lead plug during a background measurement, so that the difference between readings with and without the lead plug is not a true measure of the radiation passing through the hole in the collimator. In order to study the importance of this effect, the measurements were repeated with the background determined by placing a two inch diameter by six inch long lead plug in front of the collimator midway between the collimator and the

water surface. The resulting angular distribution curves were not appreciably altered by this change in the experimental arrangement. It is concluded from this that the results obtained are substantially correct.

A striking feature of the angular distribution measurement is the fact that there are two maxima, at approximately eight degrees on either side of the vertical axis. This is presumably an indication that a large fraction of the observed gamma radiation is due to neutron capture in the walls of the tank and the surrounding medium near the bottom of the tank. If this is the case, then further measurements would be expected to show that there is a cone of radiation originating in a ring-shaped source near the bottom of the tank. There is some indication of this in the north-south traverses near the bottom of the tank (Figures 43 and 44). Further measurements will be required in order to verify this point completely.

IV. DISCUSSION OF RESULTS

Although the sphere results show substantial agreement between the ion chamber and shielded GM counter measurements, there is an appreciable discrepancy in the case of the cylinder measurements.

It is seen from Figure 27 that the effect of the void on the peak value of N/No as measured by the ion chamber is less than the effect as measured by the GM counter. This difference is presumably due to the fact that the GM counter, shielded by two and one-half inches of lead, is mainly responsive to penetrating primary radiation which is traveling

in a nearly vertical direction. This view is supported by the fact that no difference in N/No was observed when the nose of the lead shield was cut away to present the same amount of lead to radiation from all directions. This view is also supported by the fact that the attenuation length in the water tank (Figure 30) is longer in the case of the GM counter measurements than in the case of the ion chamber measurements. Finally, the angular distribution measurements (Figures 48 and 49) exhibit some features which are also in accord with this view. These measurements indicate that the radiation emerging at various angles shows a cutoff at about $\neq 15^{\circ}$ when measured with a shielded counter, whereas the unshielded counter detects an appreciable amount of radiation at larger angles.

The excess leakage integral (Figures 28 and 29) is approximately the same in most cases whether measured with the ion chamber or with the GM counter. Apparently, the total emerging flux, the determination of which requires an integration over the entire shield face, is much less sensitive to the angular distribution than is the peak value of N/No. Thus, the larger peak value of N/No which is obtained with a detector responding to the vertical flux appears to be compensated by the larger spread in angle of the radiation detected by a detector responding to the isotropic components of the flux.

The measurements with the ion chamber, which has an approximately tissue-equivalent energy response, are to be considered more reliable than those with the shielded GM counter. The GM counter

measurements are of interest, however, in showing the influence of angular distribution on the effect of a void. In particular, it may be pointed out that the "scaling down" process of expressing all dimensions in terms of the attenuation length of the observed radiation may lead to some error if the angular distribution is not taken into account. Thus, although the attenuation length as observed with the GM counter is greater than that observed with the ion chamber, the effect of a given size of void on the peak value of N/No is greater. This is the reverse of the situation that would be predicted by scaling down the dimensions of the void by the attenuation length factor. Comparison of the excess leakage integrals measured with the ion chamber and with the GM counter indicates that the excess leakage integral is not particularly sensitive to the angular distribution. Thus, the excess leakage integral results presented here may be of fairly general interest.

V. FIGURES

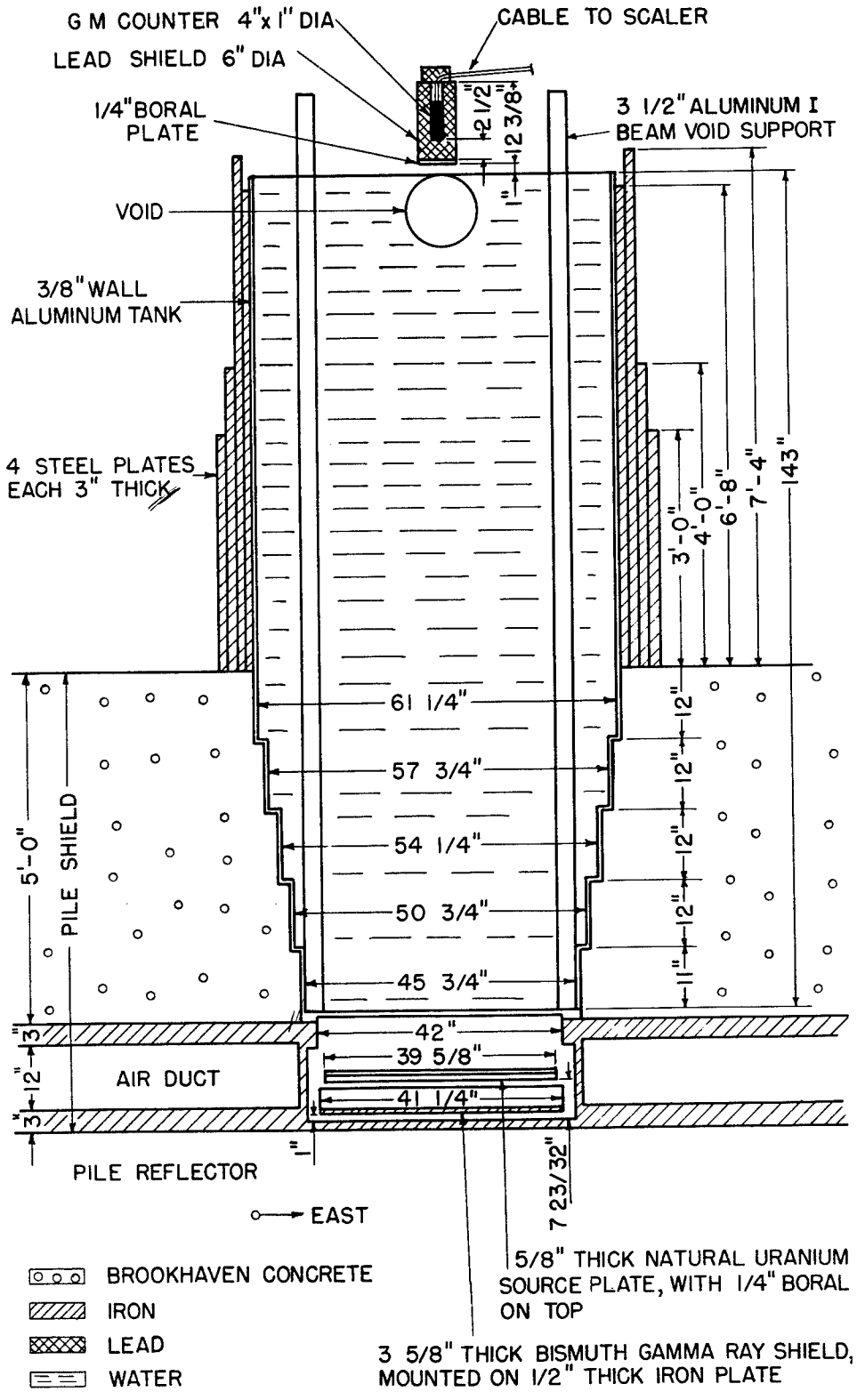

Figure 1 (Above). Water tank facility and associated equipment. BNL Log No. D-1995.

FIG. 2 GAMMA RAY FLUX WITH NO VOIDS (ION CHAMBER)

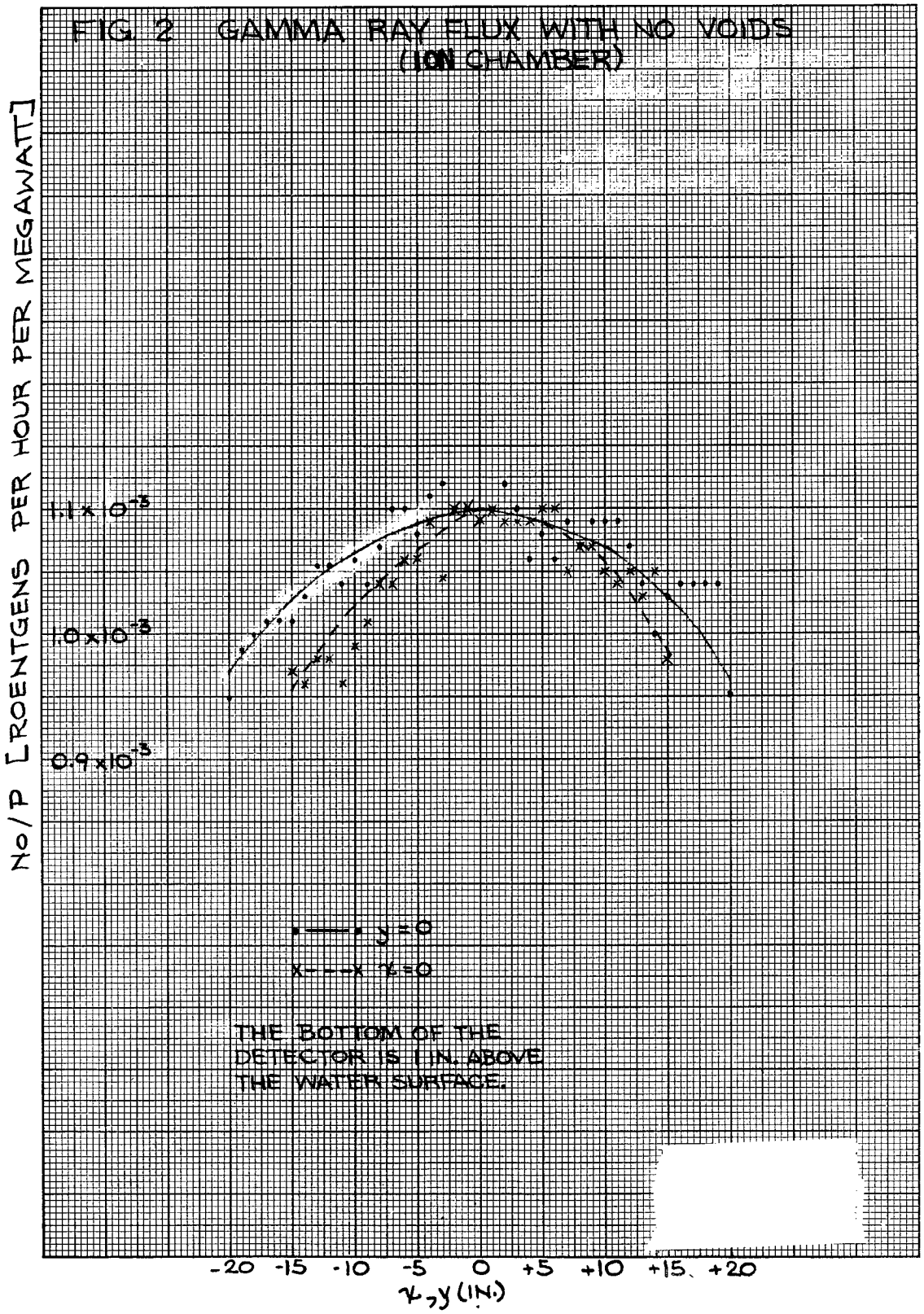

FIG. 3 GAMMA RAY FLUX WITH NO VOIDS
(G M COUNTER)

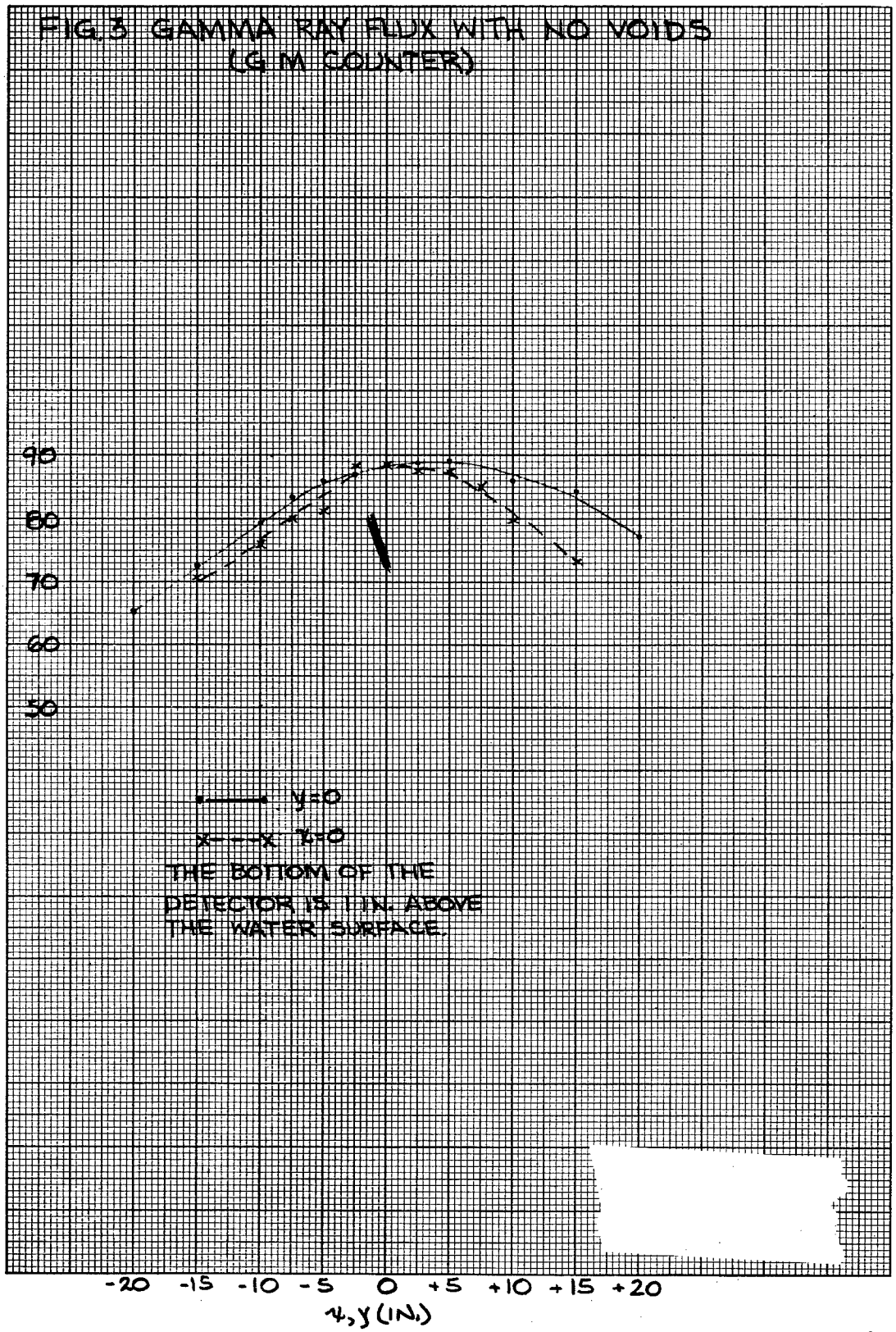

FIG. 4 GAMMA RAY LEAKAGE THROUGH 18" DIA. SPHERE (ION CHAMBER MEASUREMENTS)

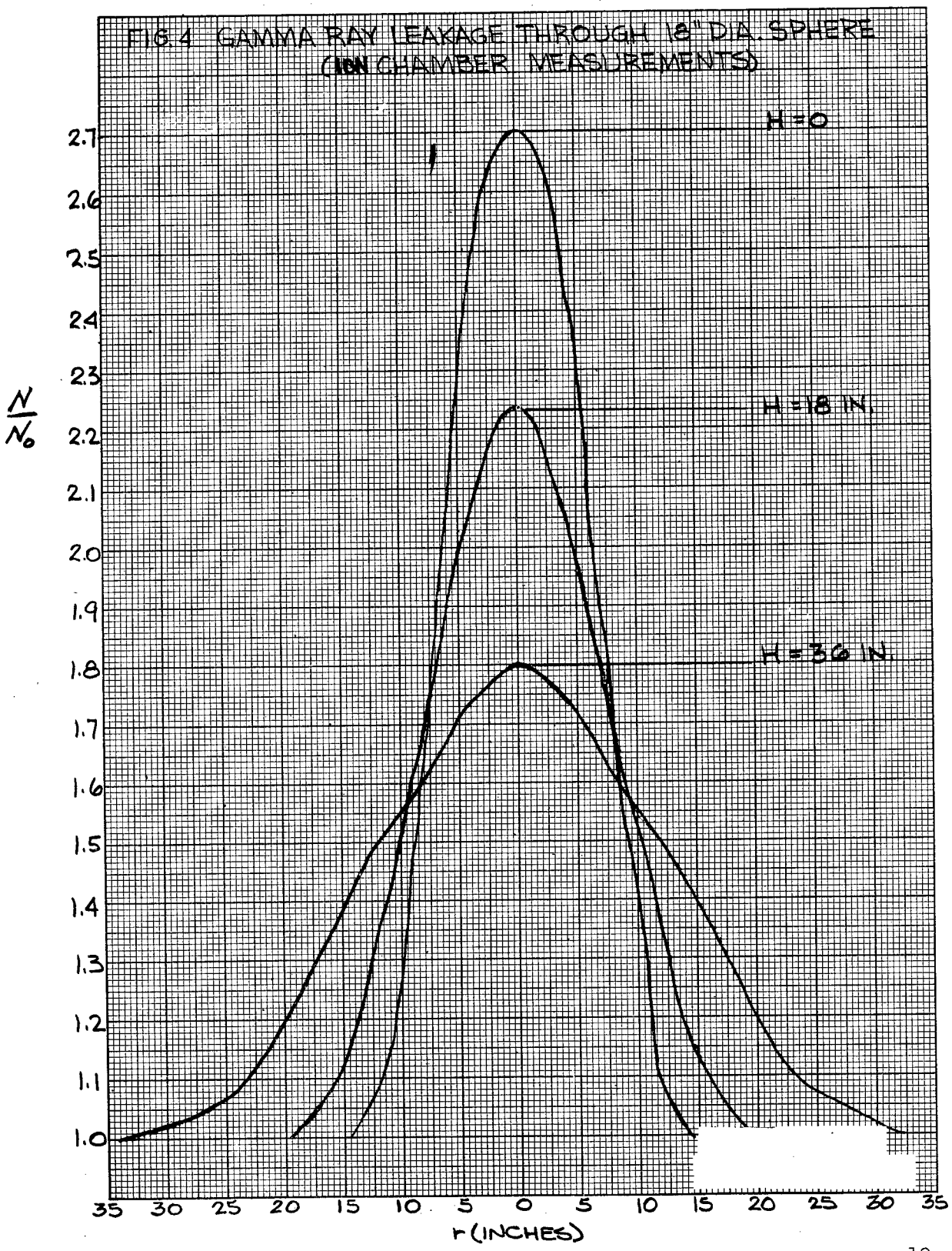

FIG. 5 GAMMA RAY LEAKAGE THROUGH 12" DIA. SPHERE
(ION CHAMBER MEASUREMENTS)

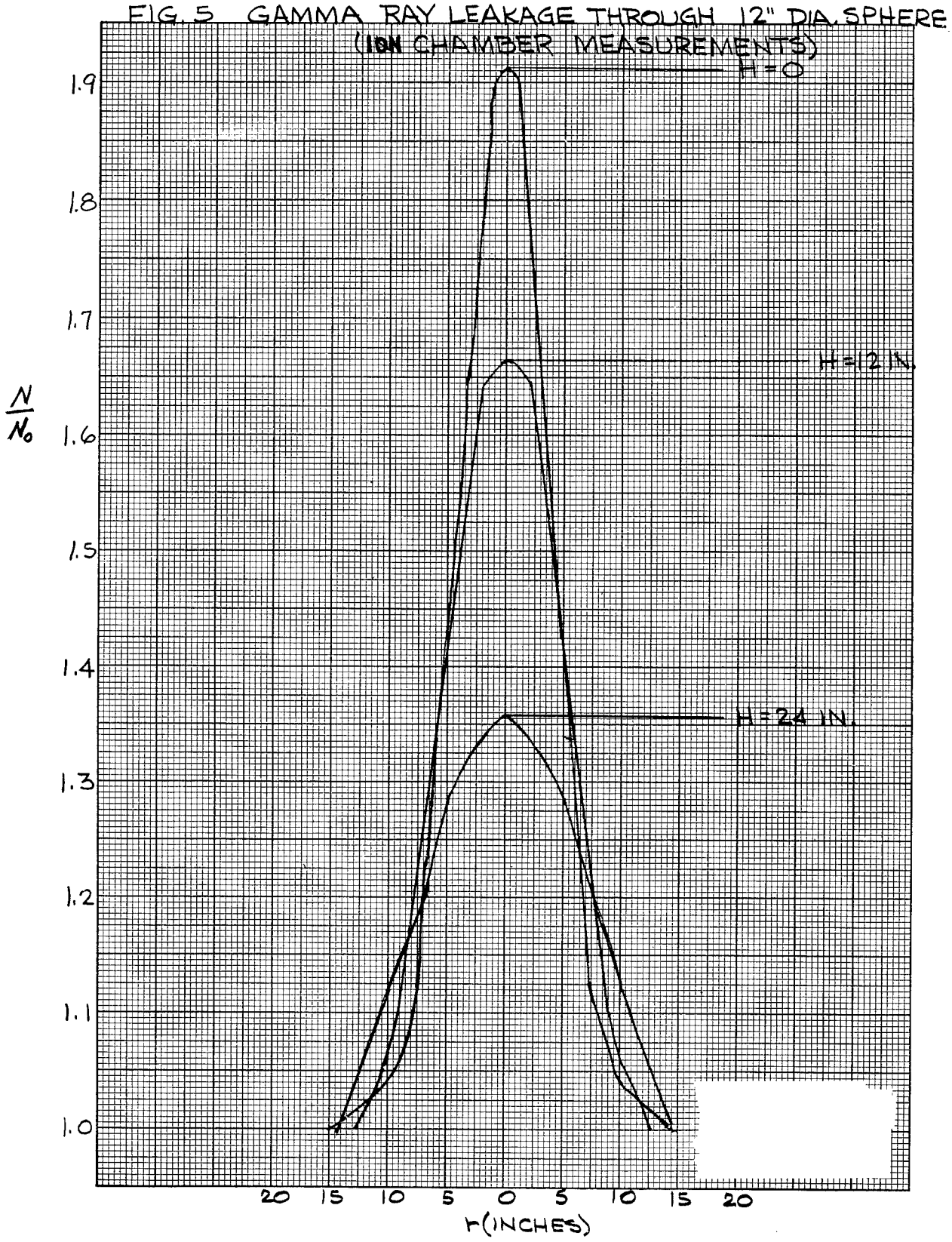

FIG. 6 GAMMA RAY LEAKAGE THROUGH 8" DIA. SPHERE
(ION CHAMBER MEASUREMENTS)

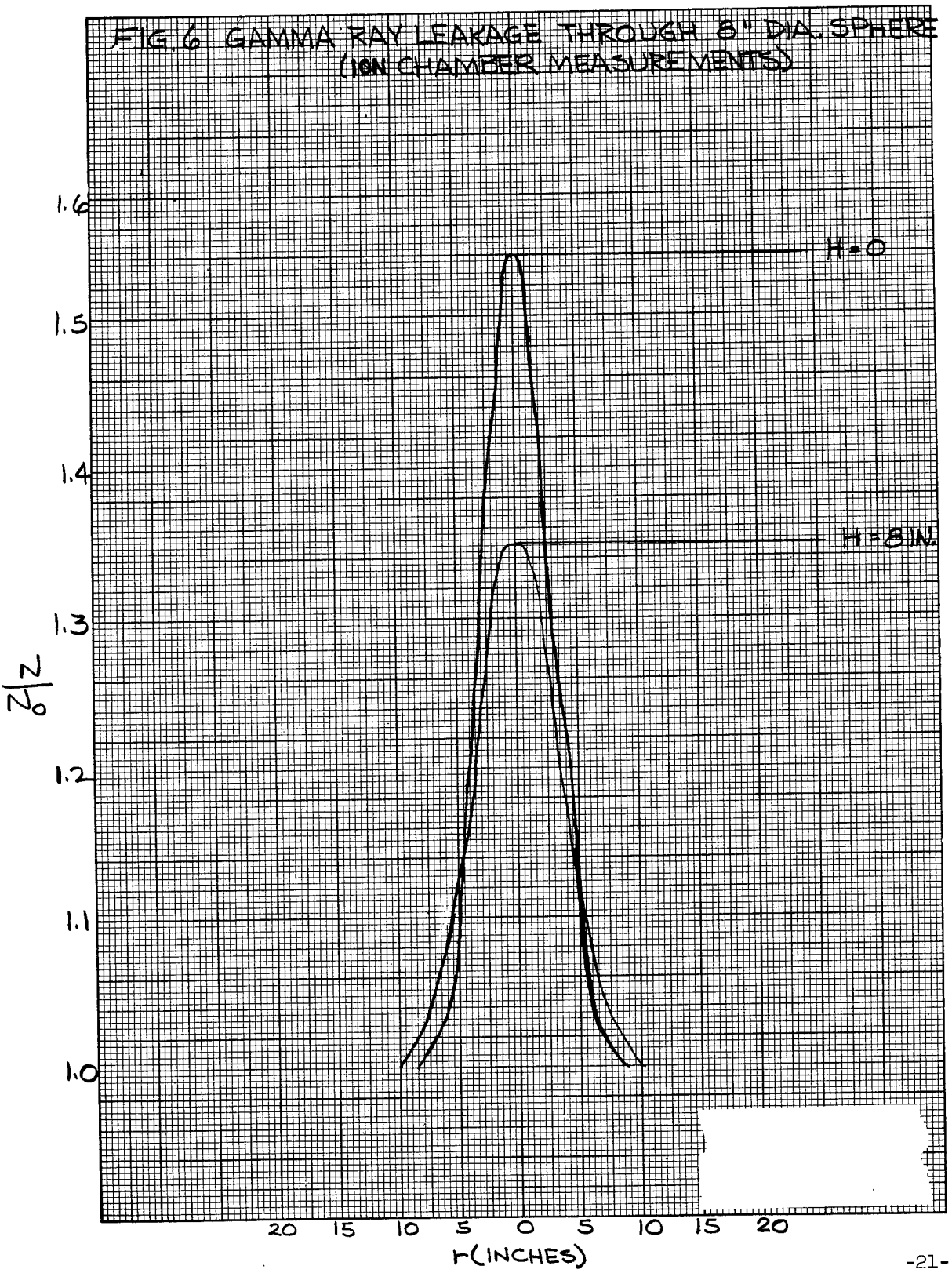

FIG. 7 GAMMA RAY LEAKAGE THROUGH 6" DIA. SPHERE
(ION CHAMBER MEASUREMENTS)

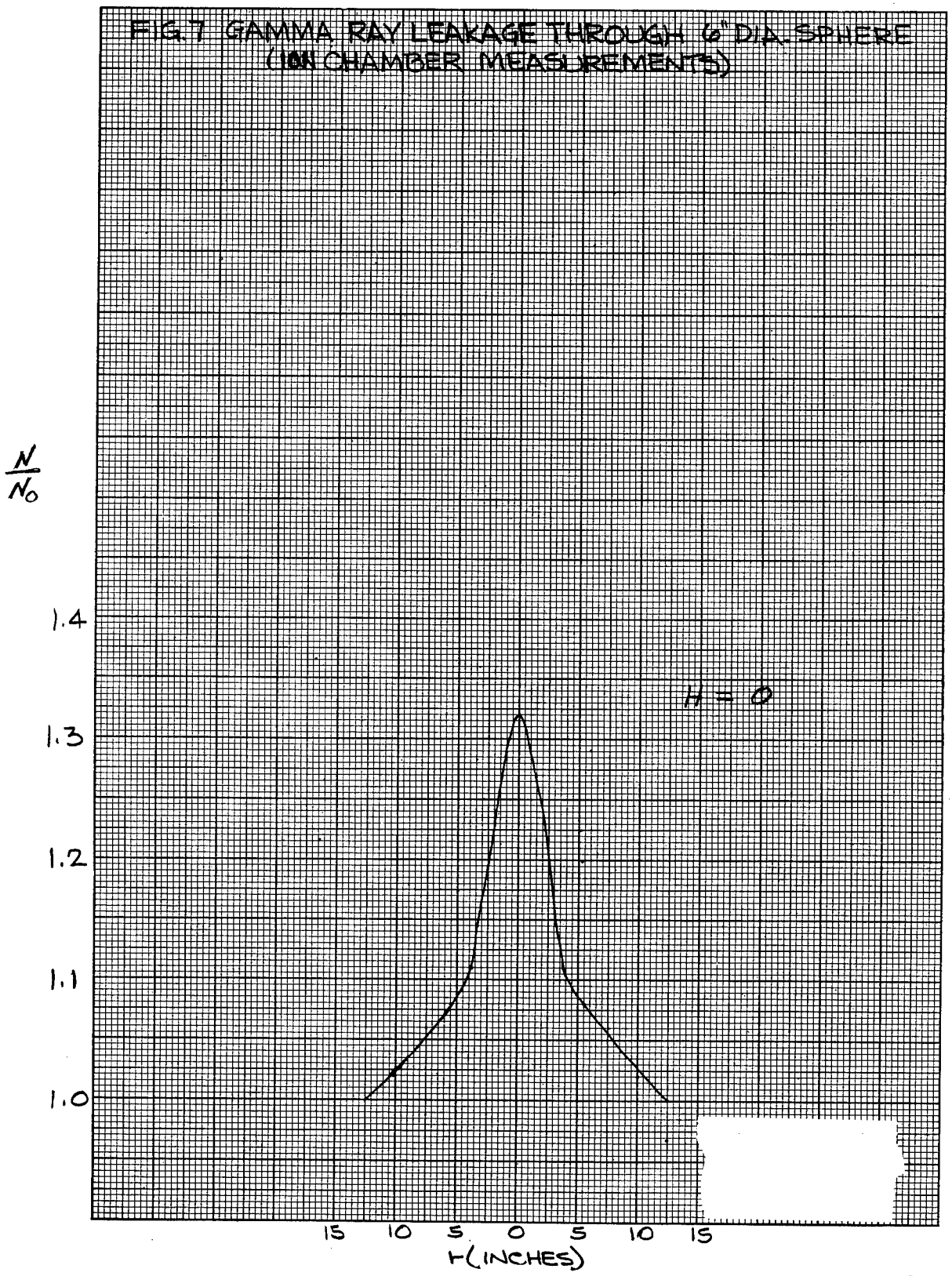

FIG. 8 GAMMA RAY LEAKAGE THROUGH 4" DIA. SPHERE
(ION CHAMBER MEASUREMENTS)

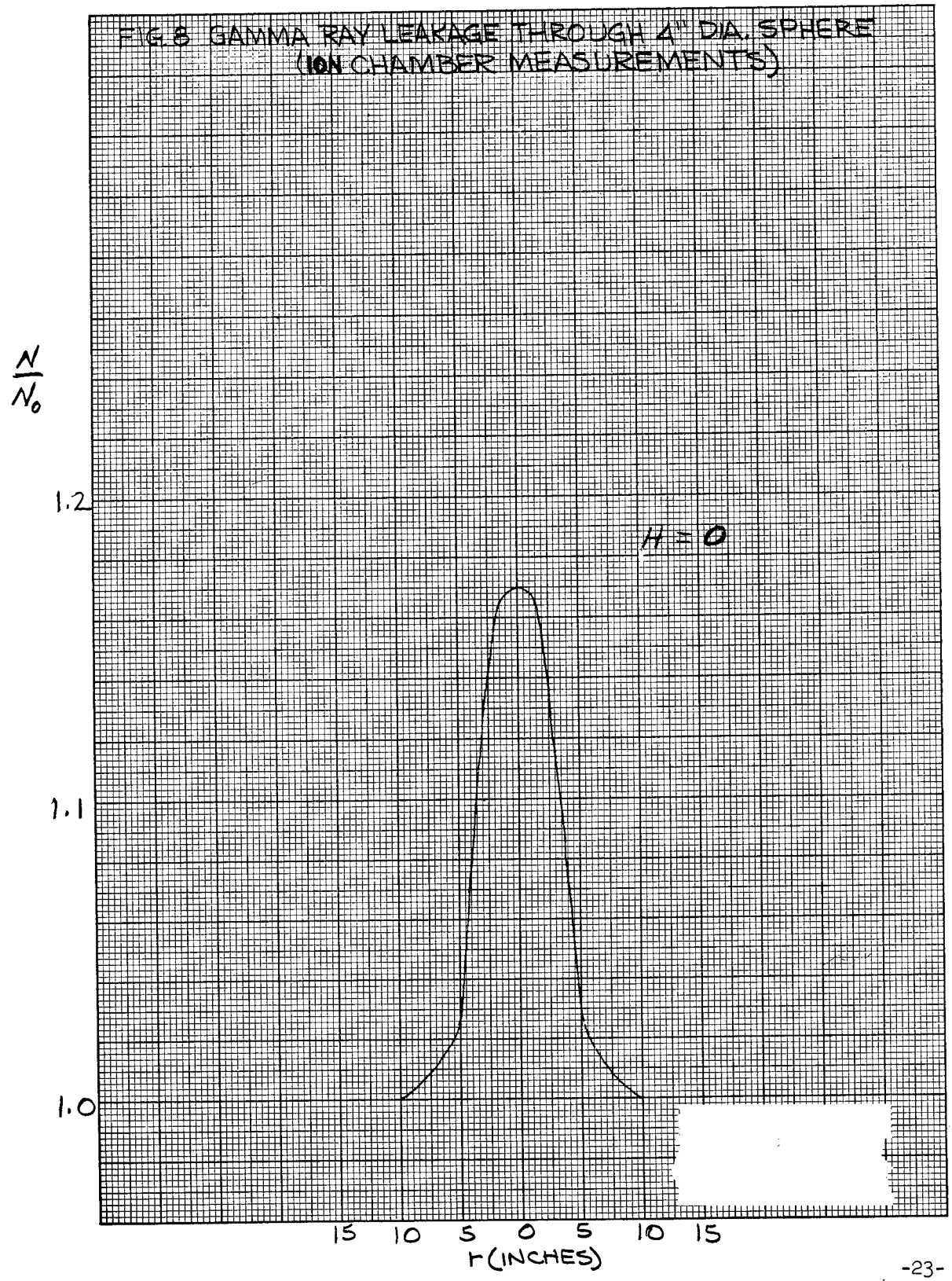

FIG. 9 GAMMA RAY LEAKAGE THROUGH 18" DIA. CYLINDER
(ION CHAMBER MEASUREMENTS)

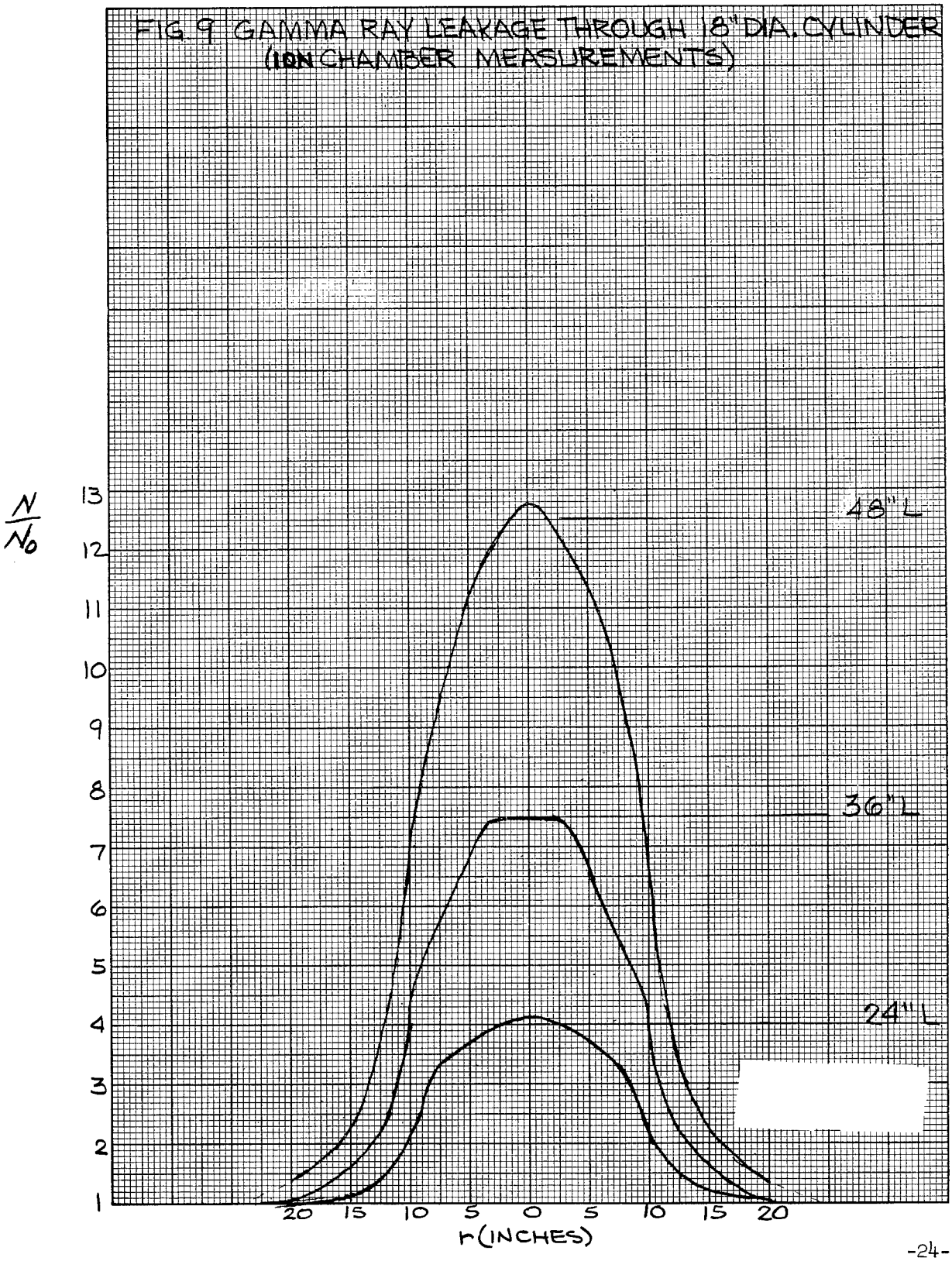

FIG 10 GAMMA RAY LEAKAGE THROUGH 12" DIA. CYLINDER
(ION CHAMBER MEASUREMENTS)

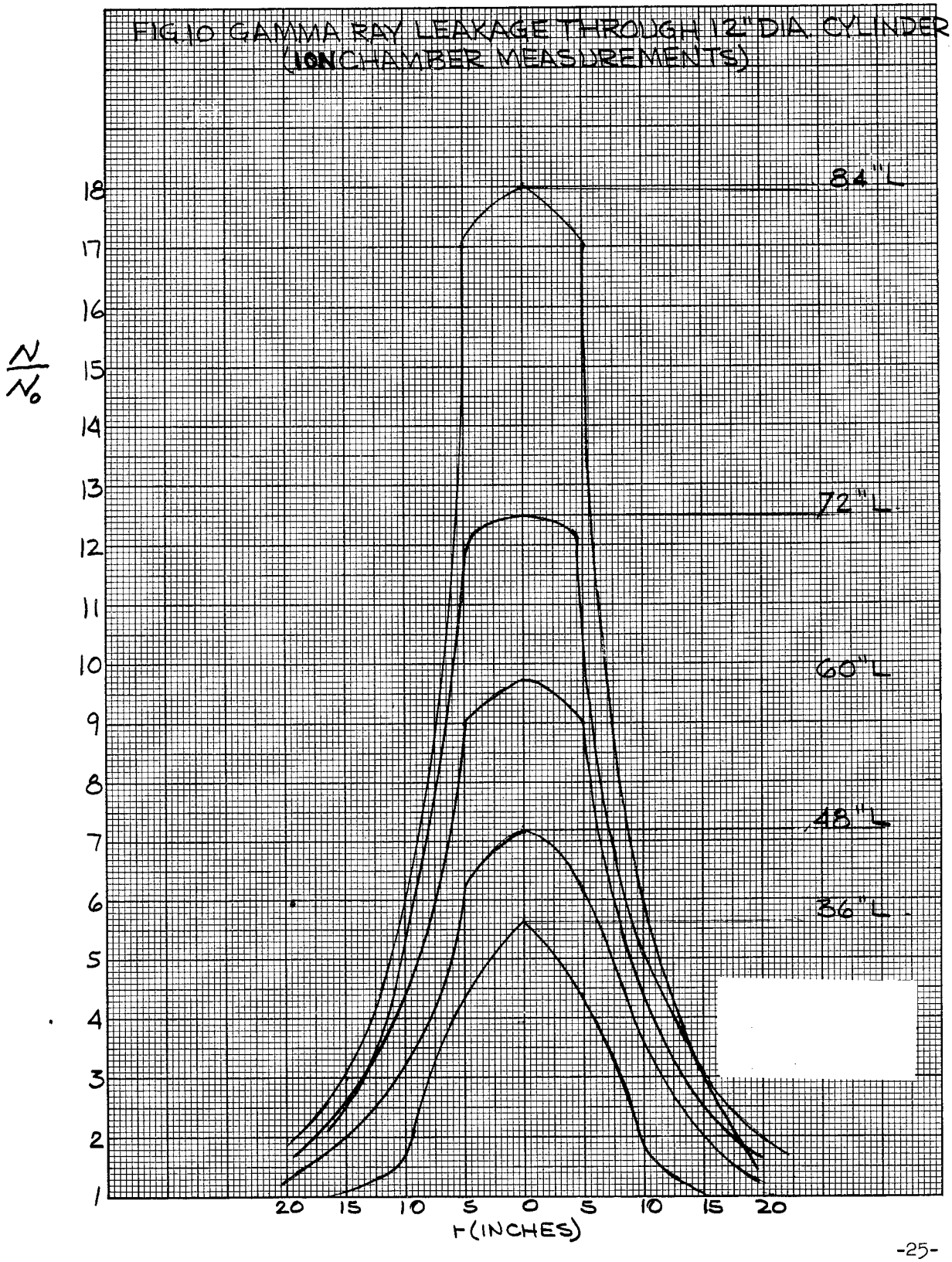

FIG. 11 GAMMA RAY LEAKAGE THROUGH 8" DIA. CYLINDER (CHAMBER MEASUREMENTS)

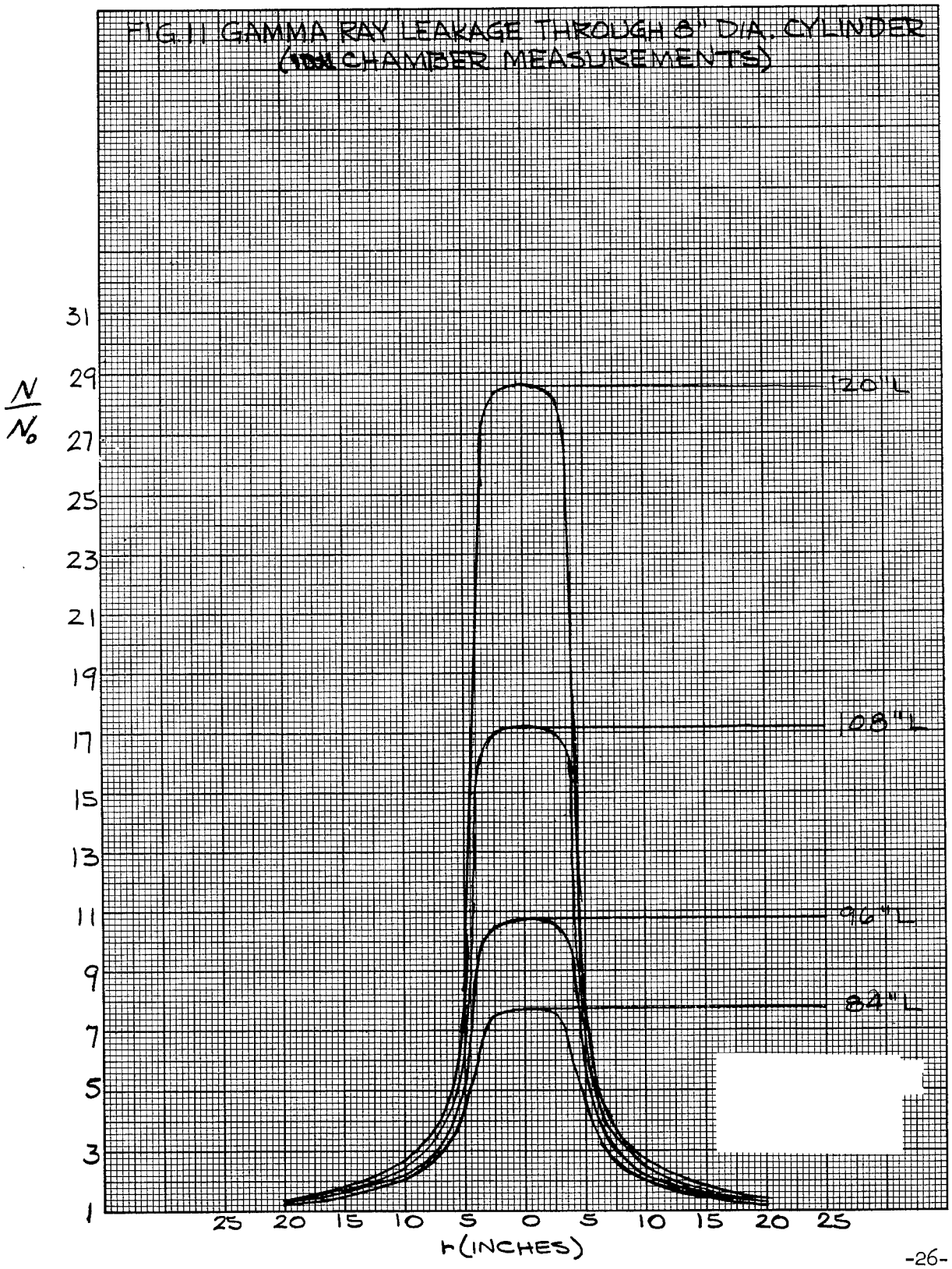

FIG. 12 GAMMA RAY LEAKAGE THROUGH 8" DIA. CYLINDER
(ION CHAMBER MEASUREMENTS)

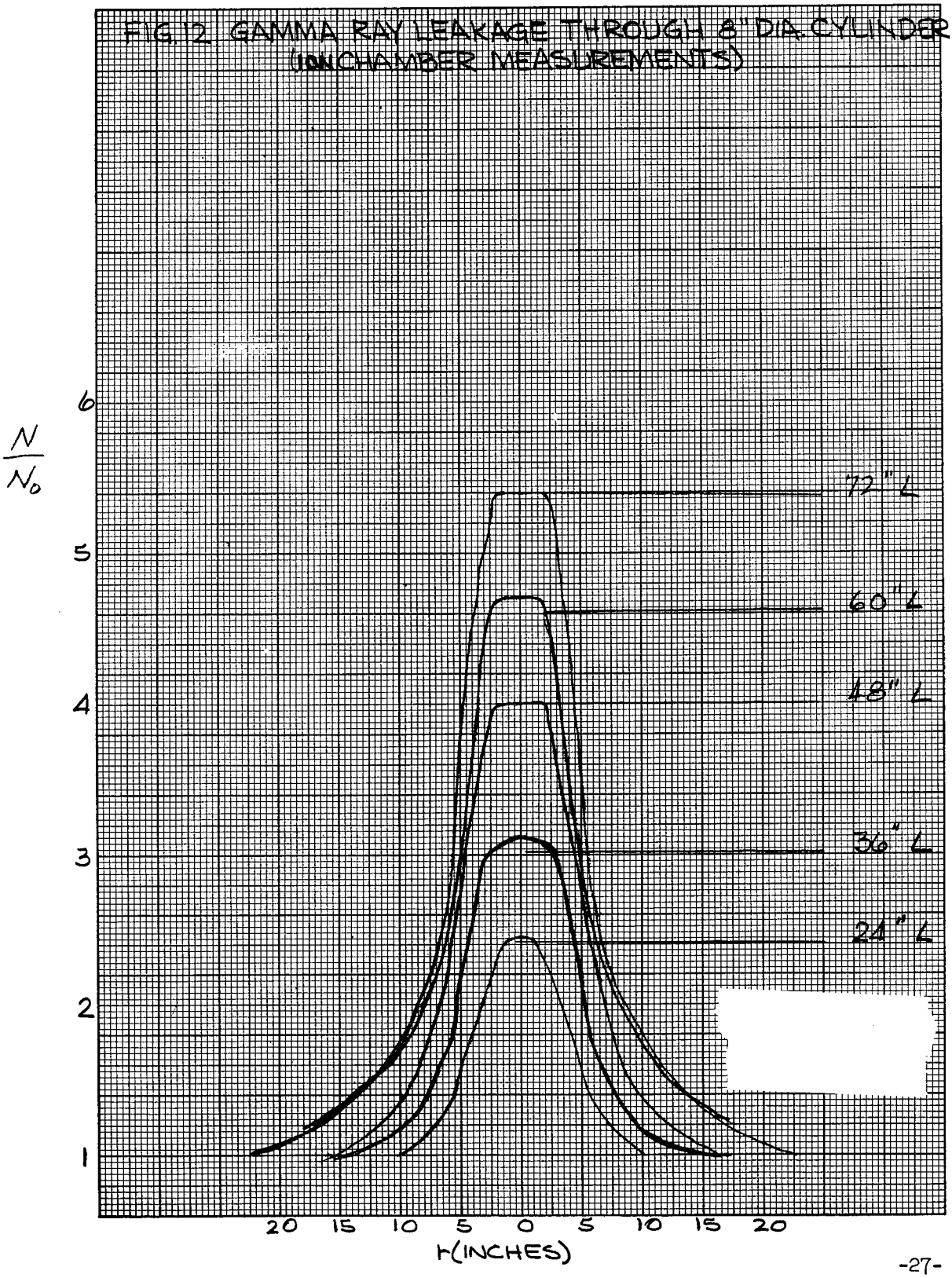

FIG. 13 GAMMA RAY LEAKAGE THROUGH 6" DIA. CYLINDER
(IN CHAMBER MEASUREMENTS)

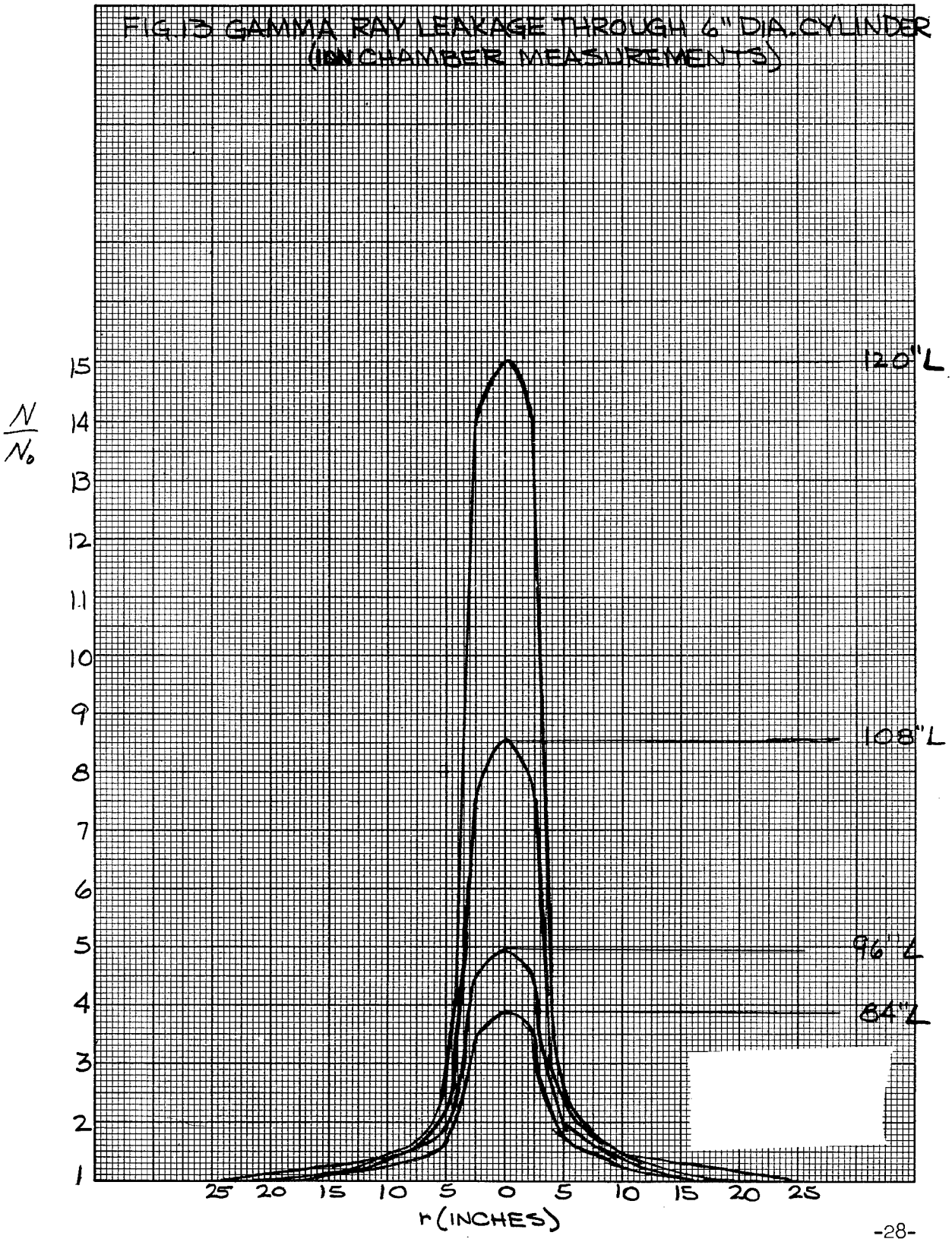

FIG. 4 GAMMA RAY LEAKAGE THROUGH 6" DIA. CYLINDER
(ION CHAMBER MEASUREMENTS)

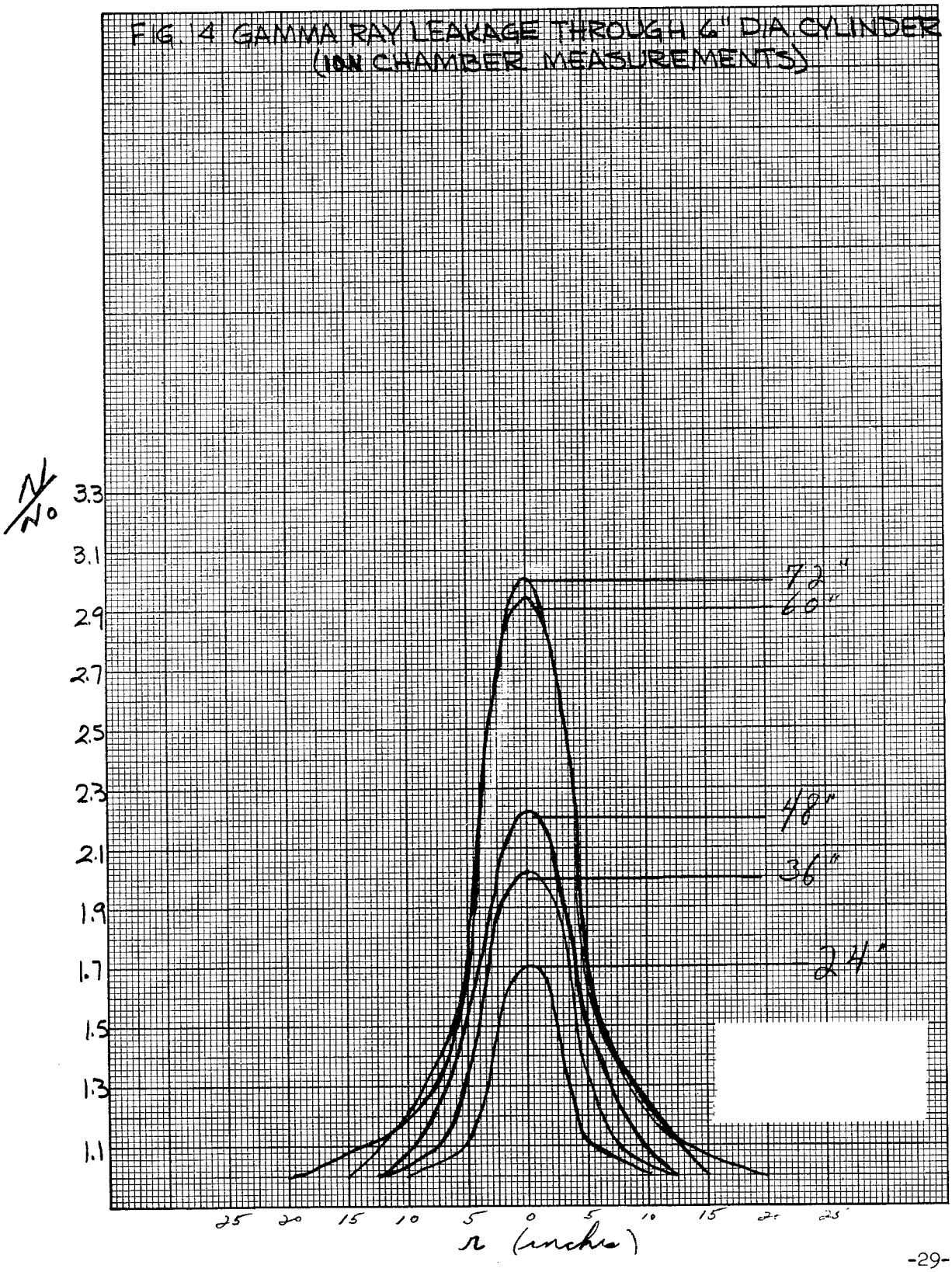

FIG 15 GAMMA RAY LEAKAGE THROUGH 4" DIA. CYLINDER
(ION CHAMBER MEASUREMENTS)

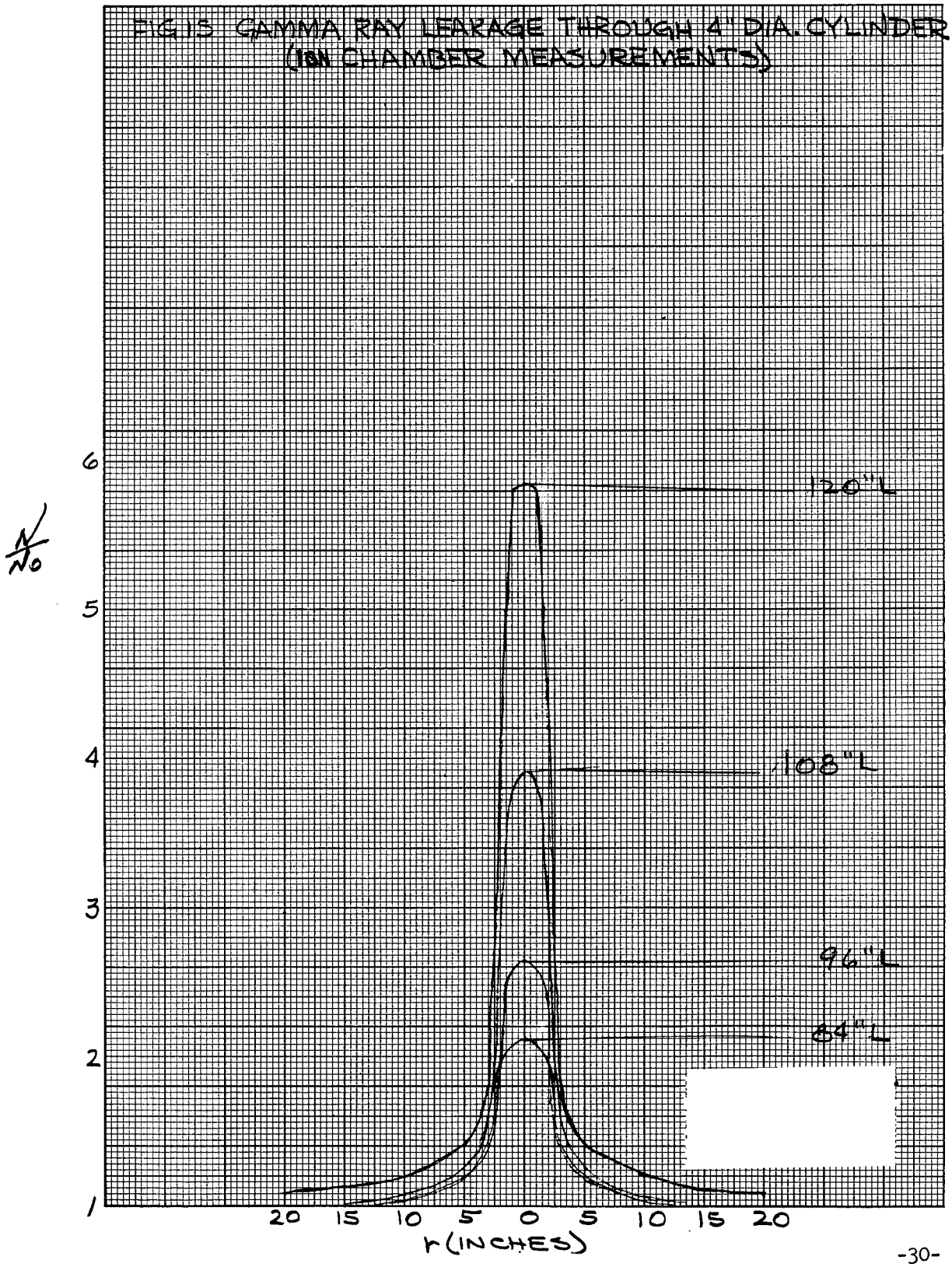

FIG 16 GAMMA RAY LEAKAGE THROUGH 4" DIA. CYLINDER

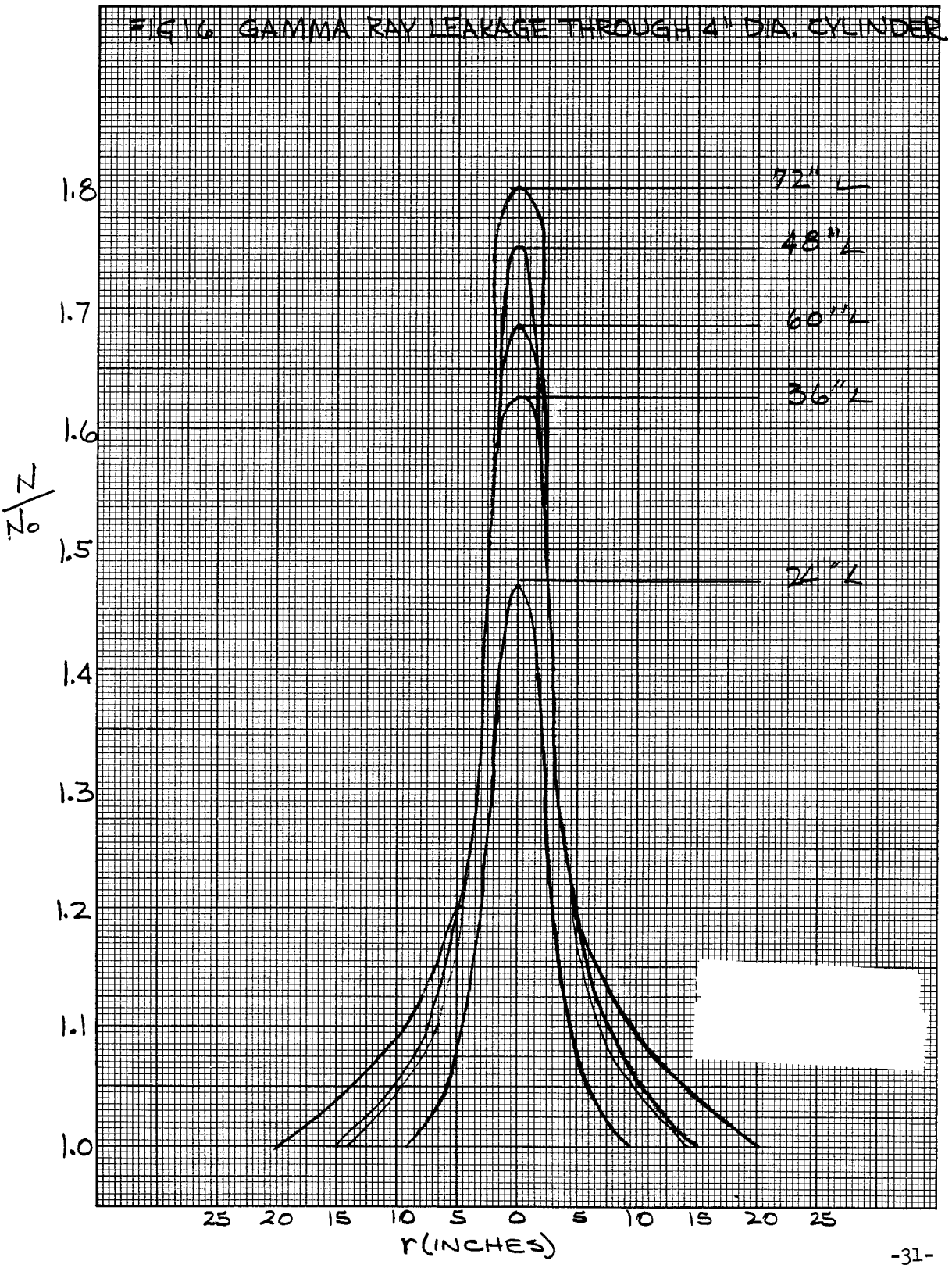

FIG. 17 GAMMA RAY LEAKAGE THROUGH 2' DIA. CYLINDER
(CHAMBER MEASUREMENTS)

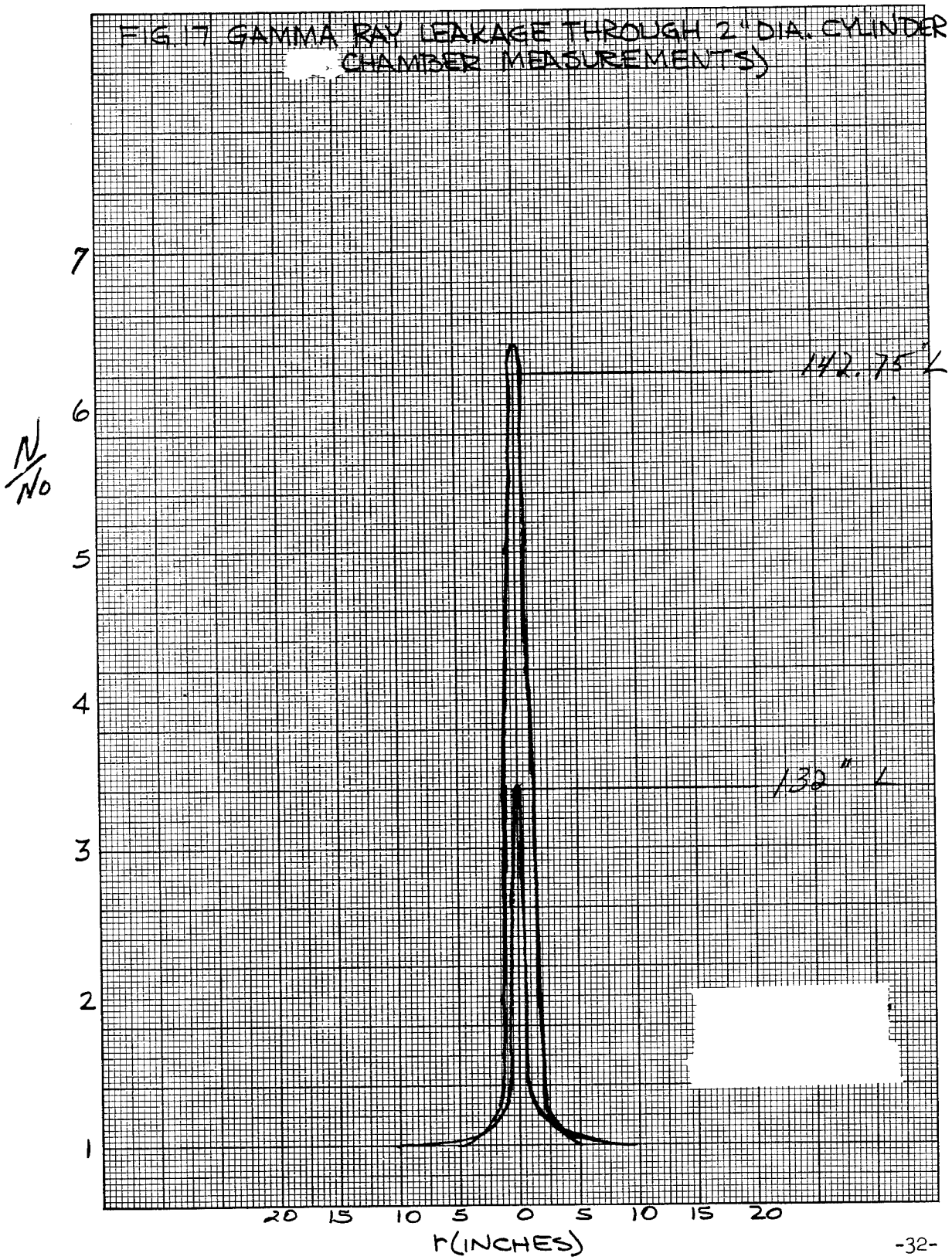

FIG. 18 GAMMA RAY LEAKAGE THROUGH 2" DIA. CYLINDER
(IN CHAMBER MEASUREMENTS)

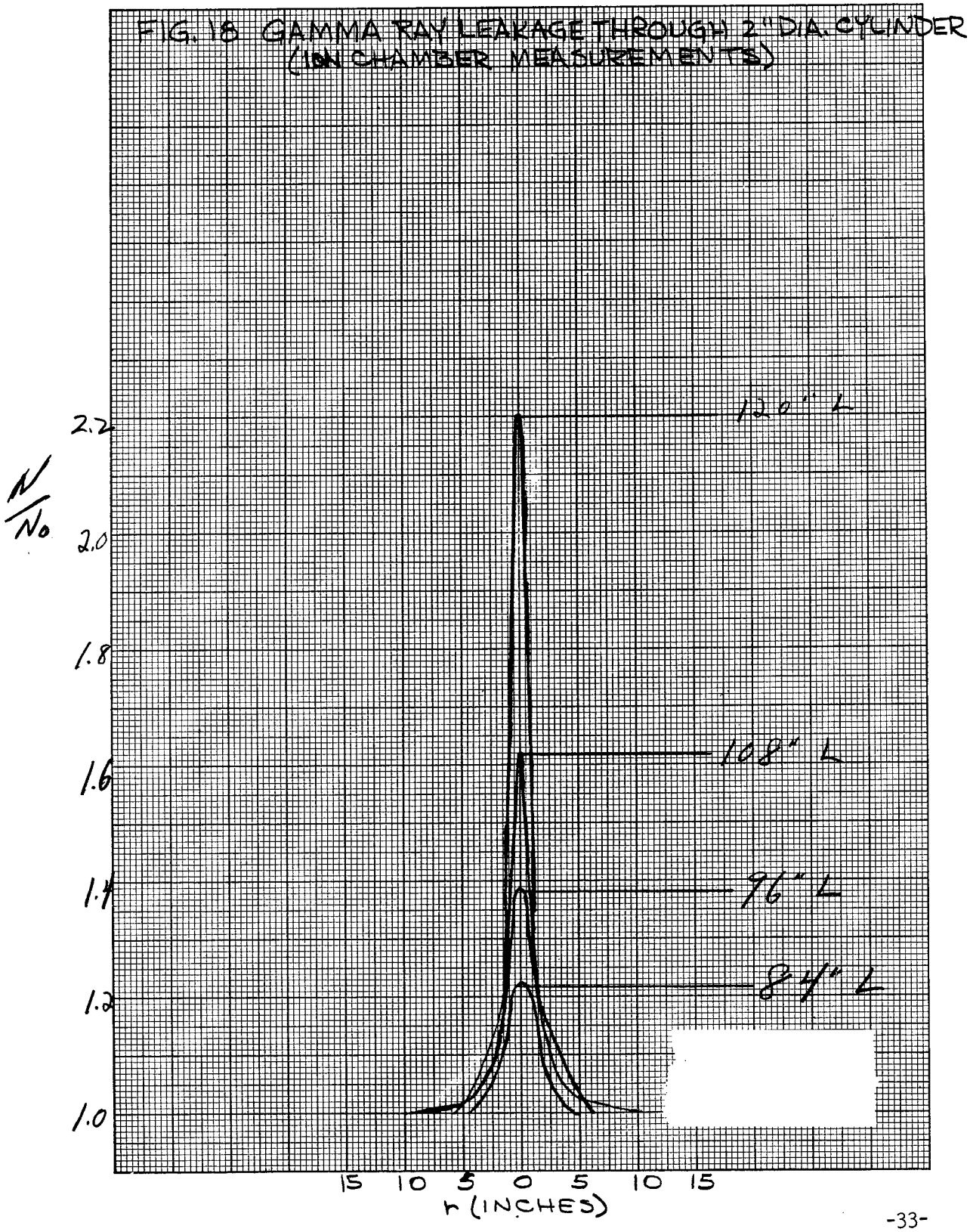

FIG. 19 GAMMA RAY LEAKAGE THROUGH 18" DIA. CYLINDER
(GM COUNTER MEASUREMENTS)

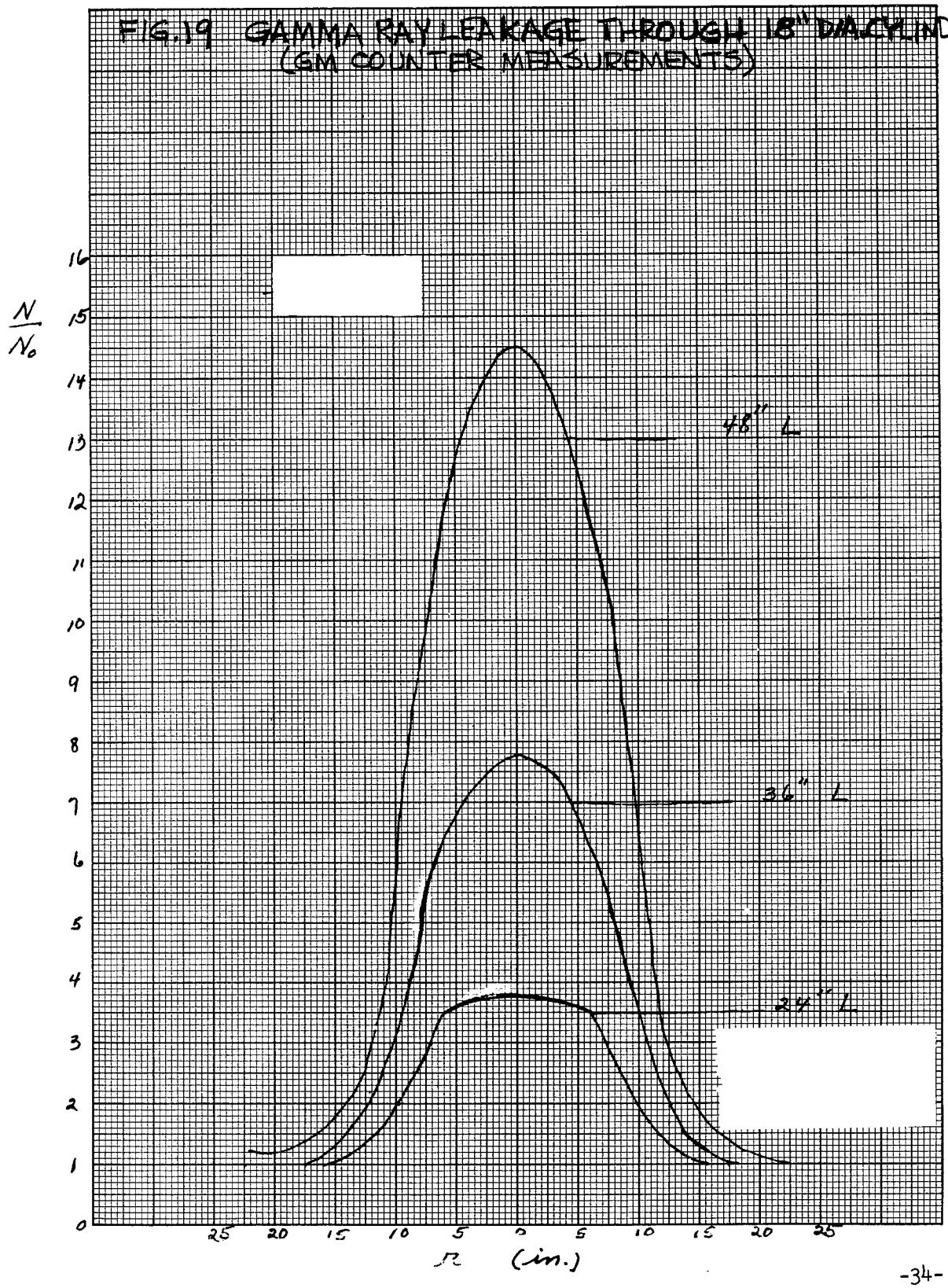

FIG 20 GAMMA RAY LEAKAGE THROUGH 12" DIA. CYLINDER
(GM COUNTER MEASUREMENTS)

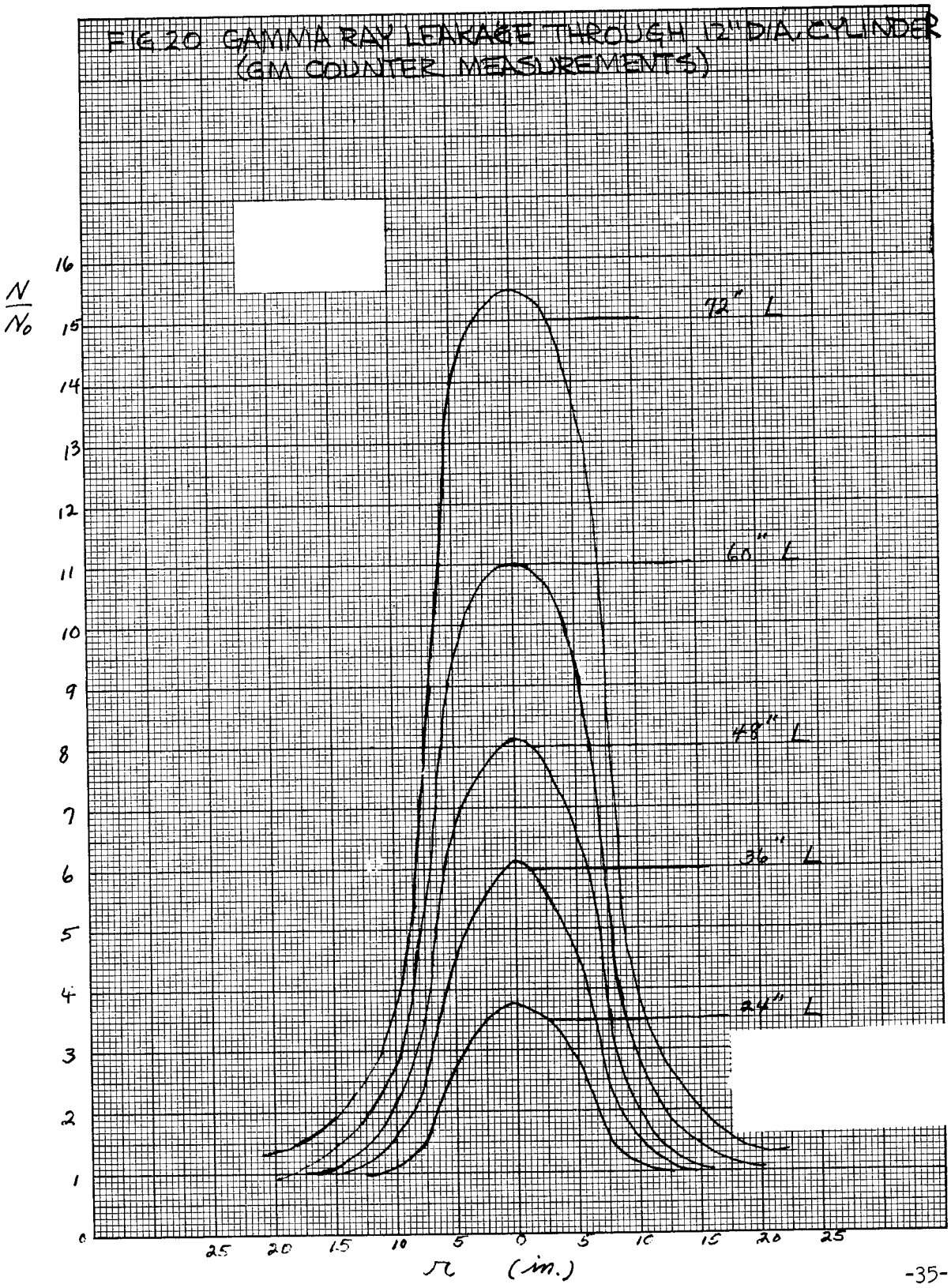

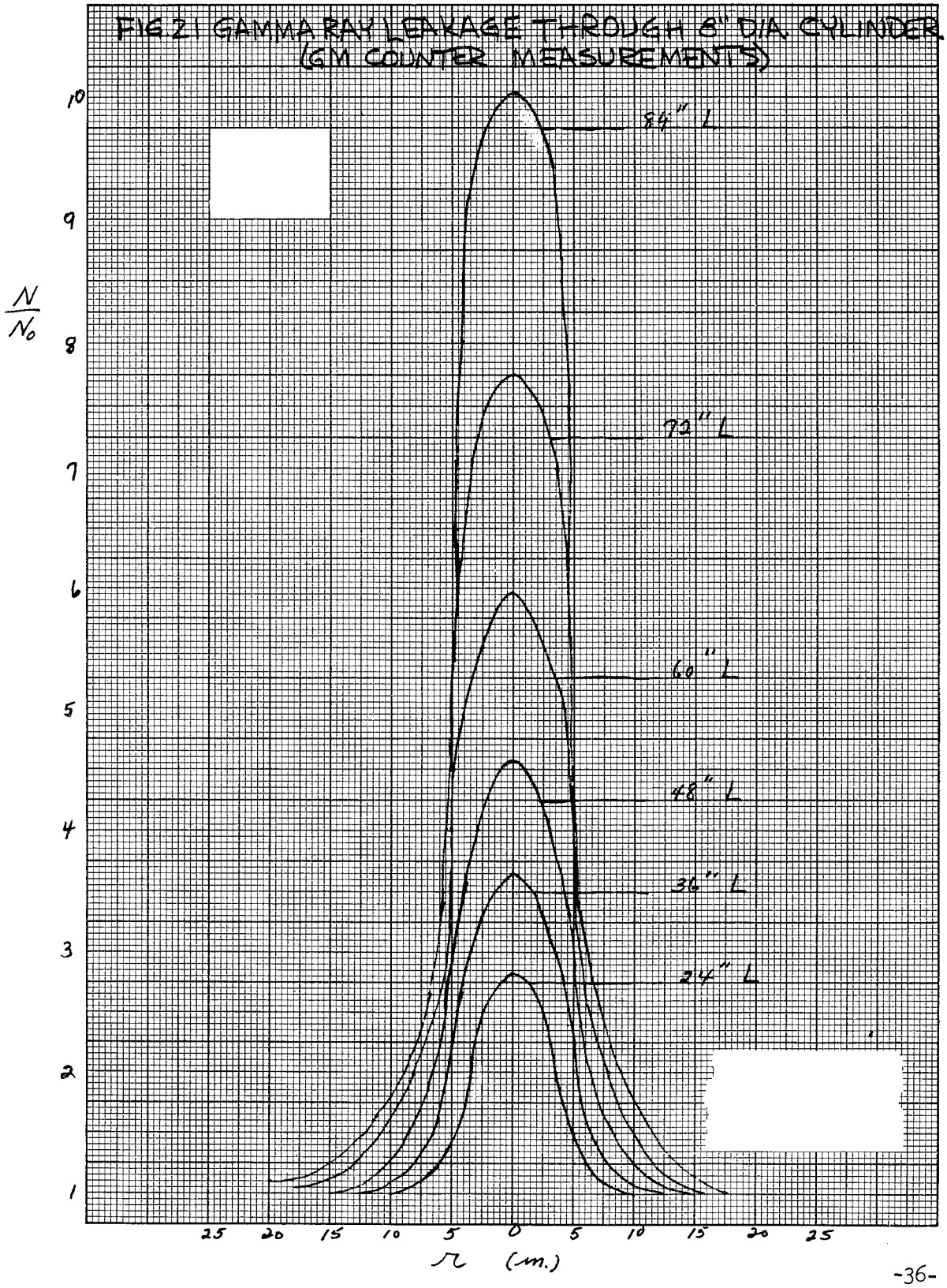
FIG 21 GAMMA RAY LEAKAGE THROUGH 8" DIA CYLINDER
(GM COUNTER MEASUREMENTS)
84" L
72" L
60" L
48" L
36" L
24" L
N/N0
10
9
8
7
6
5
4
3
2
1
25 20 15 10 5 0 5 10 15 20 25
r (in.)

FIG 22 GAMMA RAY LEAKAGE THROUGH 6" DIA. CYLINDER
(GM COUNTER MEASUREMENTS)

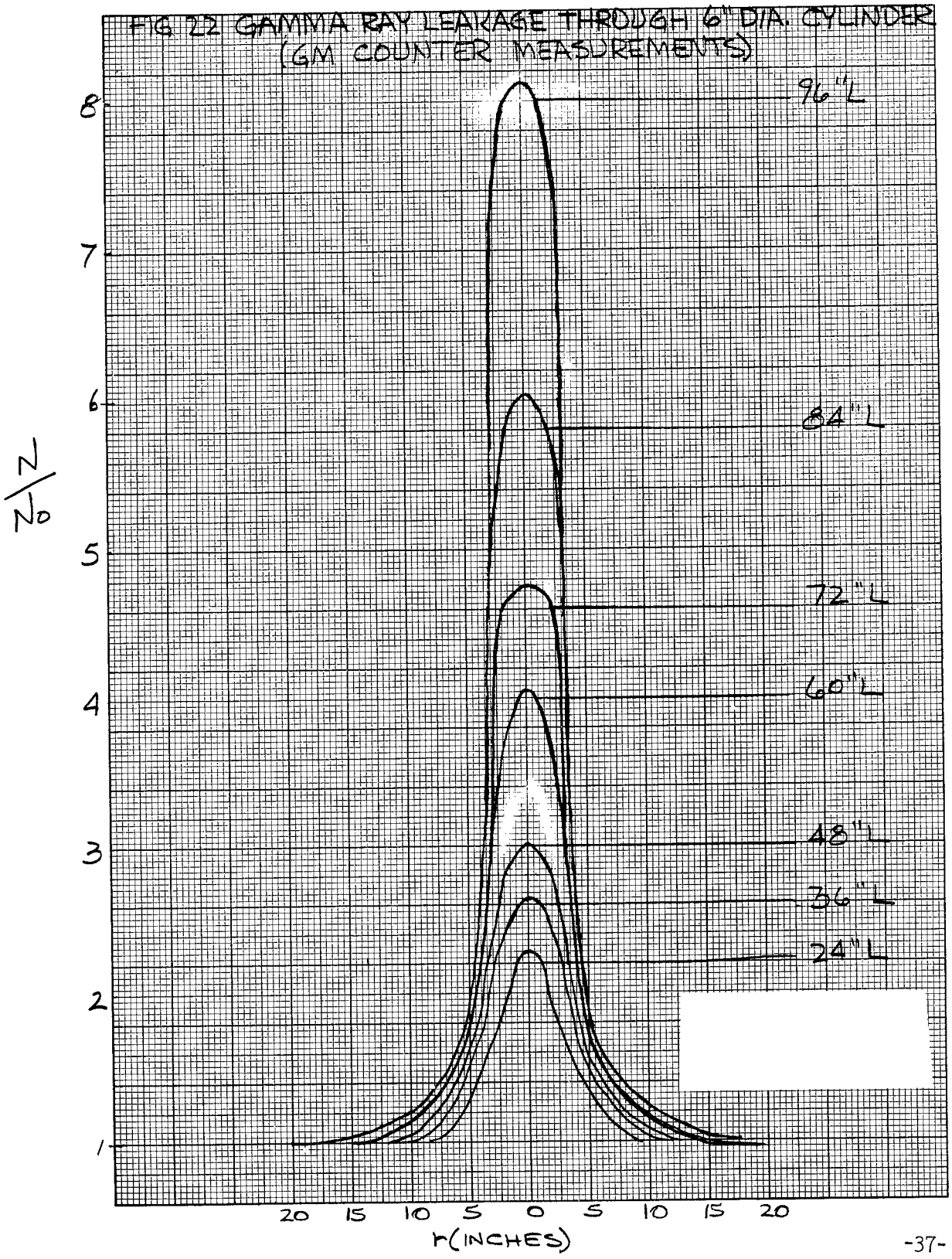

FIG. 23 GAMMA RAY LEAKAGE THROUGH 4" DIA. CYLINDER (GM COUNTER MEASUREMENTS)

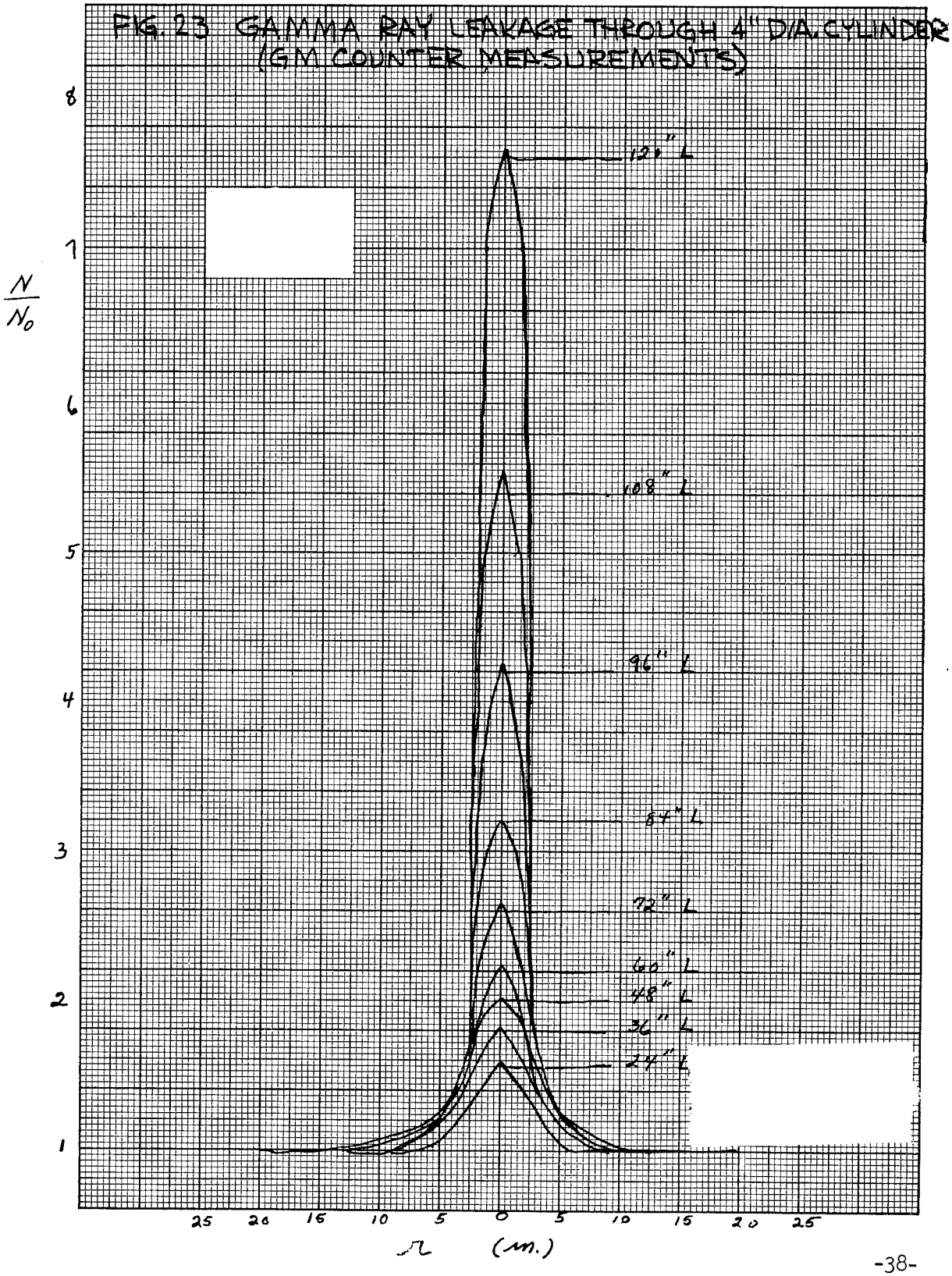

FIG. 24 GAMMA RAY LEAKAGE THROUGH 2" DIA. CYLINDER (GM COUNTER MEASUREMENTS)

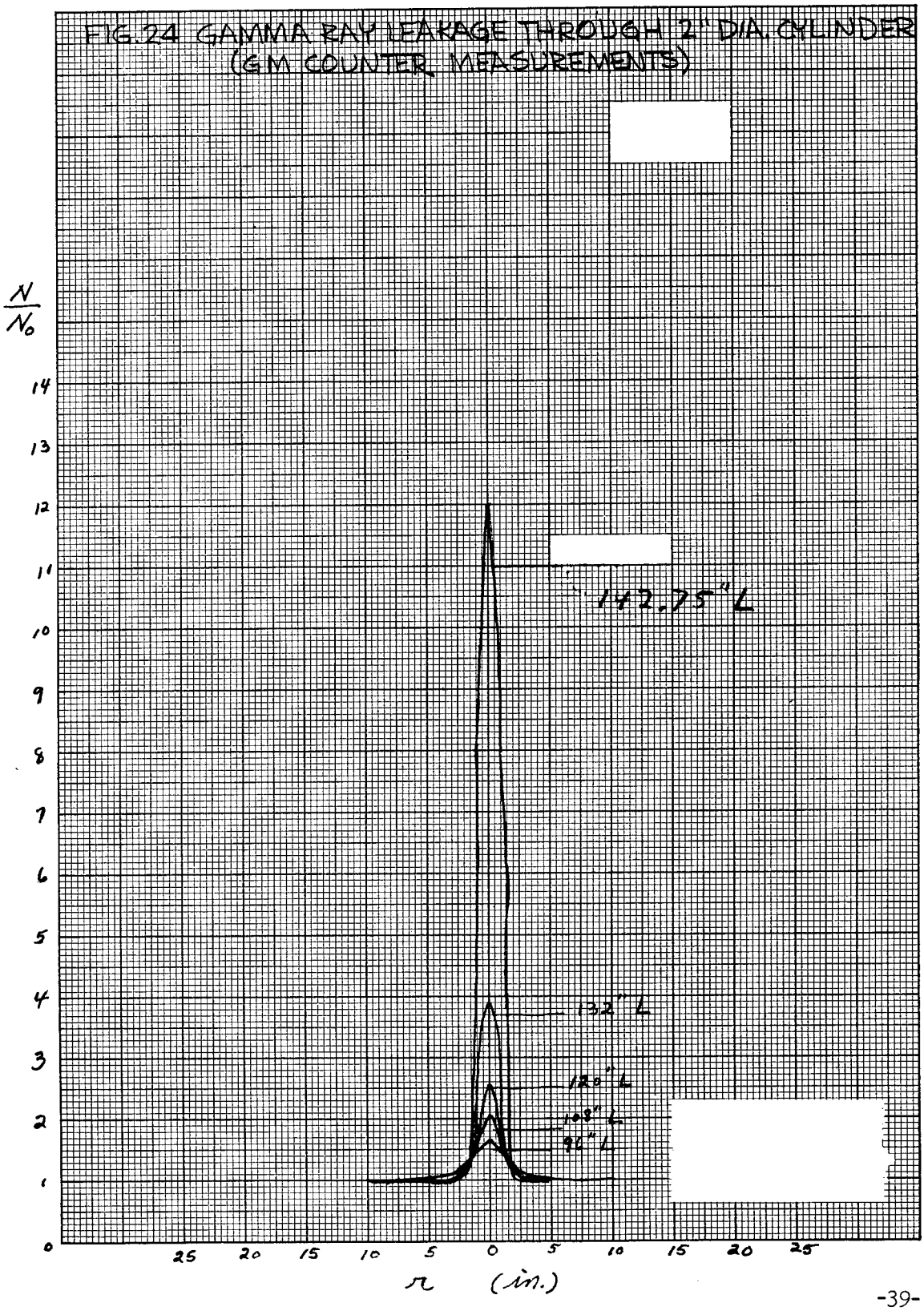

FIG 2.5 GAMMA RAY LEAKAGE THROUGH 2" DIA. CYLINDER
(GM COUNTER MEASUREMENTS)

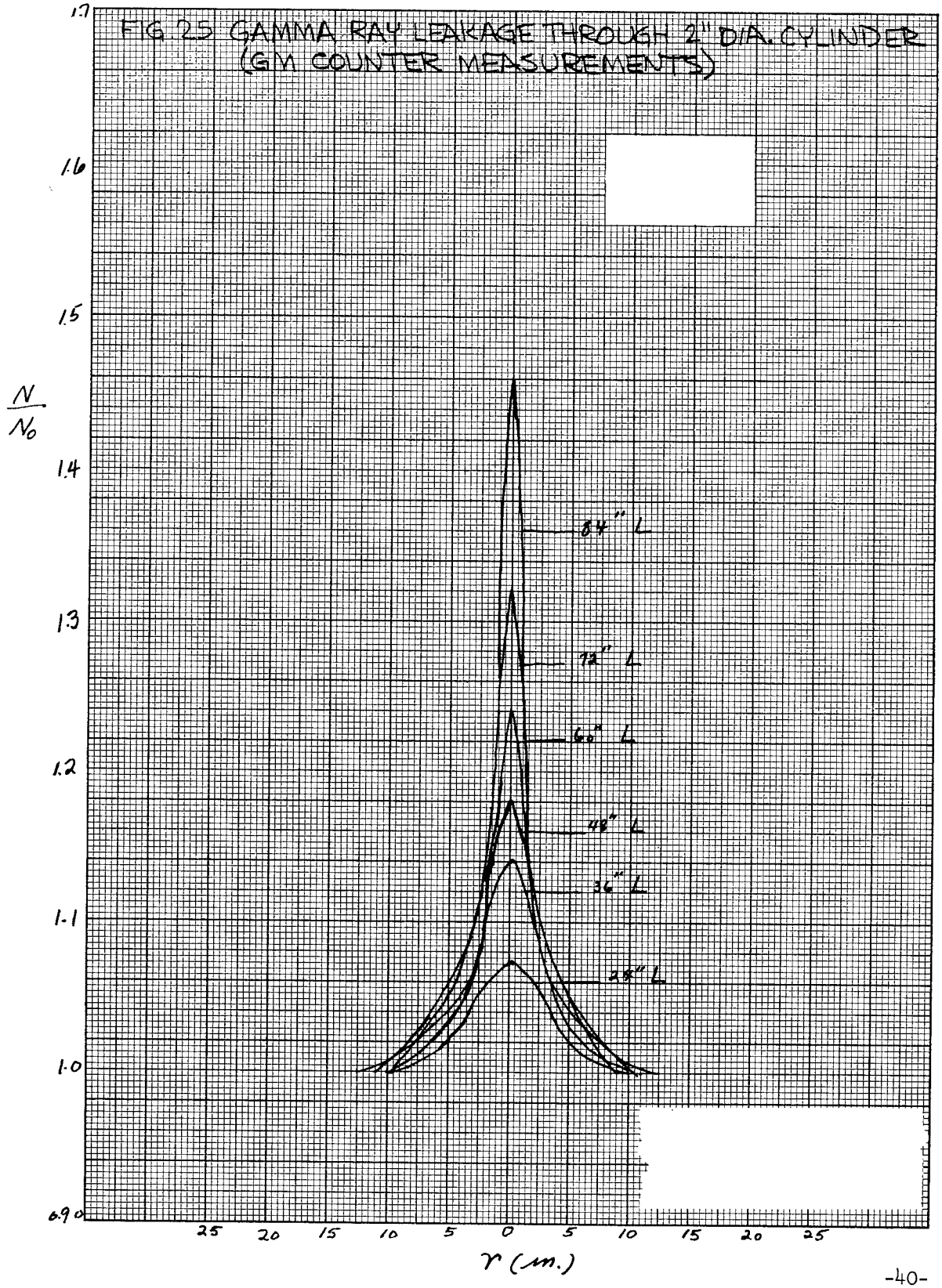

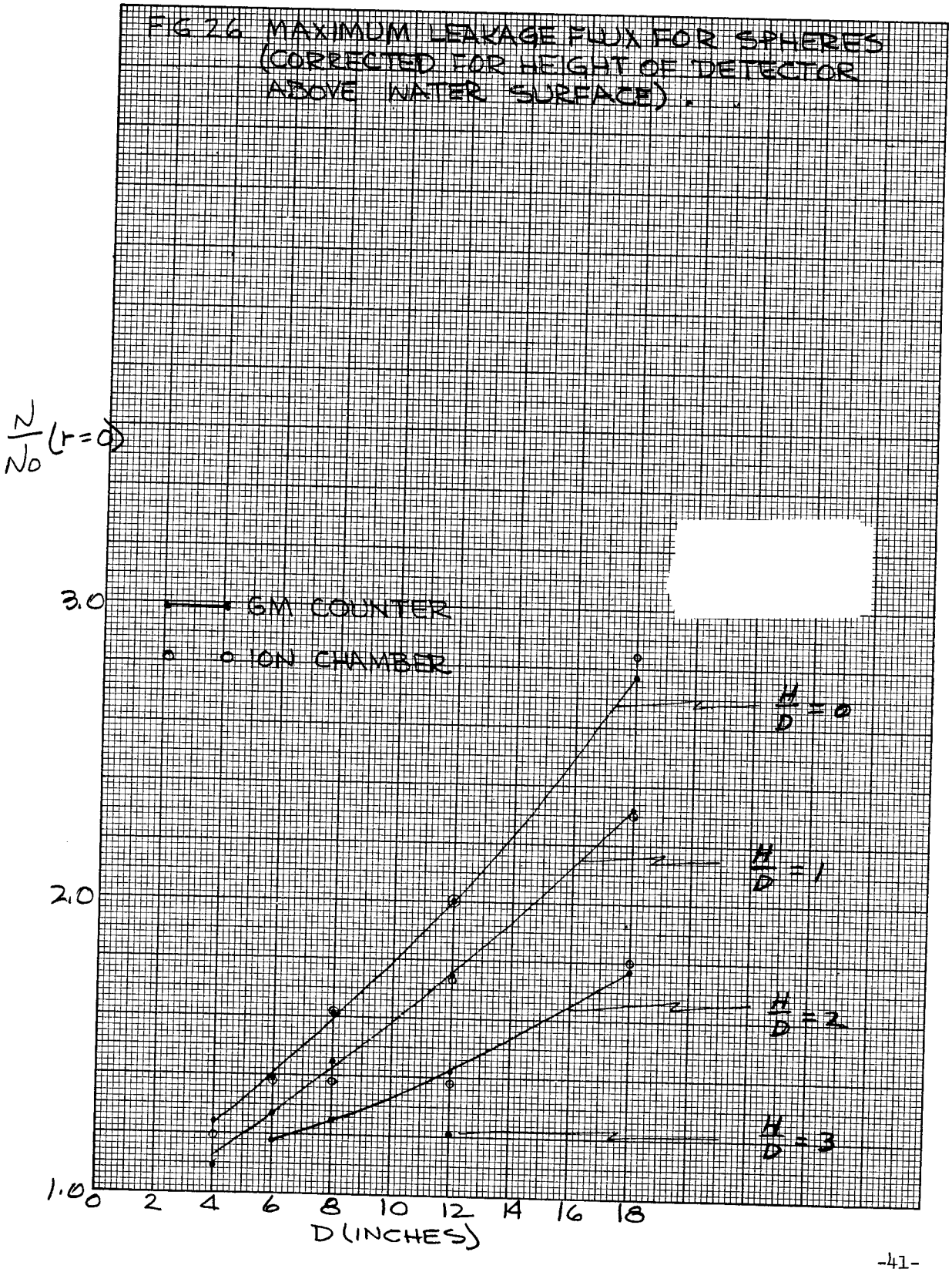
FIG 26 MAXIMUM LEAKAGE FLUX FOR SPHERES (CORRECTED FOR HEIGHT OF DETECTOR ABOVE WATER SURFACE).
N/No (r=0)
3.0
2.0
1.0
GM COUNTER
ION CHAMBER
H/D = 0
H/D = 1
H/D = 2
H/D = 3
0 2 4 6 8 10 12 14 16 18
D (INCHES)

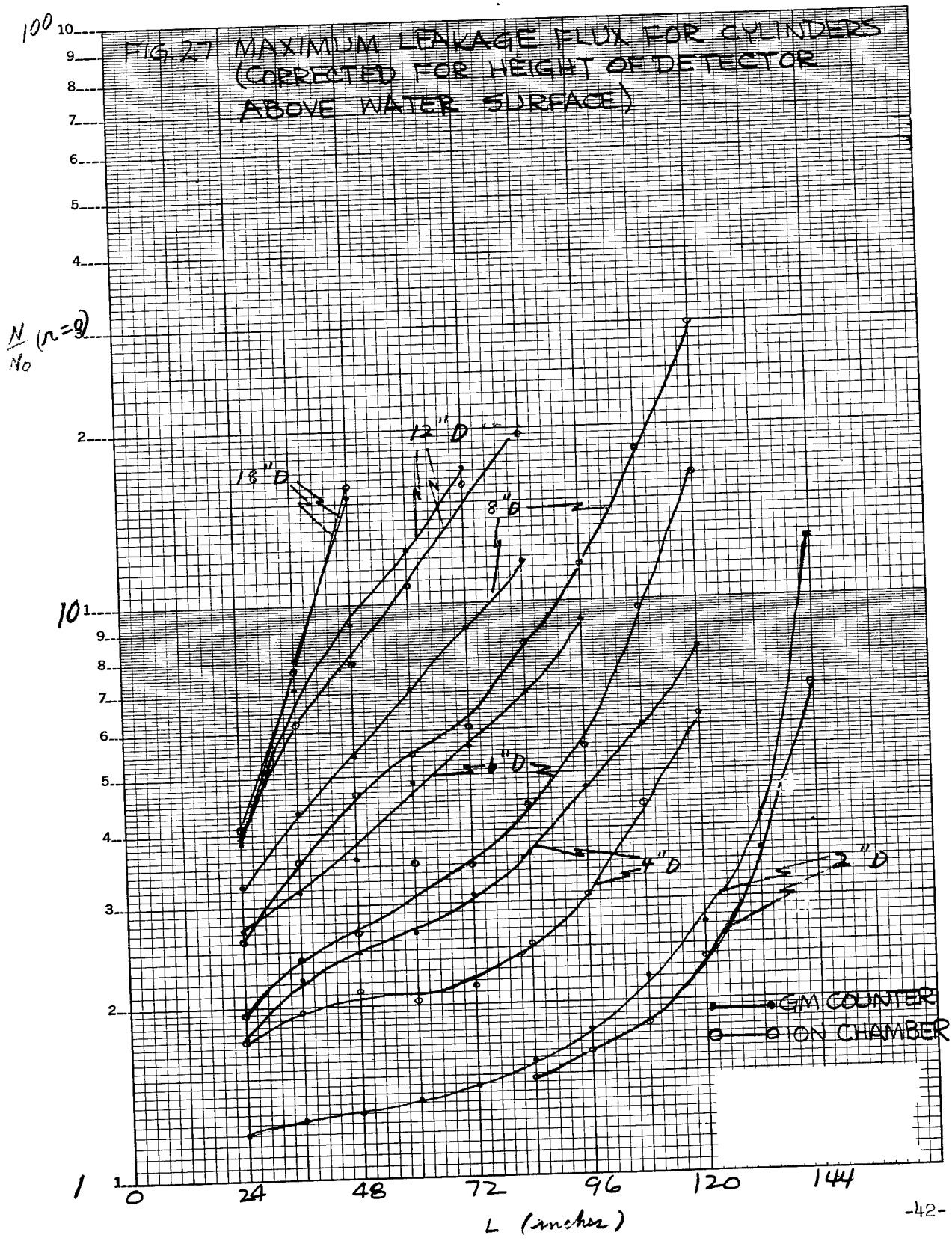
FIG. 27 MAXIMUM LEAKAGE FLUX FOR CYLINDERS (CORRECTED FOR HEIGHT OF DETECTOR ABOVE WATER SURFACE)
100
10
1
N/No (n=0)
18"D
12"D
8"D
6"D
4"D
2"D
GM COUNTER
ION CHAMBER
0
24
48
72
96
120
144
L (inches)

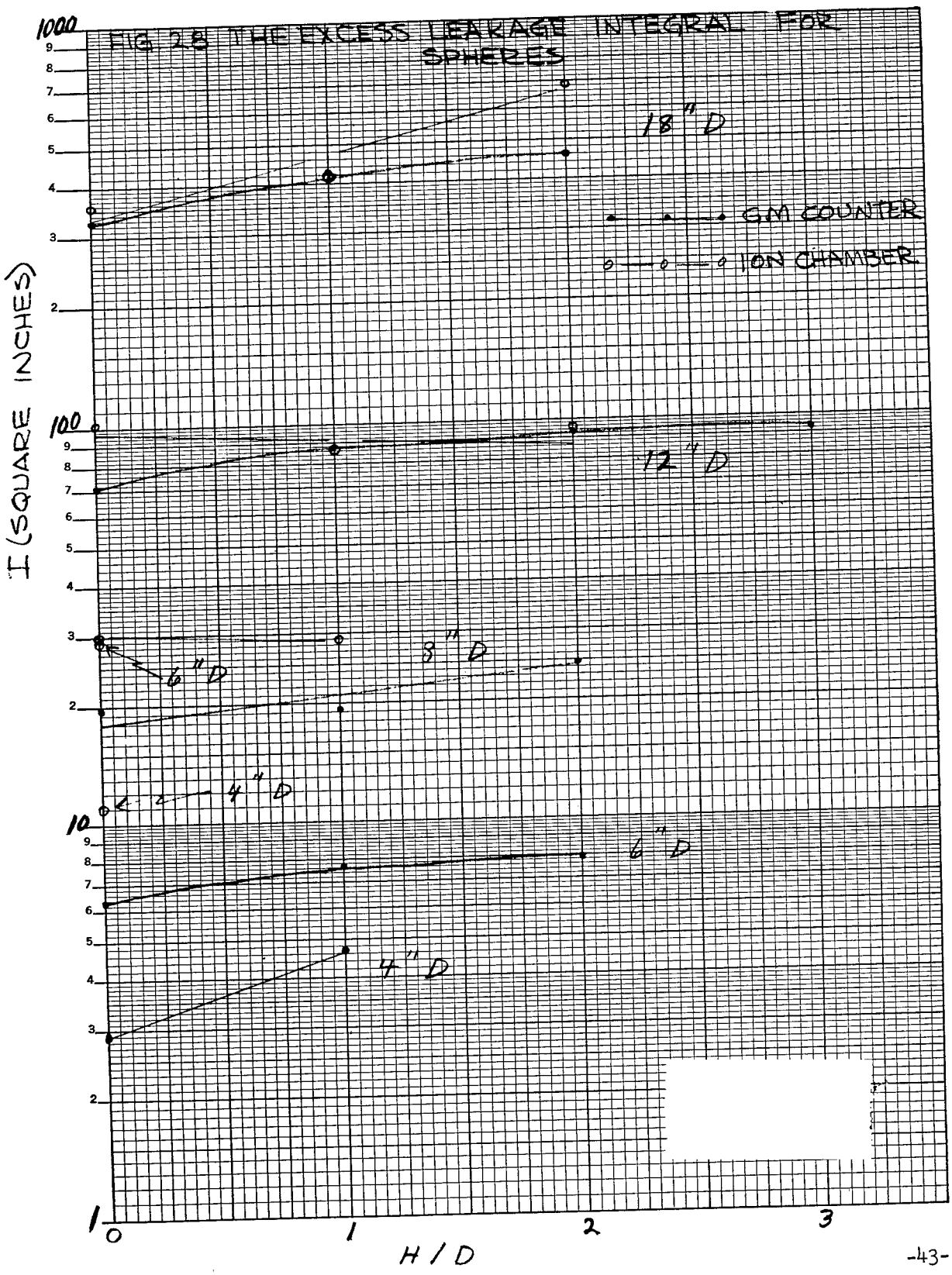
FIG. 28 THE EXCESS LEAKAGE INTEGRAL FOR SPHERES
18" D
GM COUNTER
ION CHAMBER
12" D
8" D
6" D
4" D
6" D
4" D
H (SQUARE INCHES)
H / D
1000
100
10
1
0
1
2
3

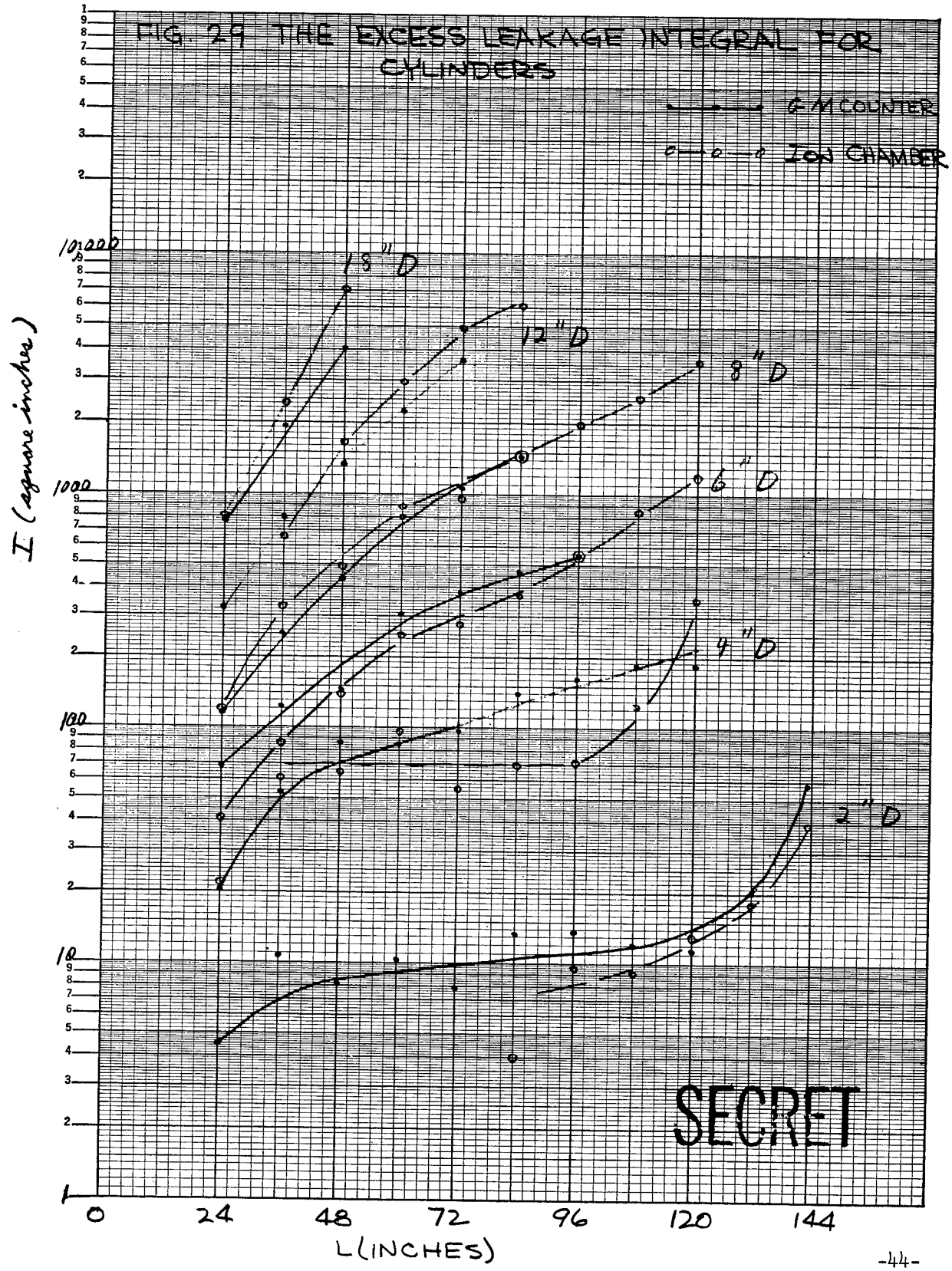
FIG. 29 THE EXCESS LEAKAGE INTEGRAL FOR CYLINDERS
G-M COUNTER
ION CHAMBER
15" D
12" D
8" D
6" D
4" D
2" D
I (square inches)
L (INCHES)
0
24
48
72
96
120
144
SECRET

MODEL

DATE

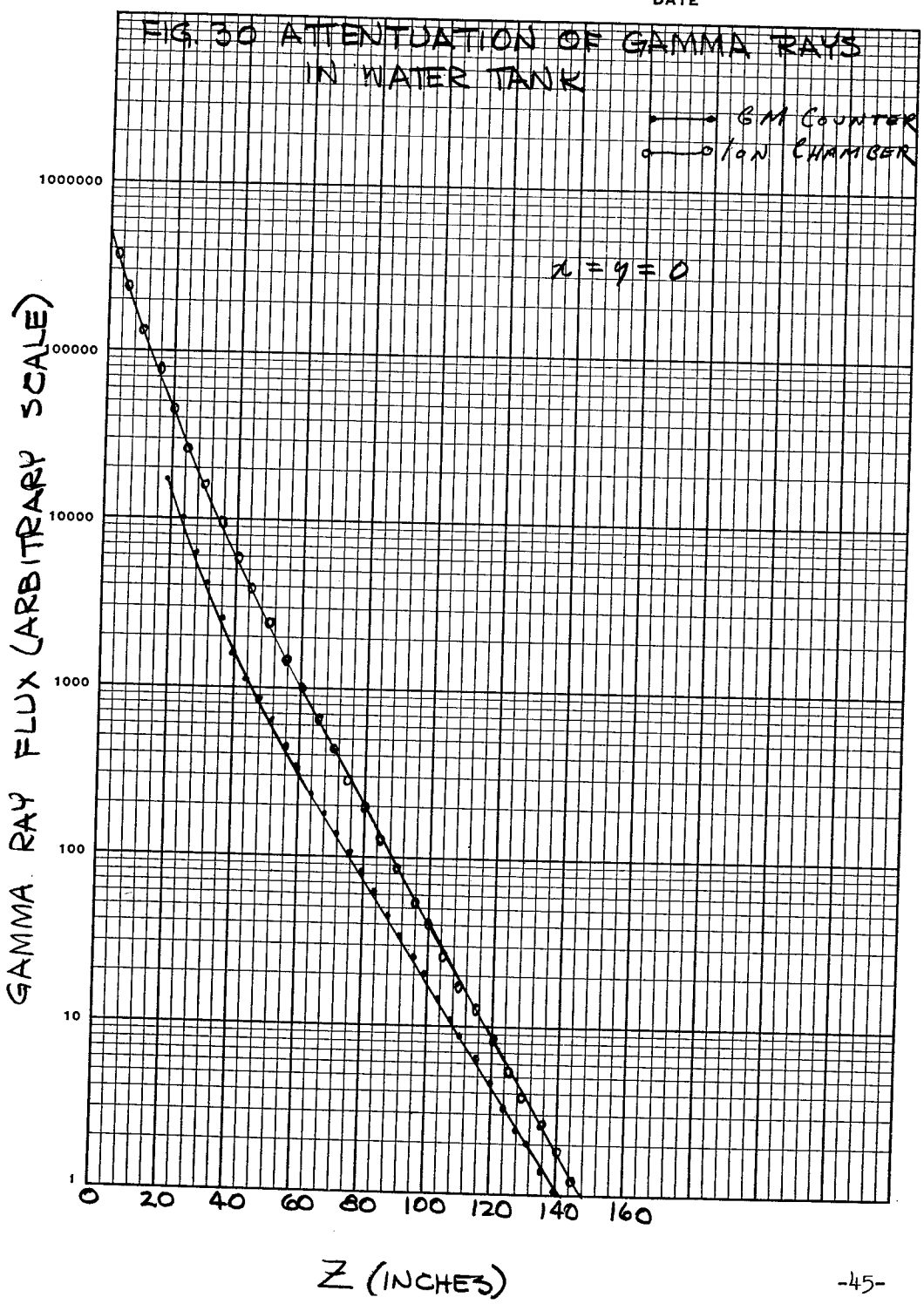
FIG. 30 ATTENTUATION OF GAMMA RAYS IN WATER TANK
GM COUNTER
ION CHAMBER
x = y = 0
GAMMA RAY FLUX (ARBITRARY SCALE)
1000000
100000
10000
1000
100
10
1
0
20
40
60
80
100
120
140
160
Z (INCHES)

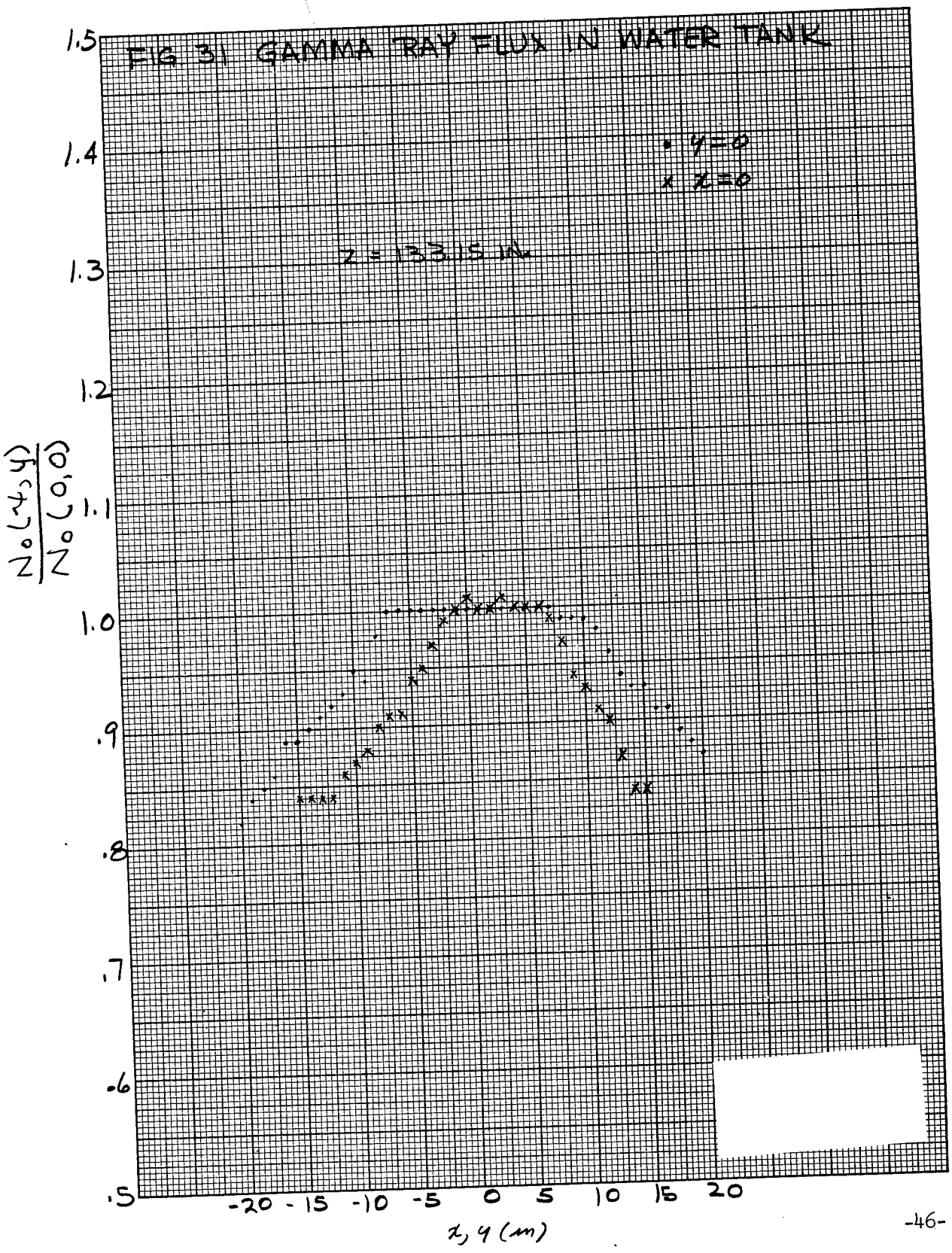
FIG. 31 GAMMA RAY FLUX IN WATER TANK
• y=0
x z=0
z = 133.15 in.
1.5
1.4
1.3
1.2
1.1
1.0
.9
.8
.7
.6
.5
N°(x,y) / N°(0,0)
-20 -15 -10 -5 0 5 10 15 20
x, y (in)

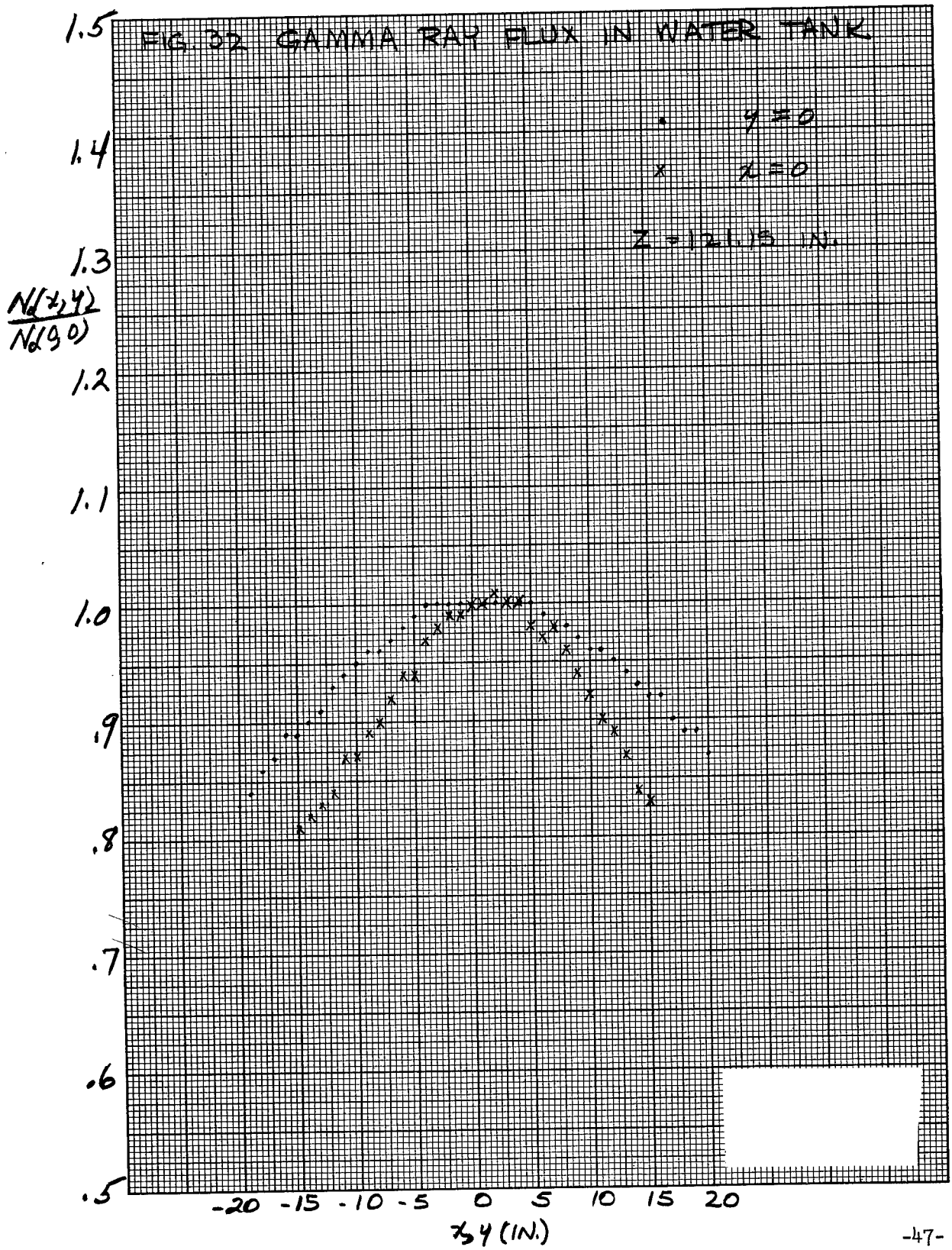
FIG. 32 GAMMA RAY FLUX IN WATER TANK
y = 0
x = 0
Z = 121.15 IN.
N(x,y) / N(0,0)
1.5
1.4
1.3
1.2
1.1
1.0
.9
.8
.7
.6
.5
-20 -15 -10 -5 0 5 10 15 20
x, y (IN.)

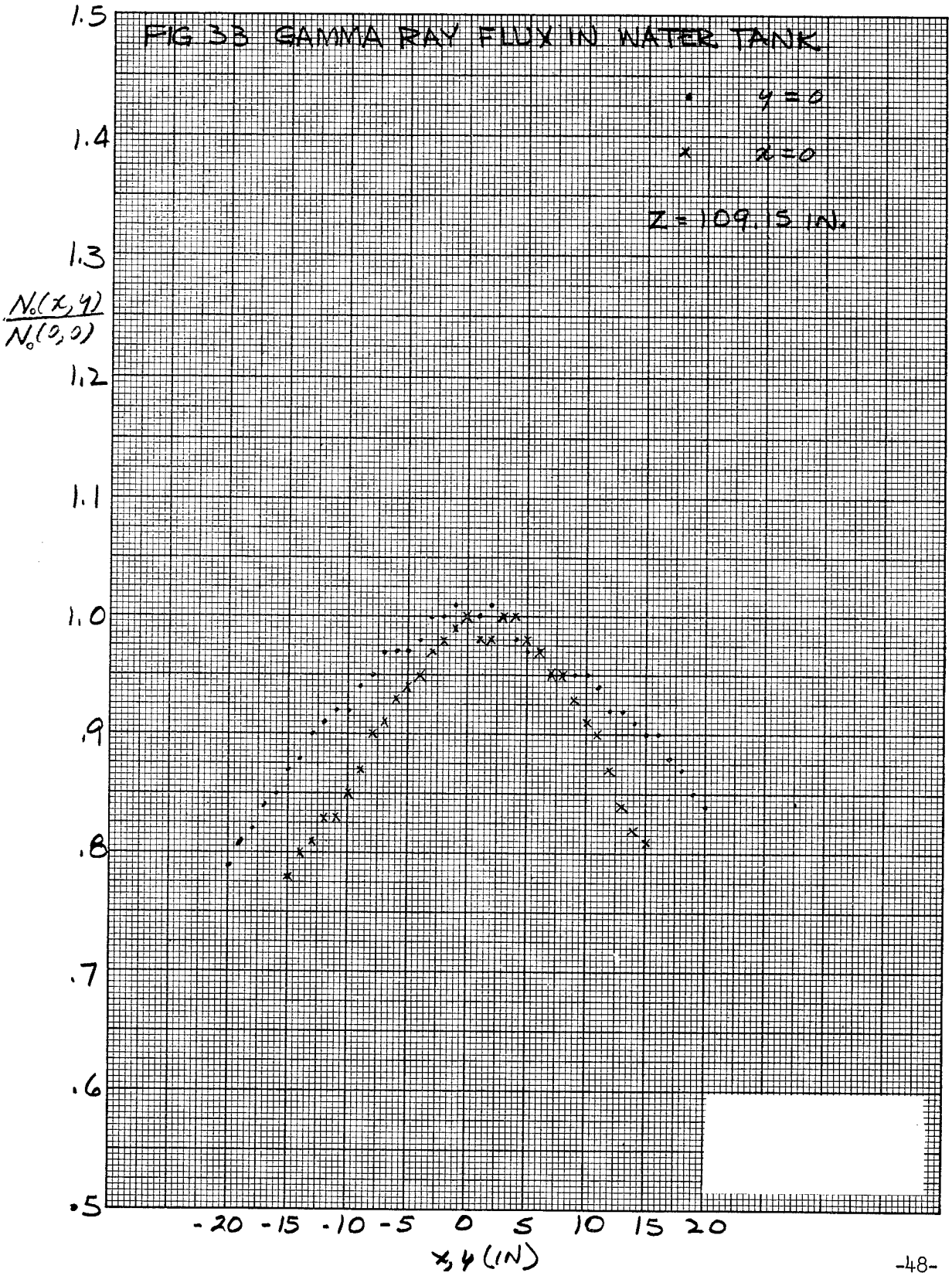
FIG 33 GAMMA RAY FLUX IN WATER TANK
y = 0
x = 0
Z = 109.5 IN.
1.5
1.4
1.3
1.2
1.1
1.0
.9
.8
.7
.6
.5
N₀(x,y) / N₀(0,0)
-20 -15 -10 -5 0 5 10 15 20
x, y (IN)

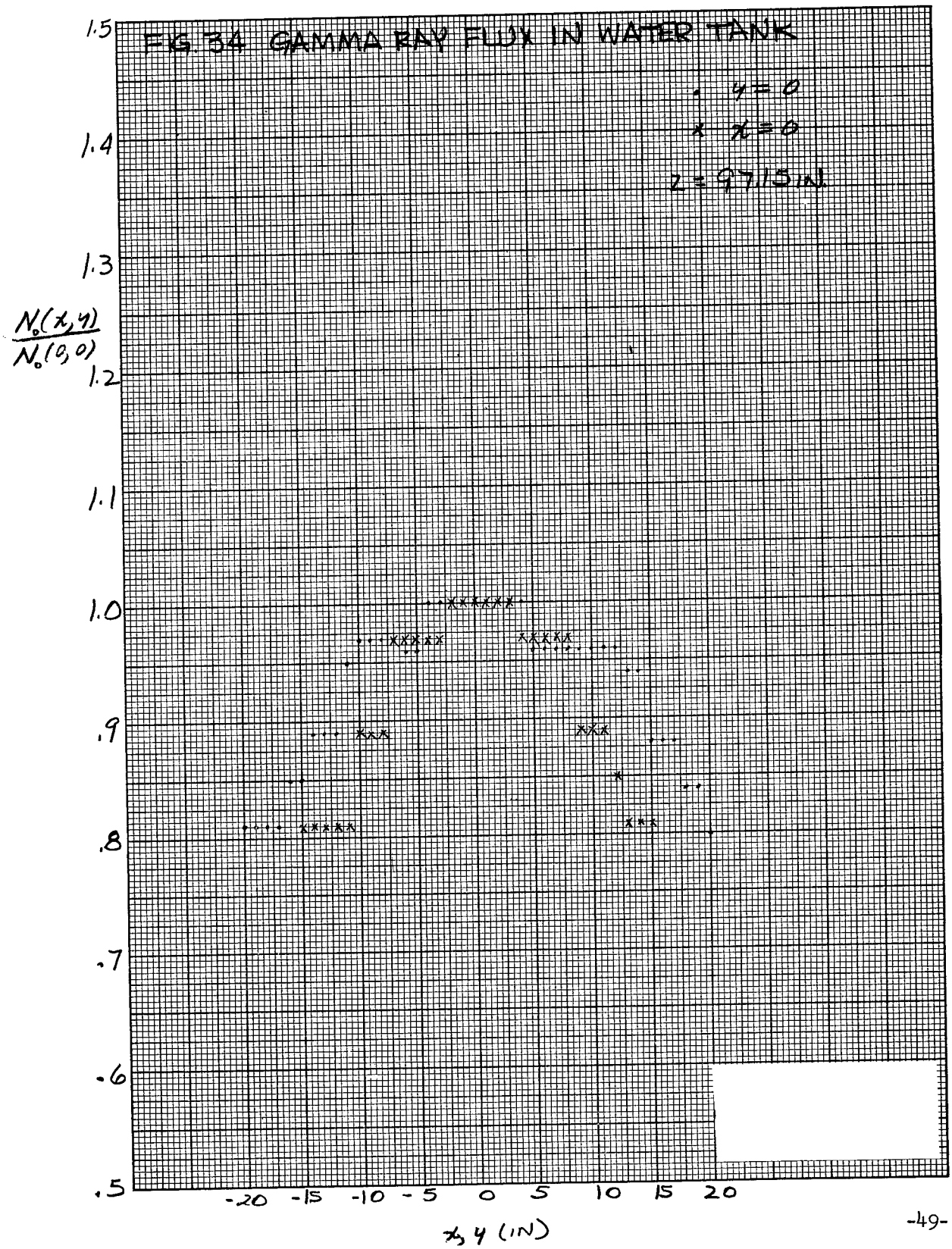
FIG. 34 GAMMA RAY FLUX IN WATER TANK
y = 0
x
x = 0
z = 97.15 IN.
1.5
1.4
1.3
N₀(x,y) / N₀(0,0)
1.2
1.1
1.0
.9
.8
.7
.6
.5
-20 -15 -10 -5 0 5 10 15 20
x, y (IN)

FIG 35 GAMMA RAY FLUX IN WATER TANK

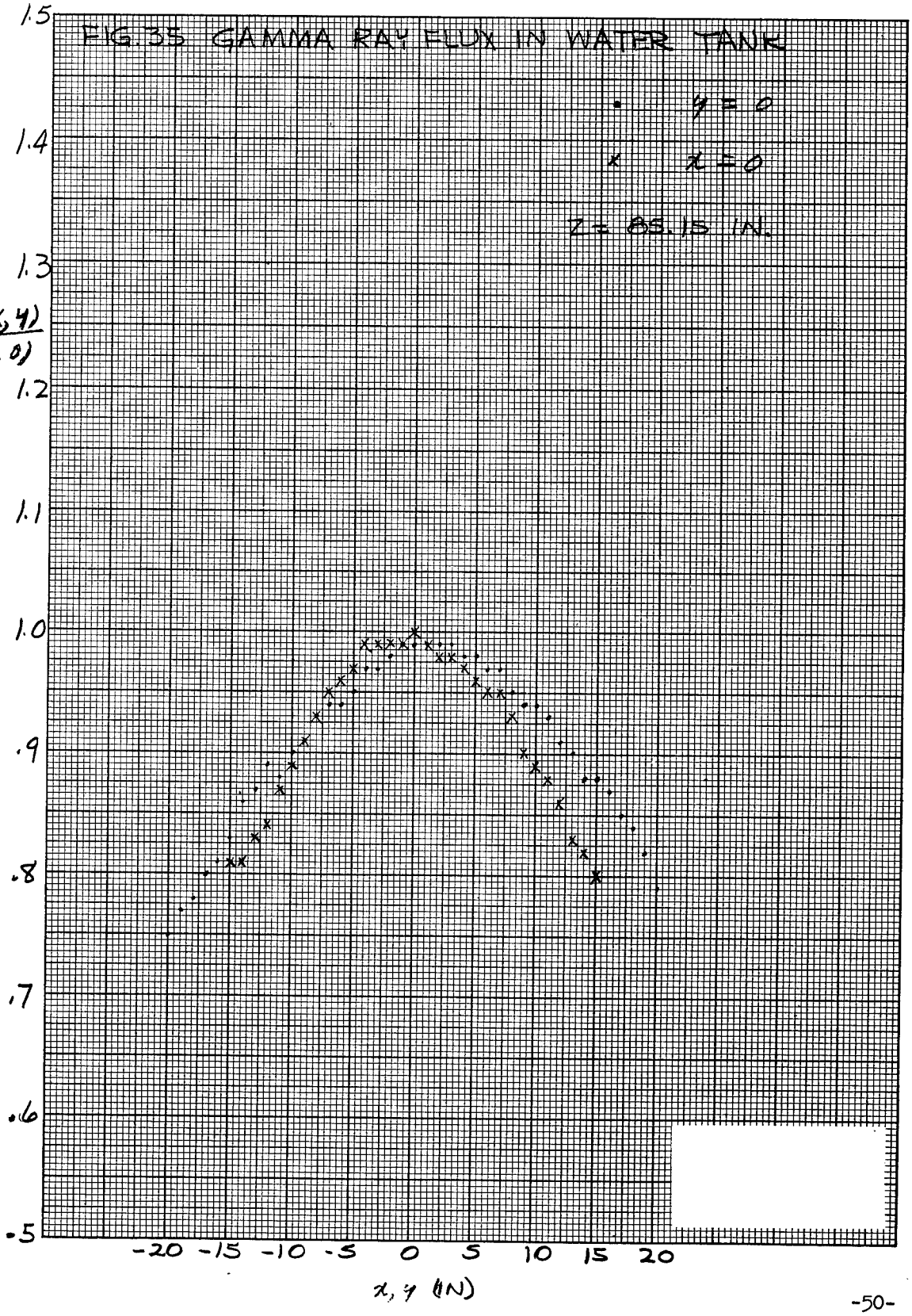

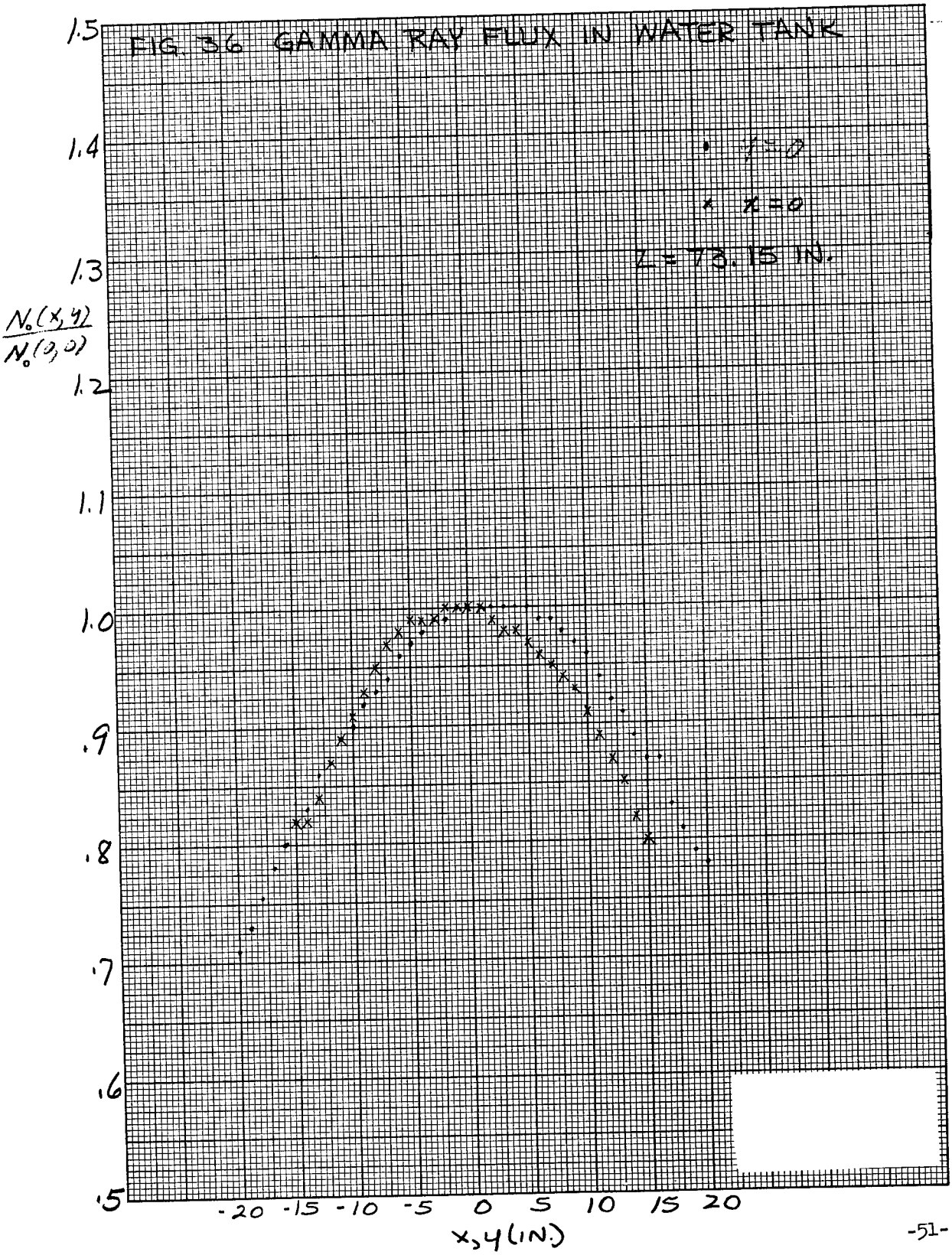
FIG. 36 GAMMA RAY FLUX IN WATER TANK
Y = 0
X = 0
Z = 73.15 IN.
$\frac{N_0(x,y)}{N_0(0,0)}$
1.5
1.4
1.3
1.2
1.1
1.0
.9
.8
.7
.6
.5
-20 -15 -10 -5 0 5 10 15 20
x,y (IN.)

FIG. 37 GAMMA RAY FLUX IN WATER TANK

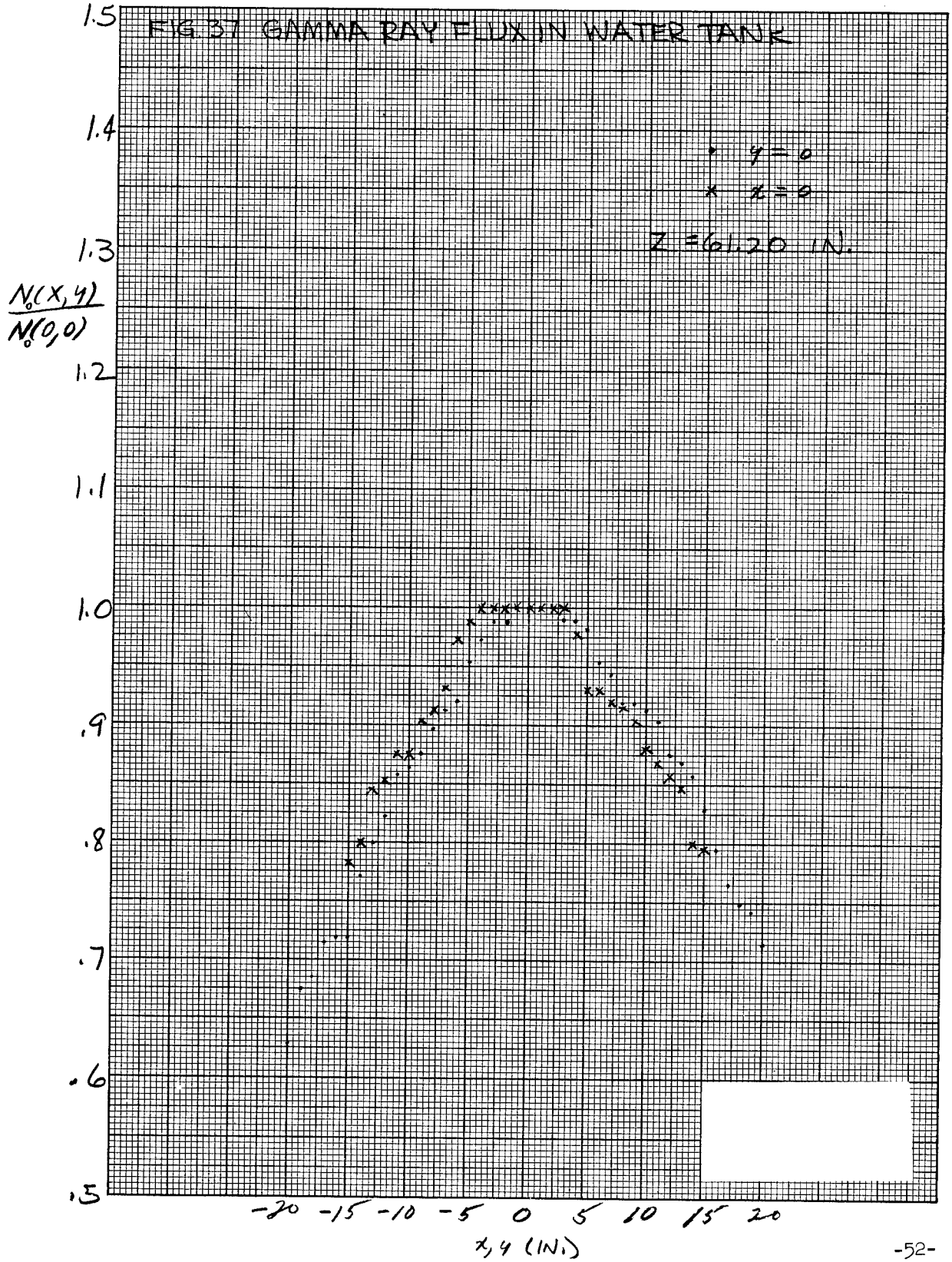

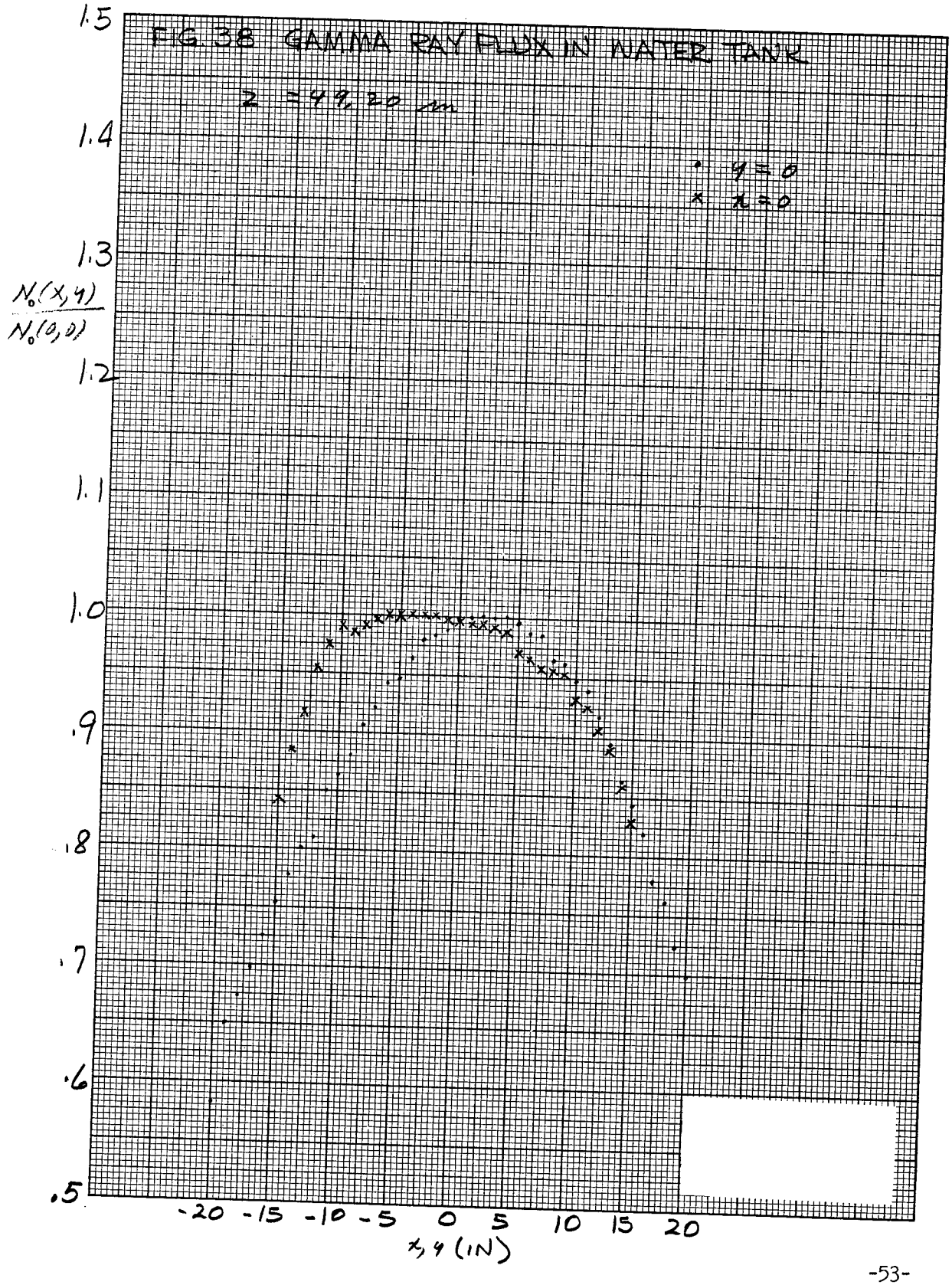
FIG. 38 GAMMA RAY FLUX IN WATER TANK
z = 49.20 in
y = 0
x = 0
1.5
1.4
1.3
1.2
1.1
1.0
.9
.8
.7
.6
.5
N₀(x,y) / N₀(0,0)
-20 -15 -10 -5 0 5 10 15 20
x, y (IN)

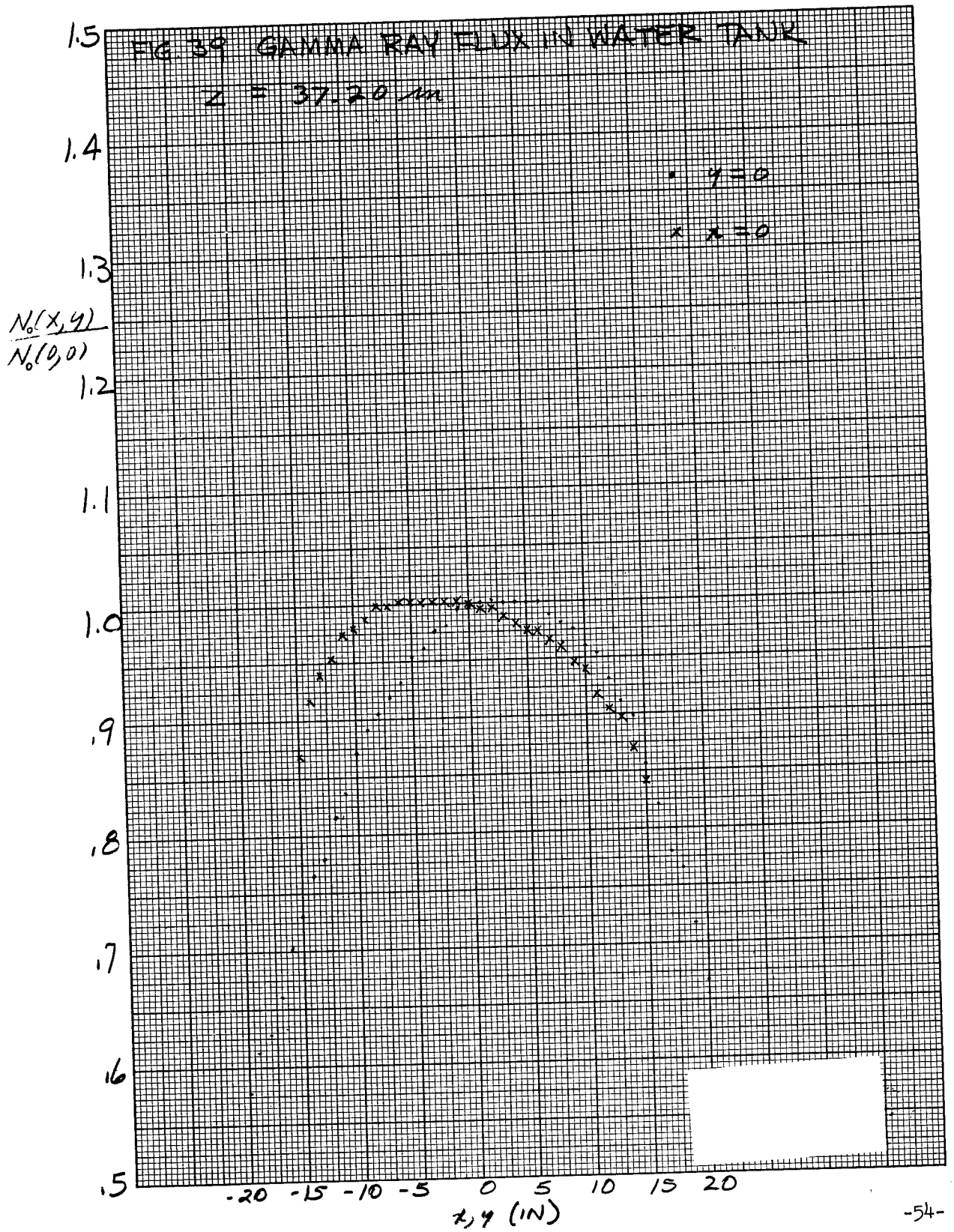
FIG 39 GAMMA RAY FLUX IN WATER TANK
Z = 37.20 cm
• y=0
× x=0
N₀(x,y) / N₀(0,0)
1.5
1.4
1.3
1.2
1.1
1.0
.9
.8
.7
.6
.5
-20 -15 -10 -5 0 5 10 15 20
x, y (IN)

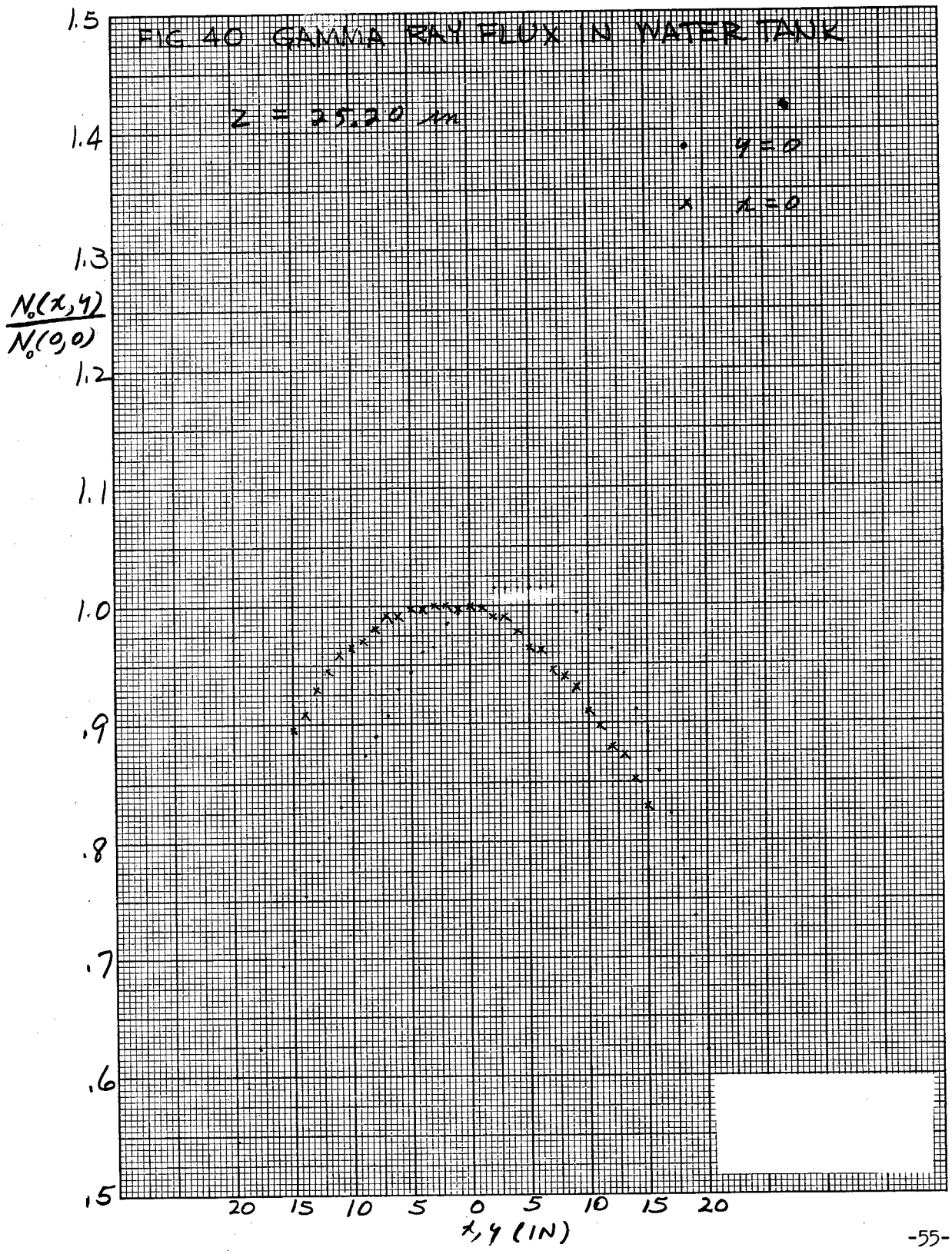
FIG 40 GAMMA RAY FLUX IN WATER TANK
Z = 25.20 in
y = 0
x = 0
1.5
1.4
1.3
1.2
1.1
1.0
.9
.8
.7
.6
.5
N₀(x,y) / N₀(0,0)
20 15 10 5 0 5 10 15 20
x, y (IN)

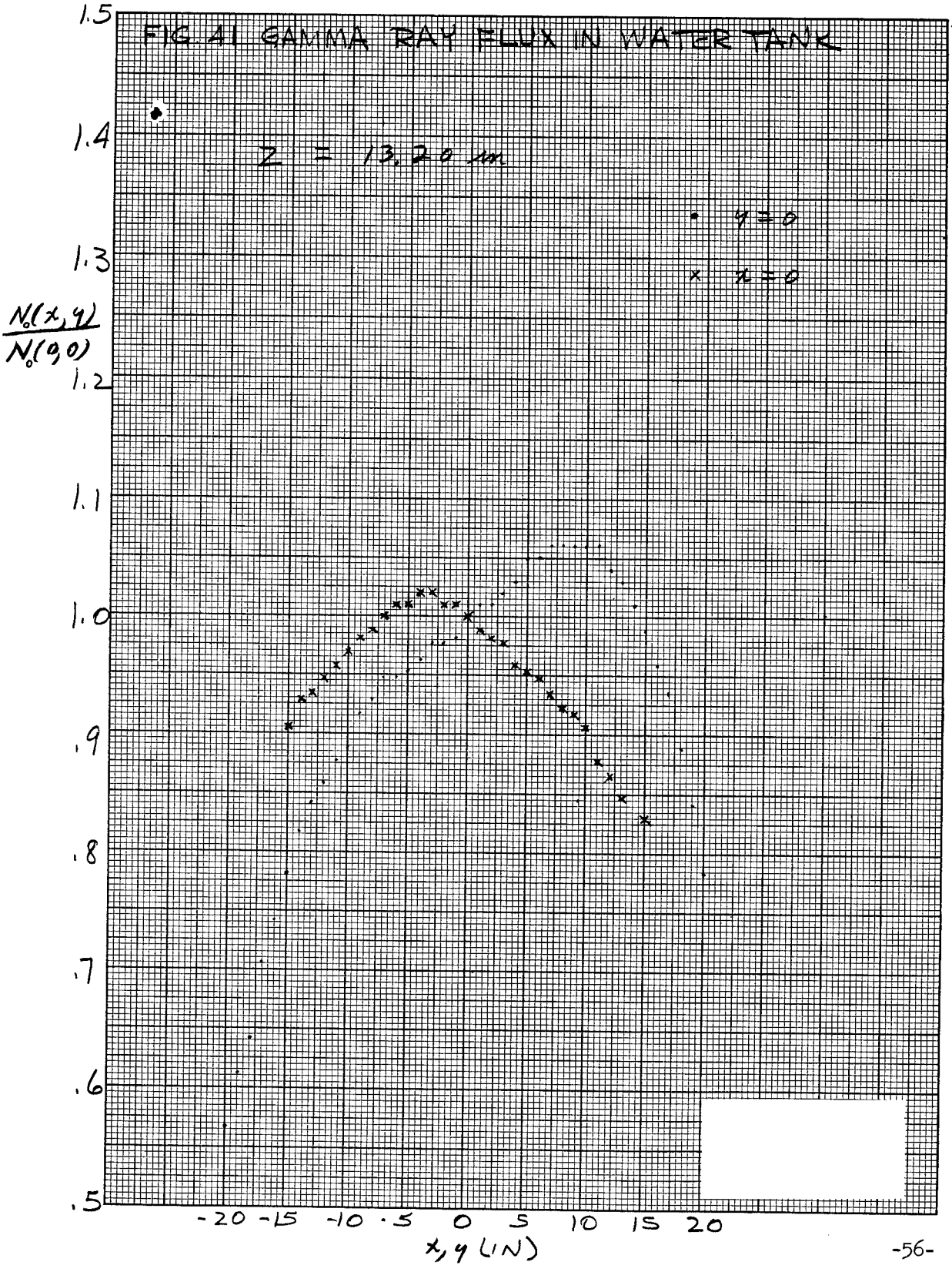
FIG. 41 GAMMA RAY FLUX IN WATER TANK
Z = 13.20 in.
• y = 0
× x = 0
N₀(x,y) / N₀(0,0)
1.5
1.4
1.3
1.2
1.1
1.0
.9
.8
.7
.6
.5
-20 -15 -10 -5 0 5 10 15 20
x, y (IN)

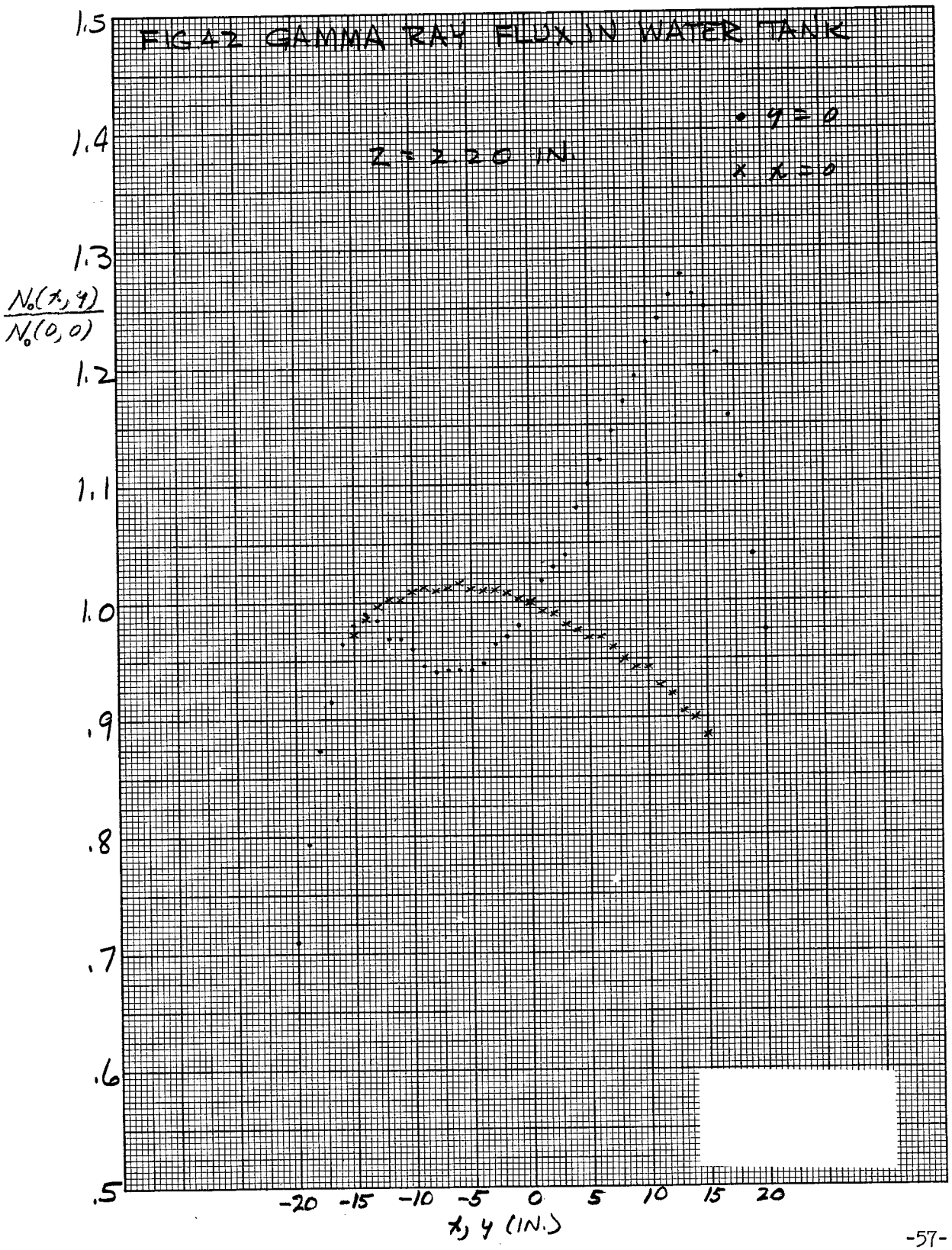
FIG 42 GAMMA RAY FLUX IN WATER TANK
Z = 2.20 IN.
• Y = 0
× X = 0
1.5
1.4
1.3
1.2
1.1
1.0
.9
.8
.7
.6
.5
N₀(x, y) / N₀(0, 0)
-20 -15 -10 -5 0 5 10 15 20
x, y (IN.)

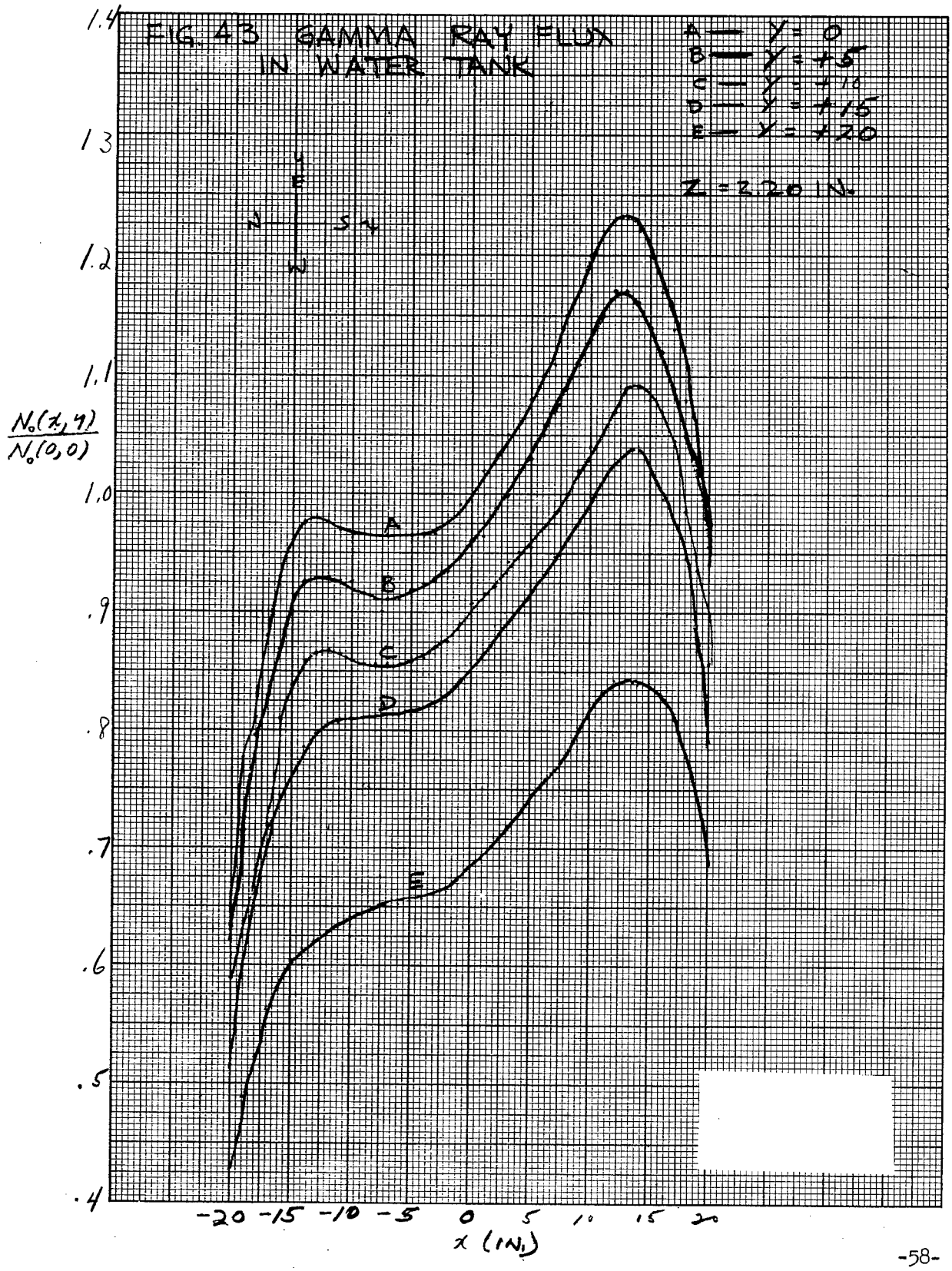
FIG. 43 GAMMA RAY FLUX IN WATER TANK
A — Y = 0
B — Y = +5
C — Y = +10
D — Y = +15
E — Y = +20
Z = 2.20 IN.
N
S
E
W
A
B
C
D
E
1.4
1.3
1.2
1.1
1.0
.9
.8
.7
.6
.5
.4
$\frac{N_0(x,y)}{N_0(0,0)}$
-20 -15 -10 -5 0 5 10 15 20
x (IN.)

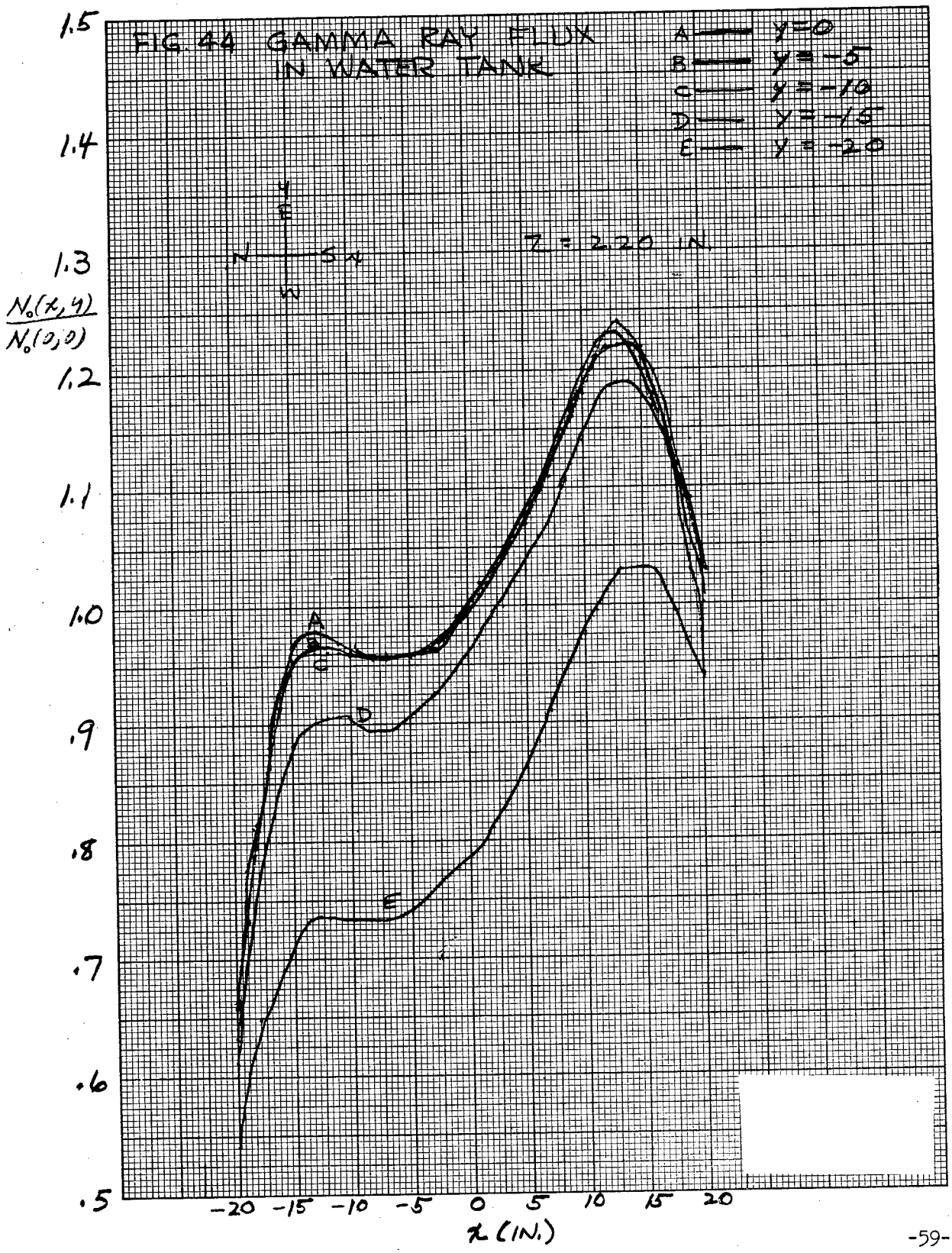
FIG. 44 GAMMA RAY FLUX IN WATER TANK
A —— Y=0
B —— Y=-5
C —— Y=-10
D —— Y=-15
E —— Y=-20
Z = 2.20 IN.
N
S
W
y
x
$\frac{N_0(x,y)}{N_0(0,0)}$
1.5
1.4
1.3
1.2
1.1
1.0
.9
.8
.7
.6
.5
A
C
D
E
-20 -15 -10 -5 0 5 10 15 20
x (IN.)

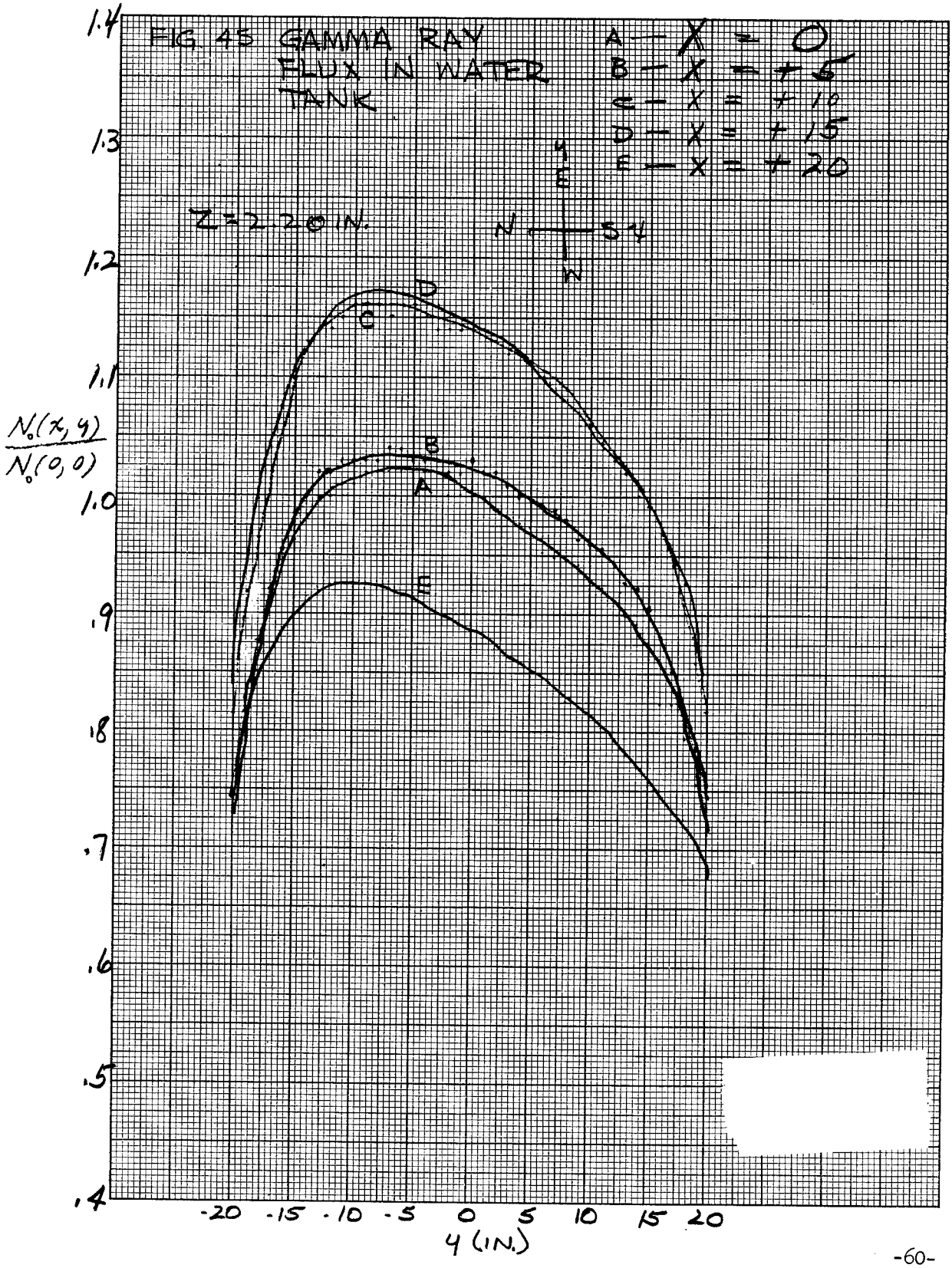
FIG. 45 GAMMA RAY FLUX IN WATER TANK
A — X = 0
B — X = ± 5
C — X = ± 10
D — X = ± 15
E — X = ± 20
Z = 2.26 IN.
N
S
E
W
A
B
C
D
E
1.4
1.3
1.2
1.1
1.0
.9
.8
.7
.6
.5
.4
N₀(x, y) / N₀(0, 0)
-20 -15 -10 -5 0 5 10 15 20
Y (IN.)

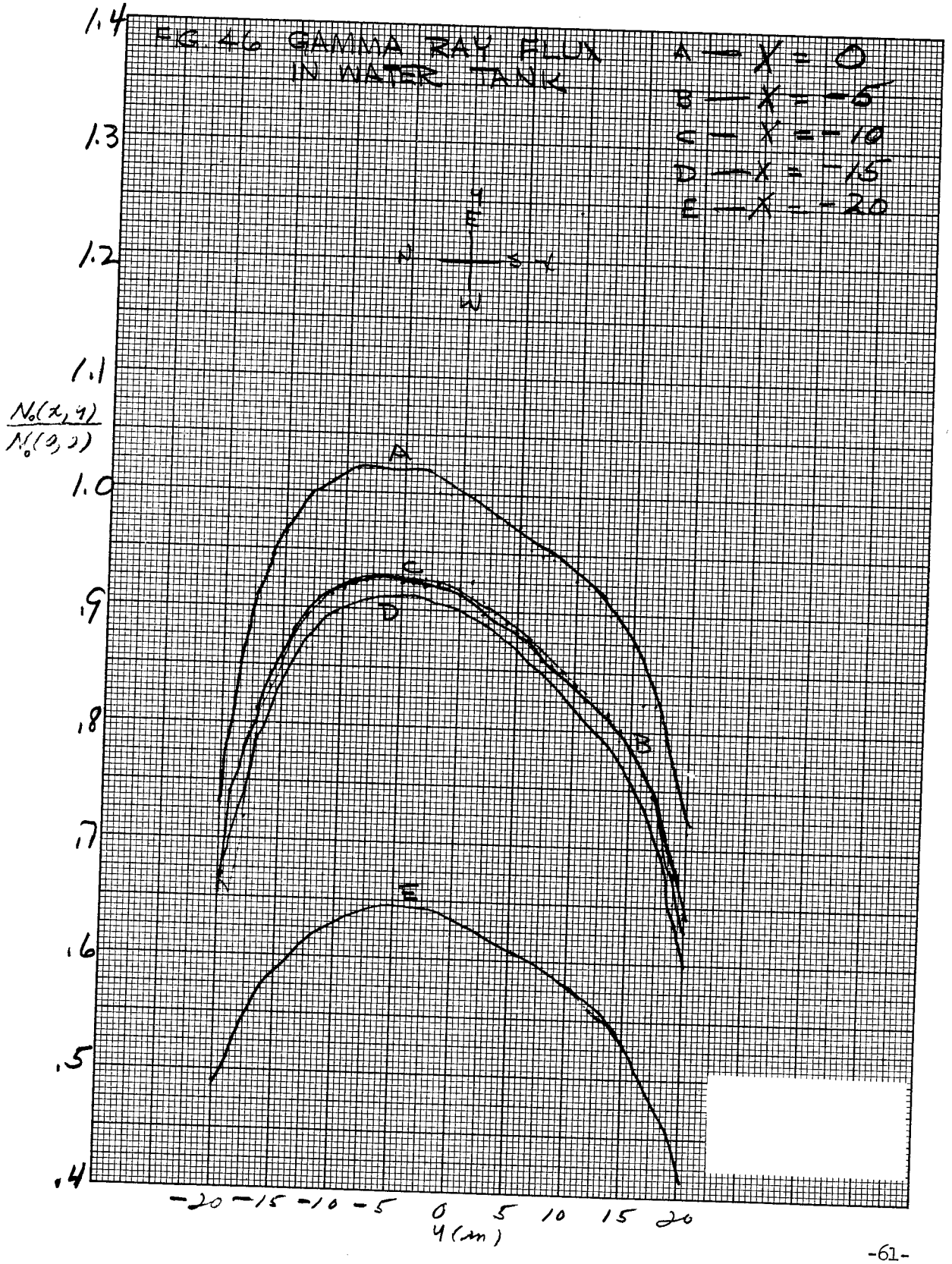
FIG. 46 GAMMA RAY FLUX IN WATER TANK
A — X = 0
B — X = -5
C — X = -10
D — X = -15
E — X = -20
N
S
E
W
Y
$\frac{N_0(x,y)}{N_0(0,0)}$
1.4
1.3
1.2
1.1
1.0
.9
.8
.7
.6
.5
.4
A
B
C
D
E
-20 -15 -10 -5 0 5 10 15 20
Y (cm)

FIG 47 APPARATUS FOR ANGULAR DISTRIBUTION MEASUREMENT

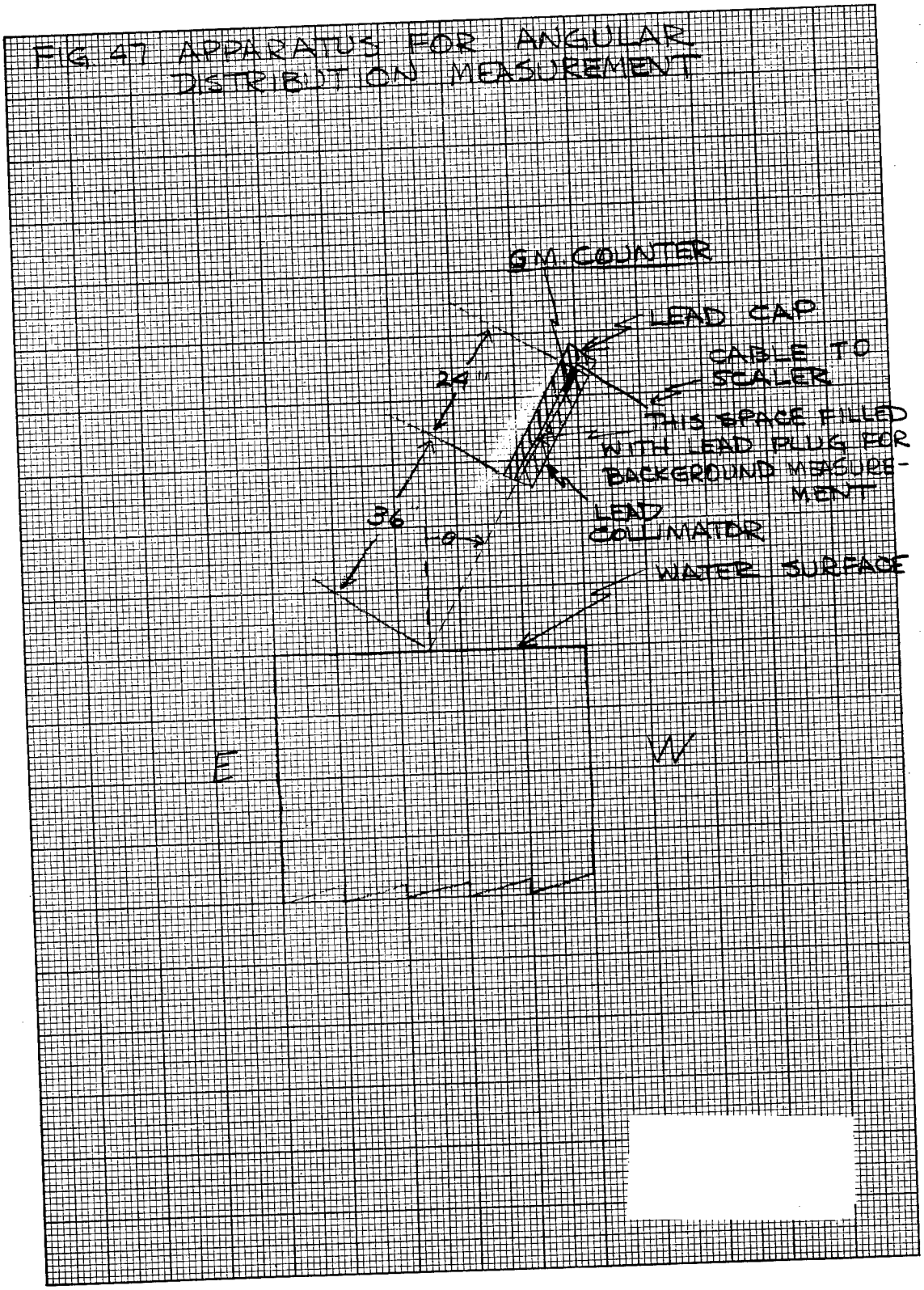

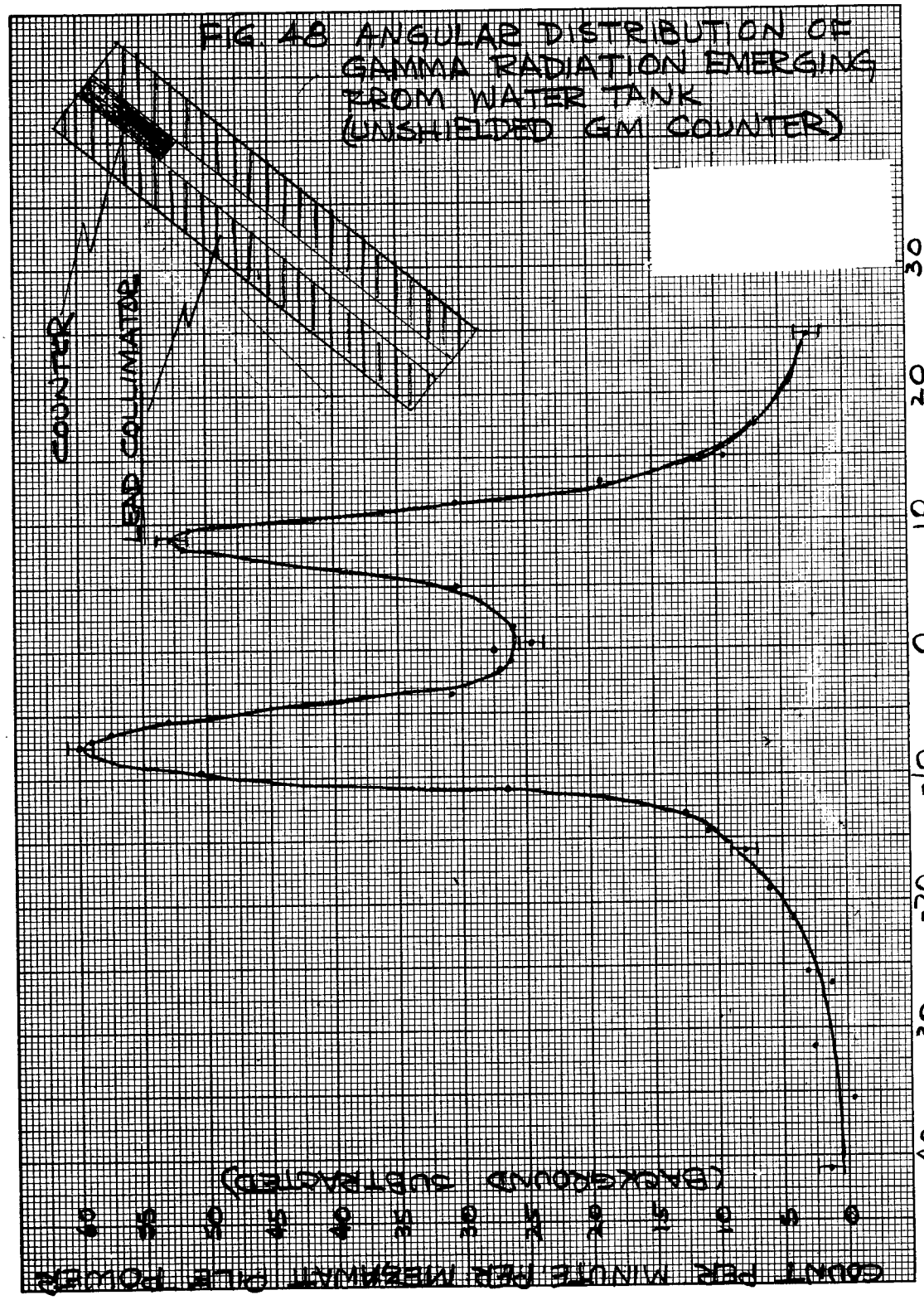
FIG 4.8 ANGULAR DISTRIBUTION OF GAMMA RADIATION EMERGING FROM WATER TANK (UNSHIELDED GM COUNTER)
SOURCE
LEAD COLLIMATOR
ANGLE (DEGREES WEST OF NORMAL)
30
20
10
0
-10
-20
-30
-40
COUNT PER MINUTE PER MILLIAMP (BACKGROUND SUBTRACTED)

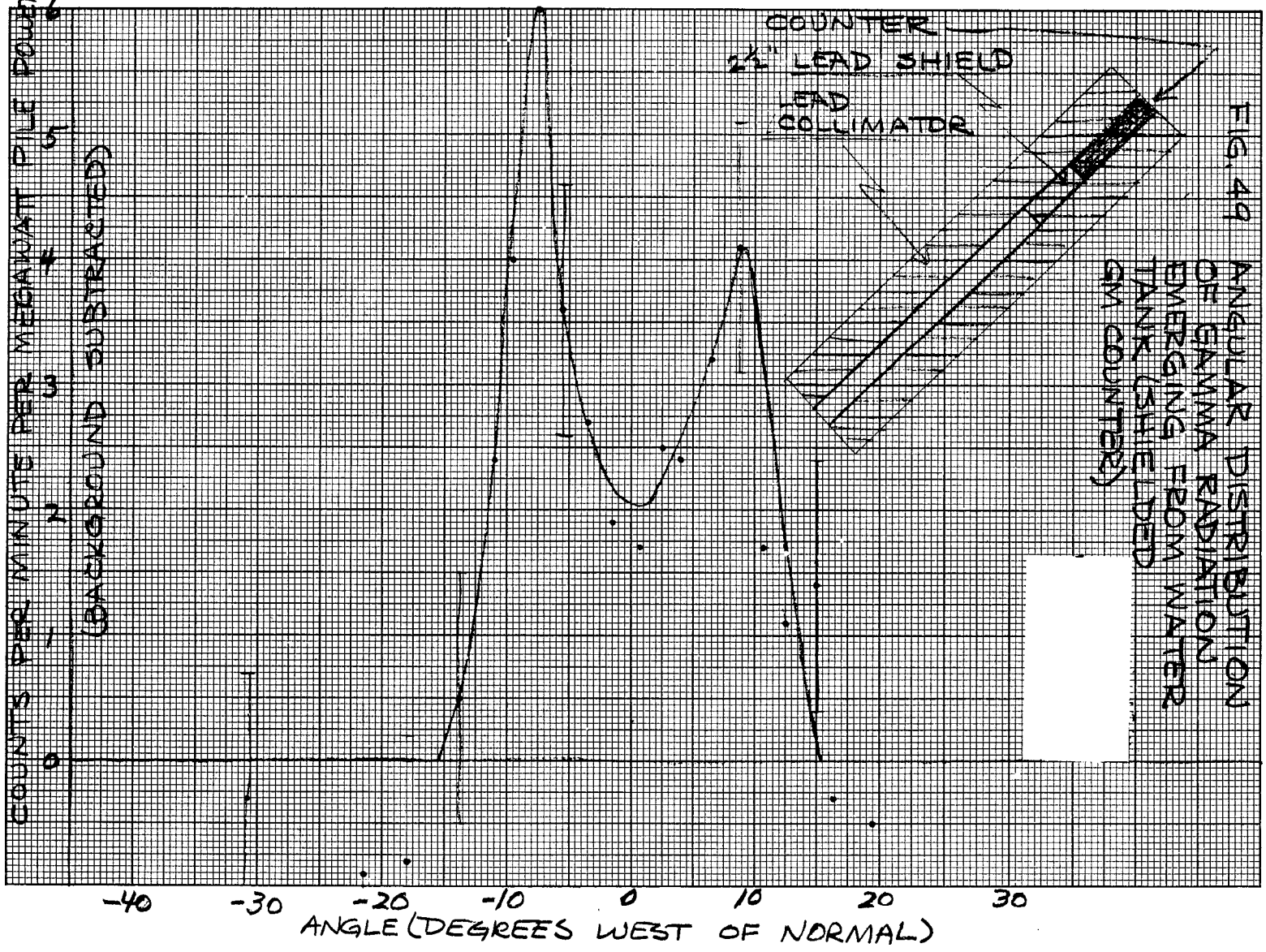

FIG. 4a ANGULAR DISTRIBUTION OF GAMMA RADIATION EMERGING FROM WATER ON COUNTER (SHIELDED AND COLLIMATED)

VI. TABLES

TABLE 1 - CORRECTION FACTOR FOR HEIGHT OF DETECTOR ABOVE WATER SURFACE

$$F = \frac{(N/No)r = 0 \text{ with detector center at water surface}}{(N/No)r = 0 \text{ with entire detector above water surface}}$$

SPHERE MEASUREMENTS

D (inches)	H (inches)	F (Ion Chamber)	F (GM Counter)
18	0	1.05	1.06
18	18	1.03	1.04
18	36	1.01	1.03
12	0	1.05	1.07
12	12	1.04	1.06
12	24	1.02	1.05
12	36	----	1.03
8	0	1.05	1.09
8	8	1.02	1.08
8	16	----	1.06
6	0	1.05	1.07
6	6	----	1.06
6	12	----	1.05
4	0	1.02	1.06
4	4	----	1.00

CYLINDER MEASUREMENTS

D (inches)	L (inches)	F (Ion Chamber)	F (GM counter)
18	24	1.00	1.03
18	36	1.03	1.04
18	48	1.06	1.06
12	24	1.01	1.06
12	36	1.09	1.17
12	48	1.10	1.14
12	60	1.10	1.13
12	72	1.09	1.11
12	84	1.08	----
8	24	1.08	1.15
8	36	1.14	1.19
8	48	1.16	1.20
8	60	1.15	1.19
8	72	1.12	1.17

TABLE 1 ——continued

CYLINDER MEASUREMENTS			
D (inches)	L (inches)	F (Ion Chamber)	F (GM Counter)
8	84	1.10	1.15
8	96	1.08	——
8	108	1.06	——
8	120	1.04	——
6	24	1.14	1.20
6	36	1.20	1.20
6	48	1.21	1.20
6	60	1.19	1.20
6	72	1.16	1.18
6	84	1.13	1.16
6	96	1.11	1.14
6	108	1.10	——
6	120	1.09	——
4	24	1.21	1.12
4	36	1.21	1.22
4	48	1.21	1.22
4	60	1.20	1.20
4	72	1.20	1.17
4	84	1.18	1.14
4	96	1.16	1.11
4	108	1.13	1.09
4	120	1.08	1.08
2	24	——	1.11
2	36	——	1.11
2	48	——	1.10
2	60	——	1.10
2	72	——	1.09
2	84	1.18	1.09
2	96	1.17	1.08
2	108	1.12	1.08
2	120	1.08	1.07
2	132	1.07	1.06
2	142.75	1.06	1.06

TABLE 2 - ION CHAMBER SPHERE MEASUREMENTS
(Uncorrected for Height of Detector Above Water Surface)

D (inches)	H (inches)	N/No (r = 0)	W (inches)	I (Square) (inches)
18	0	2.70	14	355
18	18	2.24	18	417
18	36	1.78	30	686
12	0	1.91	10	102
12	12	1.66	11	87
12	24	1.35	18	96
8	0	1.54	7	30
8	8	1.35	8	29
6	0	1.32	6	29
4	0	1.17	8	11

TABLE 3 - GM COUNTER SPHERE MEASUREMENTS
(Uncorrected for Height of Detector Above Water Surface)

D (inches)	H (inches)	N/No (r = 0)	W (inches)	I (Square) (inches)
18	0	2.61	15	324
18	18	2.23	16	426
18	36	1.72	24	460
12	0	1.87	10	71.0
12	12	1.65	10	87.6
12	24	1.35	15	92.9
12	36	1.17	25	92.7
8	0	1.48	6	19.6
8	8	1.34	7	19.4
8	16	1.18	10	24.9
6	0	1.30	4.5	6.3
6	6	1.20	6	7.7
6	12	1.12	8	7.9
4	0	1.17	4	2.9
4	4	1.09	7	4.7

TABLE 4 - ION CHAMBER CYLINDER MEASUREMENTS
(Uncorrected for Height of Detector Above Water Surface)

D (inches)	L (inches)	N/No (r = 0)	W (inches)	I (Sq. inches)
18	24	4.10	19	809
18	36	7.45	20	2420
18	48	12.8	20	7080
12	36	5.70	13	656
12	48	7.20	15	1640
12	60	9.70	16	2950
12	72	12.5	17	4910
12	84	18.0	15	6090
8	24	2.43	8	122
8	36	3.13	10	333
8	48	4.00	11	490
8	60	4.72	11	889
8	72	5.40	11	953
8	84	7.70	10	1430
8	96	10.7	10	1986
8	108	17.2	9	2528
8	120	28.7	9	3560
6	24	1.70	6.5	41
6	36	2.02	8	86
6	48	2.22	9	139
6	60	2.95	8.5	249
6	72	3.00	8	277
6	84	3.90	8	372
6	96	5.00	7	559
6	108	8.80	6	855
6	120	15.0	7	1200
4	24	1.48	5.5	22
4	36	1.62	6.5	61
4	48	1.75	7	65
4	60	1.69	5	96
4	72	1.80	5	55
4	84	2.15	5	69
4	96	2.65	5	71
4	108	3.90	5.5	124
4	120	5.80	4.5	353
2	84	1.25	3	4
2	96	1.39	2.5	9.6
2	108	1.62	2.5	9.3
2	120	2.20	2	13
2	132	3.40	1.5	18
2	142.75	6.60	2	39

TABLE 5 - GM COUNTER CYLINDER MEASUREMENTS
(Uncorrected for Height of Detector Above Water Surface)

D (inches)	L (inches)	N/No (r = 0)	W (inches)	I (sq. inches)
18	24	3.75	17	766
18	36	7.75	18	1921
18	48	14.5	18	4025
12	24	3.75	11	325
12	36	6.10	12.5	800
12	48	8.10	14	1331
12	60	11.0	10	2215
12	72	15.5	10	3645
8	24	2.83	8	115
8	36	3.64	10	252
8	48	4.55	10	436
8	60	5.95	10	803
8	72	7.75	10	1074
8	84	10.3	10	1458
6	24	2.26	6	68.1
6	36	2.64	9	122
6	48	3.00	8	146
6	60	4.05	8	309
6	72	4.75	7	380
6	84	6.00	7	468
6	96	8.10	6	551
4	24	1.58	6	20.6
4	36	1.82	6	53.3
4	48	2.02	6	86.8
4	60	2.24	5	85.8
4	72	2.65	5	97.4
4	84	3.20	5	140
4	96	4.25	5	161
4	108	5.55	4.5	185
4	120	7.65	4.5	185
2	24	1.08	7	4.5
2	36	1.14	6	10.8
2	48	1.18	5	8.1
2	60	1.24	4	10.3
2	72	1.32	3	7.9
2	84	1.46	3	13.4
2	96	1.66	2.5	13.8
2	108	2.05	2	12.0
2	120	2.55	2	11.4
2	132	3.90	2	20.3
2	142.75	12.0	2	58.6

TABLE 6 - SPHERE MEASUREMENTS (Corrected for Height of Detector Above Water Surface)

D (inches)	H (inches)	$(N/No)_{r=0}$ Ion Chamber	$(N/No)_{r=0}$ GM Counter
18	0	2.84	2.77
18	18	2.30	2.32
18	36	1.80	1.77
12	0	2.00	2.00
12	12	1.73	1.75
12	24	1.38	1.42
12	36	——	1.21
8	0	1.62	1.61
8	8	1.38	1.45
8	16	——	1.25
6	0	1.38	1.39
6	6	——	1.27
6	12	——	1.18
4	0	1.19	1.24
4	4	——	1.09

TABLE 7 - CYLINDER MEASUREMENTS (Corrected for Height of Detector Above Water Surface)

D (inches)	L (inches)	(N/No)r = 0 Ion Chamber	(N/No)r = 0 GM Counter
18	24	4.10	3.86
18	36	7.68	8.06
18	48	13.6	15.4
12	24	——	3.98
12	36	6.20	7.14
12	48	7.91	9.25
12	60	10.7	12.4
12	72	13.6	17.2
12	84	19.5	——
8	24	2.62	3.26
8	36	3.57	4.33
8	48	4.65	5.45
8	60	5.42	7.08
8	72	6.05	9.06
8	84	8.46	11.8
8	96	11.6	——
8	108	18.2	——
8	120	29.8	——
6	24	1.94	2.72
6	36	2.42	3.17
6	48	2.68	3.60
6	60	3.51	4.86
6	72	3.48	5.61
6	84	4.41	6.95
6	96	5.55	9.23
6	108	9.70	——
6	120	16.4	——
4	24	1.79	1.77
4	36	1.96	2.22
4	48	2.12	2.49
4	60	2.03	2.69
4	72	2.16	3.10
4	84	2.54	3.65
4	96	3.07	4.72
4	108	4.40	6.05
4	120	6.27	8.26
2	24	——	1.20
2	36	——	1.27
2	48	——	1.30
2	60	——	1.36
2	72	——	1.44
2	84	1.48	1.59
2	96	1.63	1.79
2	108	1.82	2.21
2	120	2.38	2.73
2	132	3.64	4.14
2	142.75	7.00	12.7

TABLE 8 - ATTENUATION OF GAMMA RAYS IN WATER TANK (ION CHAMBER MEASUREMENTS)

Water Depth Z (inches)	R/MWH[x]	Water Depth Z (inches)	R/MWH[x]	Water Depth Z (inches)	R/MWH[x]
2.20	3.86(2)	49.20	2.66(0)	96.15	5.44(-2)
3.20	3.37(2)	50.20	2.43(0)	97.15	5.01(-2)
4.20	2.95(2)	51.20	2.22(0)	98.15	4.58(-2)
5.20	2.60(2)	52.20	2.02(0)	99.15	4.29(-2)
6.20	2.25(2)	53.20	1.85(0)	100.15	4.01(-2)
7.20	1.99(2)	54.20	1.72(0)	101.15	3.72(-2)
8.20	1.76(2)	55.20	1.57(0)	102.15	3.44(-2)
9.20	1.52(2)	56.20	1.47(0)	103.15	3.15(-2)
10.20	1.35(2)	57.20	1.30(0)	104.15	2.86(-2)
11.20	1.22(2)	58.20	1.21(0)	105.15	2.69(-2)
12.20	1.07(2)	59.20	1.10(0)	106.15	2.49(-2)
13.20	9.54(1)	60.20	1.00(0)	107.15	2.29(-2)
14.20	8.69(1)	61.20	9.05(-1)	108.15	2.13(-2)
15.20	7.74(1)	62.20	8.55(-1)	109.15	1.98(-2)
16.20	6.90(1)	63.20	7.94(-1)	110.15	1.82(-2)
17.20	6.18(1)	64.20	7.34(-1)	111.15	1.69(-2)
18.20	5.52(1)	65.20	6.63(-1)	112.15	1.56(-2)
19.20	4.93(1)	66.20	6.07(-1)	113.15	1.43(-2)
20.20	4.42(1)	67.20	5.62(-1)	114.15	1.32(-2)
21.20	3.94(1)	68.20	5.20(-1)	115.15	1.22(-2)
22.20	3.59(1)	69.20	4.72(-1)	116.15	1.13(-2)
23.20	3.24(1)	70.20	4.41(-1)	117.15	1.04(-2)
24.20	2.95(1)	71.20	4.03(-1)	118.15	9.59(-3)
25.20	2.65(1)	72.20	3.71(-1)	119.15	8.87(-3)
26.20	2.41(1)	73.20	3.41(-1)	120.15	8.30(-3)
27.20	2.17(1)	74.20	3.17(-1)	121.15	7.59(-3)
28.20	1.93(1)	75.20	2.89(-1)	122.15	7.01(-3)
29.20	1.74(1)	76.15	2.72(-1)	123.15	6.44(-3)
30.20	1.60(1)	77.15	2.50(-1)	124.15	6.01(-3)
31.20	1.43(1)	78.15	2.30(-1)	125.15	5.58(-3)
32.20	1.37(1)	79.15	2.12(-1)	126.15	5.15(-3)
33.20	1.18(1)	80.15	1.98(-1)	127.15	4.72(-3)
34.20	1.14(1)	81.15	1.80(-1)	128.15	4.44(-3)
35.20	9.65(0)	82.15	1.65(-1)	129.15	4.15(-3)
36.20	9.27(0)	83.15	1.53(-1)	130.15	3.86(-3)
37.20	8.11(0)	84.15	1.42(-1)	131.15	3.58(-3)
38.20	7.39(0)	85.15	1.30(-1)	132.15	3.29(-3)
39.20	6.68(0)	86.15	1.20(-1)	133.15	3.01(-3)
40.20	6.06(0)	87.15	1.12(-1)	134.15	2.69(-3)
41.20	5.63(0)	88.15	1.03(-1)	135.15	2.46(-3)
42.20	5.20(0)	89.15	9.45(-2)	136.15	2.29(-3)
43.20	4.62(0)	90.15	8.73(-2)	137.15	2.09(-3)
44.20	4.19(0)	91.15	8.02(-2)	138.15	1.95(-3)
45.20	3.82(0)	92.15	7.44(-2)	139.15	1.80(-3)
46.20	3.48(0)	93.15	6.87(-2)	140.15	1.57(-3)
47.20	3.17(0)	94.15	6.44(-2)	141.15	1.43(-3)
48.20	2.95(0)	95.15	5.87(-2)		

x Roentgens per hour per megawatt pile power. A figure in parentheses denotes a power of 10. Attenuation length for $Z \geq 55$ inches is 31.6 cm. $x = y = 0$

TABLE 9 - ATTENUATION OF GAMMA RAYS IN WATER TANK (GM COUNTER MEASUREMENTS)

Water Depth Z (inches)	C/MMW[x]
18.50	1.812(6)
23.25	1.108(6)
26.81	6.563(5)
31.00	4.088(5)
35.00	2.683(5)
39.25	1.768(5)
42.88	1.232(5)
47.50	8.761(4)
51.12	6.479(4)
55.00	4.742(4)
58.69	3.561(4)
63.38	2.628(4)
67.12	1.944(4)
70.94	1.472(4)
74.69	1.136(4)
78.69	8.349(3)
83.00	6.353(3)
87.12	4.830(3)
91.19	3.567(3)
95.25	2.775(3)
98.94	2.116(3)
103.31	1.541(3)
107.25	1.130(3)
111.38	8.770(2)
115.00	6.607(2)
119.31	4.882(2)
123.06	3.774(2)
127.25	2.794(2)
131.25	2.065(2)
134.94	1.582(2)
139.25	1.182(2)
143.00	8.84(1)

[x] Counts per minute per megawatt pile power.

A figure in parenthesis denotes a power of 10.

Attenuation length for $Z \geq 55$ inches is 31.6 cm.

$x = y = 0$.

TABLE 10 - ANGULAR DISTRIBUTION OF GAMMA RAY FLUX EMERGING FROM WATER TANK

UNSHIELDED GM COUNTER[x]

Angle[xx] (degrees)	Flux[+] (C/M-MW)	Angle[xx] (degrees)	Flux[+] (C/M-MW)
-41.0	1.4		
-35.5	-0.4	- 3.5	30.8
-31.3	2.6	- 1.5	27.4
-26.3	1.2	- 0.8	26.1
-25.5	3.2	0	27.5
-21.3	4.2	∠ 0.5	24.5
-19.0	5.1	∠ 2.7	26.0
-16.0	7.9	∠ 5.0	30.4
-14.5	10.8	∠ 8.0	51.8
-12.5	15.6	∠ 8.8	52.8
-11.0	26.5	∠ 9.5	51.4
- 9.5	50.5	∠11.5	30.4
- 7.5	59.9	∠13.1	19.0
- 7.0	59.0	∠14.8	9.4
- 6.5	57.6	∠17.5	6.9
- 5.5	53.1	∠24.5	2.8

SHIELDED GM COUNTER[x]

-30.8	-0.3	∠ 0.7	1.7
-21.5	-0.9	∠ 2.5	2.5
-18.0	-0.8	∠ 4.4	2.4
-13.8	∠0.5	∠ 6.5	3.2
-11.0	∠2.4	∠ 8.8	4.1
- 9.5	∠4.0	∠10.7	1.7
- 7.5	∠6.0	∠12.5	1.1
- 5.5	∠3.6	∠15.0	1.4
- 3.5	∠2.7	∠16.4	-0.3
- 1.5	∠1.9	∠19.5	-0.5

[x] The unshielded GM counter refers to the counter in the collimator alone. The shielded GM counter refers to the counter in the collimator with a 2-1/2 inch lead plug directly in front of the counter.

[xx] A positive angle corresponds to radiation emerging in a direction to the west of the normal, a negative angle corresponds to radiation emerging in a direction to the east of the normal.

[+] Flux is given in counts per minute per megawatt pile power, with the background (determined by filling the collimator with a lead plug in front of the counter) subtracted. All flux values are ± 1 C/M-MW.

TABLE 11 - VOID DIMENSIONS

SPHERES

Nominal Diameter (inches)	Inside Diameter (inches)	Outside Diameter (inches)
4	3.88	4.00
6	5.88	6.00
8	7.88	8.00
12	11.88	12.00
18	17.88	18.00

CYLINDERS

Nominal Diameter (inches)	Inside Diameter (inches)	Outside Diameter (inches)	Endplate Thickness (inches)
2	1.88	2.00	0.38
4	3.81	4.00	0.38
6	5.81	6.00	0.38
8	7.81	8.00	0.38
12	11.81	12.00	0.38
18	17.75	18.00	0.38

Nominal length of cylindrical voids is the length of air space inside the void.

☆ U. S. GOVERNMENT PRINTING OFFICE: 1956 O— 376515